Characterization of mitotic checkpoint complexes

Inauguraldissertation

zur
Erlangung der Würde eines Doktors der Philosophie
vorgelegt der
Philosophisch-Naturwissenschaftlichen Fakultät
der Universität Basel
von

Luca Fava

aus Bozen, Italien

Basel, 2011

Genehmigt von der Philosophisch-Naturwissenschaftlichen Fakultät

auf Antrag von

Prof. Erich A. Nigg, Prof. Elmar Schiebel, Dr. Anna Santamaria
(Mitglieder des Dissertationskomitees)

Basel, den 18.10.2011
Prof. Martin Spiess
- Dekan –

The experiments displayed in this thesis have been performed from September 2007 to October 2011 in the laboratory of Prof. Erich A. Nigg, in the Department of Cell Biology at the Max-Planck Institute of Biochemistry and at the Biozentrum (Growth & Development), University of Basel.

Parts of this thesis have been published in:

Fava LL, Kaulich M, Nigg EA, Santamaria A (2011) Probing the in vivo function of Mad1:C-Mad2 in the spindle assembly checkpoint. *The EMBO journal* **30:** 3322-3336

Chan YW, Fava LL, Uldschmid A, Schmitz MH, Gerlich DW, Nigg EA, Santamaria A (2009) Mitotic control of kinetochore-associated dynein and spindle orientation by human Spindly. *J Cell Biol* **185:** 859-874

I herewith declare that major passages in this thesis have been adapted from Fava et al., 2011. I am primarily responsible for the work described in this publication.

Figures 23 and 37 of this thesis have been performed by and Manuel Kaulich and Anna Baron, respectively. The work performed by Anna Baron will be also displayed in a Master thesis that will be submitted to this Faculty in the near future.

Table of Contents

Summary **1**

Introduction **3**

The cell cycle and its checkpoints 3

The events of mitosis 6

The Spindle Assembly Checkpoint (SAC) 8

The vertebrate centromere/kinetochore region, the SAC sensor 10

The anaphase promoting complex or cyclosome, the SAC target 14

The Mad2 template model for SAC signaling and silencing 18

Control of mitotic timing, clock or domino? 21

The nuclear envelope and the control of cell division 22

Aim **27**

Results **29**

Generation and characterization of antibodies to Mad1, p31comet and Mad2 29

Mad1 29

p31comet 31

Mad2 31

$CM2^{276}$ recognizes C-Mad2 on the dimerization interface 35

Only liganded Mad2 adopts the Closed conformation in vivo 38

Mad1 is required for the formation of C-Mad2 in interphase 43

The Mad1:C-Mad2 complex is required to initiate the SAC 45

The Mad1:C-Mad2 complex is required to maintain the SAC 48

The Mad1:C-Mad2 complex is required to regulate mitotic timing 50

The SAC regulates mitotic timing operating intra-mitotically and not through a pre-assembled inhibitor 53

The Mad1:C-Mad2 complex undergoes p31comet dependent “capping” 56

p31comet dependent capping of C-Mad2 at NPCs and spindle poles 56

p31comet dependent capping of C-Mad2 at KTs 59

p31comet localizes at KTs during an active SAC in a C-Mad2 dependent manner 60

A role for Mps1 kinase activity in regulating p31comet dependent capping 61

A possible role for Tpr in regulating p31comet dependent capping 64

Analysis of the post-translational modifications and interaction partners of Mad1:C-Mad2 70

Discussion **76**

The two state behavior of Mad2 in the cell 76

Mad1:C-Mad2 initiating and maintaining the SAC ... 78
KT-dependent control of mitotic timing ... 79
Regulation of Mad1:C-Mad2 through p31comet dependent capping ... 82
Is there a Tpr-Mps1 axis controlling Mad1:C-Mad2? ... 84
Materials and Methods ... 88
Cloning procedures ... 88
Production and purification of recombinant proteins and antibodies ... 88
Competition assays ... 90
Peptide spots array synthesis and antibody binding assay ... 90
In vitro kinase assay ... 91
Cell culture and synchronization ... 91
SILAC labeling of cultured cells ... 91
Transient transfections of plasmid DNA and siRNA duplexes ... 92
Cell extracts, Western blots and immunoprecipitations ... 92
Mass spectrometry ... 93
Immunofluorescence microscopy and fluorescence intensity measurements ... 95
Antibody microinjection ... 96
Time-lapse microscopy ... 97
Size exclusion chromatography followed by immunoprecipitation ... 97
Appendix ... 99
Generation of additional antibodies to Mad2 ... 99
List of generated plasmids ... 102
References ... 104
Acknowledgements ... 117
***Curriculum Vitae* ... 119**

Summary

In eukaryotes, chromosome segregation critically depends on the establishment of productive contacts between kinetochores (KTs), specialized chromosomal structures, and the spindle microtubules (MTs). In mitosis, the spindle assembly checkpoint (SAC) is the major surveillance mechanism that restrains anaphase onset until all KTs become bi-oriented by spindle MTs. Several SAC proteins act in concert to relay the presence of unattached KTs to the cell cycle machinery in the cytoplasm. The SAC protein Mad2 plays a pivotal role in this signal transduction cascade, contributing both to the KT sensor and to the SAC cytoplasmic effector. Mad2 can fold into two distinct conformers, Open (O) and Closed (C), and can asymmetrically dimerize. Biophysical and structural work had demonstrated that the conformational dynamics of Mad2 is crucial for its activation *in vitro*, but models arising from this work could not be exhaustively tested in cells. Here, we describe a monoclonal antibody that specifically recognizes the dimerization interface of C-Mad2. This antibody revealed several conformation specific features of Mad2 in human cells. Notably, we show that Mad2 requires association with its KT-receptor Mad1 to adopt the Closed conformation. Furthermore, C-Mad2 antibody microinjection interfered with Mad2 asymmetric dimerization and abrogated the SAC, accelerating mitotic progression. Remarkably, microinjection of a Mad1-neutralizing antibody triggered a comparable mitotic acceleration. Finally, we show that the activity of the Mad1:C-Mad2 complex undergoes regulation by p31comet-dependent 'capping'. We also suggest that p31comet capping is negatively regulated by the SAC kinase Mps1 and the SAC regulator Tpr. Collectively, this work provides direct *in vivo* evidence

for the model that a KT complex of Mad1:C-Mad2 acts as a template to sustain the SAC and it challenges the distinction between SAC and mitotic timer.

Introduction

The cell cycle and its checkpoints

Self-reproduction is certainly the most crucial feature of cells, fundamental units of structure and function in living organisms. The principle that each cell arises from a pre-existing cell by division (*"omnis cellula e cellula"*) was divulgated by the pathologist Rudolph Virchow in the mid-19th century and laid the foundation of the modern cell theory. For unicellular organisms, each cell division represents the generation of two novel organisms arising from one. For multicellular organisms, cell division plays a crucial role not only in the organismic growth during development but also for the adult tissue homeostasis, replenishing the cellular pool otherwise depleted by the ongoing cell death. Mitotic cell divisions give rise to two genetically identical daughter cells and are always preceded by the duplication of the genetic material and other cellular components. The ordered series of events leading to cell division is defined as the **cell cycle**. In prokaryotes, the cell division occurs through a process called binary fission in which the replication of the chromosome(s) and cell growth occupy large part of the entire cell cycle, being rapidly followed by cell division. In eukaryotes, the two crucial phases of duplication (**S-phase**) and segregation (**M-phase**) of the genetic material are separated by so-called gap phases, **G1** and **G2** (Fig. 1). During G1 phase, the cell responds to both intra and extracellular growth signals that contribute to the decision of committing to one additional cell cycle, i.e. entering or not a new S phase. During G2 phase the cell with duplicated chromosome content prepares for entering the subsequent M-phase (Fig. 1). G0 refers to a state in which a cell remains metabolically active, but no longer proliferates. The G0 state is maintained until the cell receives appropriate extracellular signals.

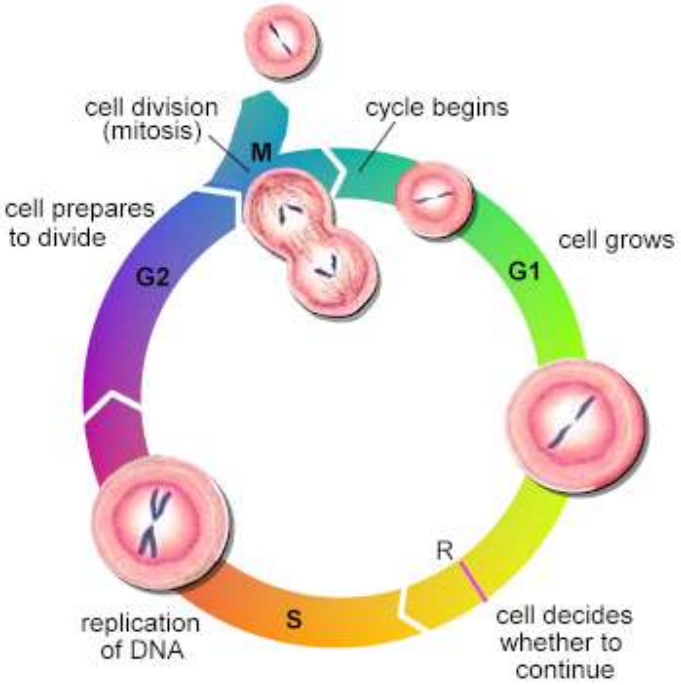

Figure 1. The eukaryotic cell cycle. The cell cycle is subdivided in four phases: **G1**, characterized by cell growth and by the presence of the restriction point (R), at which the decision to commit to a new cell cycle is taken, **S** in which the chromosomal DNA is replicated, **G2** in which the cells prepares to divide and **M**-phase, in which the chromosome are segregated (karyokinesis) and two cells separated (cytokinesis). Illustration adapted from "The Encyclopaedia of Science" (www.daviddarling.info).

A key principle of the cell cycle is that the underlying events occur in a controlled fashion displaying unidirectionality: this means that M-phase (chromosome separation) has always to be preceded by S-phase (chromosome duplication) and deviations would lead to the generation of an aberrant progeny. Key transitions in the cell cycle are controlled by surveillance mechanisms called checkpoints, systems that are devoted to monitor the correct completion of key cell cycle events and extend the duration of a given phase, providing time for error correction (Hartwell & Weinert, 1989). In the absence of perturbations the cell cycle might appear as governed by a **clock**, an autonomous oscillator dictating the duration of the different phases without any possible external input (Fig. 2A). When the cell cycle is perturbed, interfering either genetically or

chemically with the molecular devices such as the DNA replication machinery or the mitotic spindle apparatus, a checkpoint mediated cell cycle arrest occurs. In this perspective, the cell cycle appears more as a **domino**: a linear sequence of event in which the initiation of each step is dependent on the completion of the earlier step (Fig. 2B).

During the early days of cell cycle research questions were tackled by using either amphibian eggs or yeasts as model organisms. The embryological work in eggs seemed to support the “clock view” of the cell cycle, whereas results obtained by genetic approaches in yeast were consistent with the “domino model”. While increasing the molecular comprehension of the cell cycle machinery it became clear that the two views were not mutually exclusive: Cyclin protein abundances vary throughout the cell cycle determining changes in the activity of cyclin dependent kinases (CDKs); this leads in turn to the oscillation between S-phase and M-phase. Additional molecular components account for feedback mechanisms (usually absent during early embryonic development but present in somatic cells) that impose that major transitions in cyclin-CDK behavior require completion of the events triggered by the precedent cyclin-CDK transition. Therefore, evidence from both traditions has contributed to a unified view of the eukaryotic cell cycle and the elucidation of these mechanisms led to the Nobel prize in Medicine awarded to Tim Hunt, Paul Nurse and Lee Hartwell in 2001.

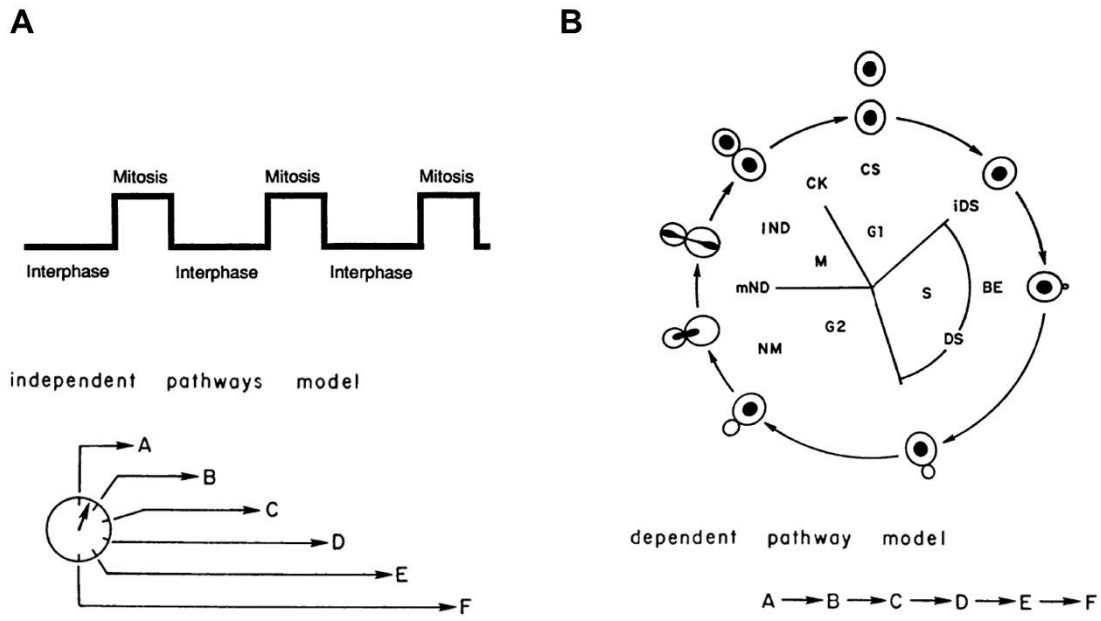

Figure 2. Cell cycle control: clock and dominoes. (A) Research performed utilizing amphibian eggs depicted the cell cycle as the alternation of interphase and mitosis, which is controlled by an autonomous **clock** or oscillator, dictating the timing regardless of the completion of the cyclic events (independent pathways model). **(B)** Research performed utilizing yeasts supported the view that initiation of events of the cell cycle required the completion of the precedent set of events, in a linear pathway (dependent pathway model). Illustrations adapted from (Hartwell et al, 1974; Murray & Kirschner, 1989).

The events of mitosis

Mitosis or nuclear division is the phase of the cell cycle in which sister chromatids (the daughter DNA molecules produced in S phase) are equally segregated to the two daughter cells. Morphologically, mitosis can be divided into distinct phases, each of them involving major structural rearrangements in the dividing cell. Despite the comparatively primitive technology available, Walther Flemming could already in 1882 describe the structural rearrangements typical of a dividing cell (Fig. 3A). Modern technology has majorly improved our ability to image living cells (Fig. 3B) and the various possibilities for genetic manipulation allowed an increasingly detailed molecular understanding of the process of cell division.

In morphological terms, mitosis can be divided into five distinct phases:

Prophase: the interphase **chromatin condenses**. The centrosomes (cellular organelle that serves as the main microtubule organizing center (MTOC), which have been duplicated during S phase, separate and move to opposite side of the nucleus. There, by nucleating MTs, the initiation of spindle assembly occurs.

Prometaphase: nuclear envelope break down (abbreviated NEBD) is completed. Specialized proteinaceous structures assembled at the centromeric regions of both sister chromatids, called kinetochores (KTs), begin establishing contacts with the spindle MTs. Such contacts will contribute to the movement of sister chromatids to the cellular equator, a process known as **chromosome congression**.

Metaphase: sister chromatids have **completed congression**, reaching bipolar attachment, i.e. sister KTs establish stable interactions with MTs emanating from opposite spindle poles.

Anaphase: sister chromatid cohesion is lost and **sister chromatids** are **segregated** to opposite poles of the spindle (anaphase A). With a variable temporal overlap, the spindle elongates and the poles move further apart from each other (anaphase B).

Telophase: chromosomes decondense and the **nuclear membrane reforms** around them.

During late mitotic stages the separation of the cytoplasms, or cytokinesis, is initiated. The contraction of an actin-myosinII-based ring-like structure leads to furrow ingression and the central spindle compacts to form the midbody. Cytokinesis is ultimated by abscission, in which the two cytoplasms are separated resulting in two new genetically identical daughter cells.

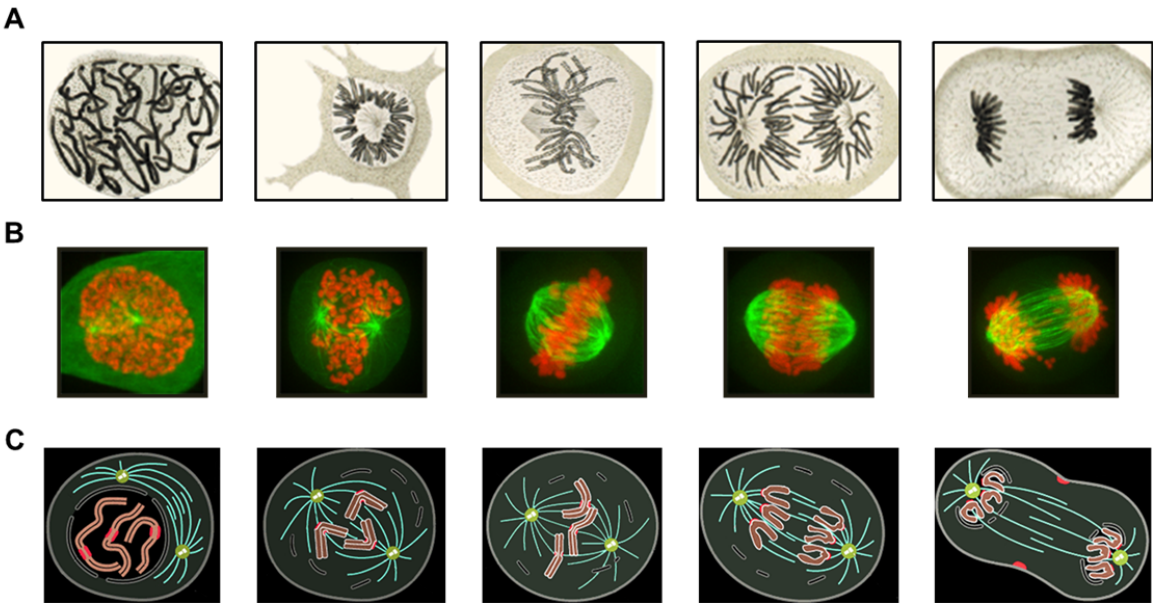

Figure 3 The phases of mitosis. Prophase, prometaphase, metaphase, anaphase and telophase as visualized by Walther Flemming **(A)**, by modern florescence microscopy (MTs labelled in green and the chromatine in red) **(B)** and in a schematic of a modern text book **(C)**. Pictures in (A) were adapted from (Paweletz, 2001), original pictures from (Flemming, 1882). Images in B are courtesy of Dr. Anna Santamaria, whereas schematics depicted in C were adapted from (Morgan, The Cell Cycle. Principles of Control).

The Spindle Assembly Checkpoint (SAC)

The major task of mitosis is to equally segregate the chromosomes to two daughter cells. This task relies on the establishment of productive contacts between sister KTs and spindle MTs emanating from opposite spindle poles, also called bipolar attachment. A quarter of a century ago, the 'search and capture' model laid the foundations for understanding the process of KT-MT attachment (Kirschner & Mitchison, 1986). The model incorporated the newly discovered dynamic instability of MTs to propose that mitotic MTs explore the space and become selectively stabilized once they reach KTs as their targets. Since the process relies on the intrinsically stochastic MT behavior, accomplishment of bipolar attachment for all 46 pairs of sister KTs present in a mitotic human cell can take a variable amount of time. In order to obtain faithful cell

division, eukaryotic cells have evolved a surveillance pathway called spindle assembly checkpoint (SAC), that extends (pro-)metaphase duration until bipolar attachment is completed (Fig. 4). As other cell cycle checkpoints, the SAC is composed of a **sensing system**, monitoring primarily KT-MT attachment, a **signal transduction module** that relays on the attachment status away from KTs in the cellular cytoplasm, and an **effector** that regulates core components of the cell cycle machinery to generate the required delay. The molecular components of the SAC were discovered two decades ago in two independent genetic screens in the budding yeast *S. cerevisiae* (Hoyt et al, 1991; Li & Murray, 1991). They are conserved among eukaryotes and include Mad1, Mad2, Bub1, Bub3, BubR1/Mad3 and Mps1, all localizing to KTs during mitosis in a dynamic fashion (reviewed in Musacchio & Salmon, 2007). The following sections will focus on the detailed description of our current knowledge on this pathway.

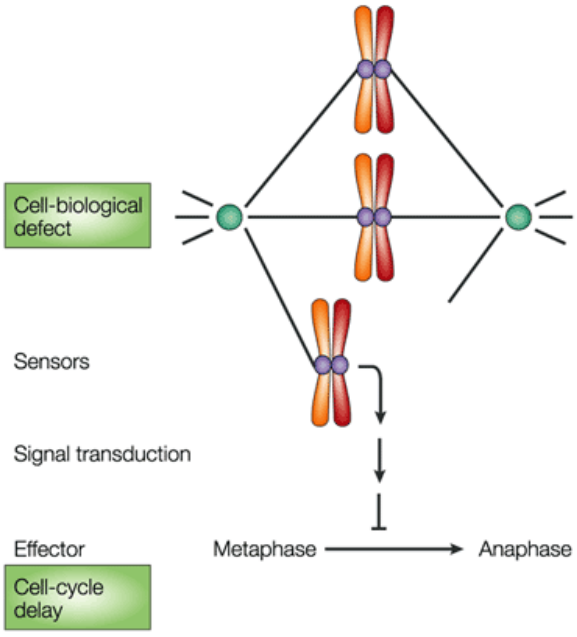

Figure 4 Checkpoint controls (also known as surveillance mechanisms) ensure the dependency of cell-cycle transitions on the completion of earlier events. They consist of three distinct sets of functions: sensors (which look out for defects and emit a signal); signal-transduction cascades (checkpoint signals need to be transmitted throughout the nucleus or cell); and effectors (a target is regulated to delay cell-cycle progression). Illustration adapted from (Musacchio & Hardwick, 2002)

.

The vertebrate centromere/kinetochore region, the SAC sensor

The understanding on how the SAC can sense a proper KT-MT attachment cannot be put aside the detailed comprehension of the structure of KTs themselves. KTs are large protein assemblies built on chromosomal *loci* named centromeres. By electron microscopy, vertebrate KTs appear as trilaminar structures, with electron dense inner and outer KT plates (Fig. 5A) (reviewed in Cleveland et al, 2003). The inner plate contains KT proteins implicated in the creation of an interface with centromeric chromatin. The outer plate contains KT proteins that interact with MTs. A fibrous corona, extending outward from the outer plate, is visible in the absence of MTs and contains MT motors, and components of the spindle checkpoint, such as the Rod-ZW10-Zwilch (RZZ) complex (reviewed in Santaguida & Musacchio, 2009). A conserved hallmark of the centromere–KT interface is a specialized nucleosome containing the histone H3 variant CENP-A (Blower et al, 2002). Regional centromeres such as those in vertebrates contain multiple CENP-A nucleosomes, incorporated at long arrays of repetitive DNA sequences (Allshire & Karpen, 2008). Human centromeres form on a small subdomain of a highly ordered array containing thousands of copies of a 171-bp repeat sequence known as α-I satellite DNA. The α-I satellite DNA contains the CENP-B box, a sequence recognized by the CENP-B protein (Masumoto et al, 1989). CENP-B is required to establish (but not maintain), centromeric chromatin (Okada et al, 2007).

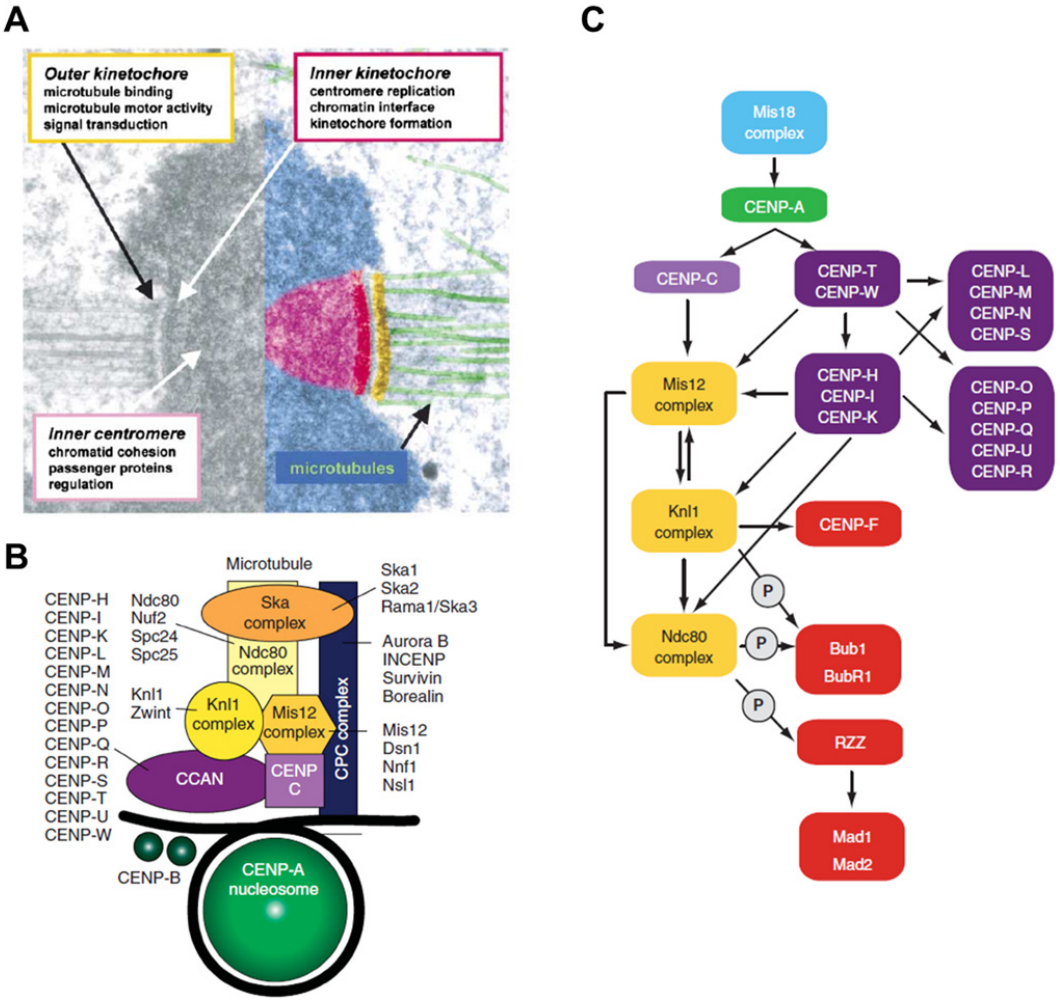

Figure 5. Overall organization of the centromere/KT. (A) A mitotic chromosome has been sectioned along the plane of the spindle axis, revealing the symmetric bipolar organization of a chromosome fully engaged on the spindle. (Right) Key elements have been pseudo colored. Violet, the inner centromere; red, the inner KT and yellow, the outer KT. **(B)** Schematic for the physical map of outer KT of metazoans. **(C)** Non-comprehensive 'epistatic' relationships between KT proteins. Arrows indicate a dependency for localization. The circles enclosing a 'P' indicate post-translational modifications. Illustrations adapted from (Cleveland et al, 2003; Santaguida & Musacchio, 2009).

The fact that α-satellite DNA not strictly required for in centromere specification, indicates the existence of epigenetic mechanisms in the establishment and maintenance of centromere identity (reviewed in Marshall et al, 2008). CENP-A interacts with at least a subset of the subunits of the constitutive centromere-associated network complex (CCAN), the major protein assembly at inner KT (Fig. 5B-C) (reviewed

in Perpelescu & Fukagawa, 2011). The molecular connection between inner and outer KT is unknown, but recent evidence suggests that Cenp-C might fulfill this duty, binding both the Cenp-A nucleosome and the major outer KT protein assembly, the KMN network (Screpanti et al, 2011). The KMN network has emerged as crucial component of the KT machinery involved in generating load-bearing MT-attachment. It is a conserved 10-subunit assembly composed of three distinct subcomplexes, known as Knl1, Mis12, and Ndc80 (acronym KMN). A growing body of evidence circumstantiates the notion that several KMN components establish direct contact with MTs allowing the establishment of load bearing attachments that can couple MT depolimerization with chromosome movement during anaphase (Cheeseman & Desai, 2008; Santaguida & Musacchio, 2009). Interestingly, RNAi mediated depletion of KMN components does not only lead to a KT-null phenotype but compromises also the SAC functionality (Cheeseman et al, 2004; DeLuca et al, 2005; Martin-Lluesma et al, 2002; McCleland et al, 2003; Meraldi et al, 2004). This suggests in turn that the same machinery responsible for the establishment for of correct attachment is required for building the SAC signaling platform itself.

Whereas only weak evidence for direct interactions between KMN components and the SAC components Mad1/Mad2 has been produced (Kops et al, 2010; Martin-Lluesma et al, 2002), it is clear that KT recruitment of Mad1/Mad2 depends on the KMN network (Fig. 5C) (Martin-Lluesma et al, 2002; McCleland et al, 2003; Meraldi et al, 2004). Mad1/Mad2 recruitment to KTs is an evolutionarily conserved event that intimately correlates with SAC signaling. Moreover, Mis12 is required for KT recruitment

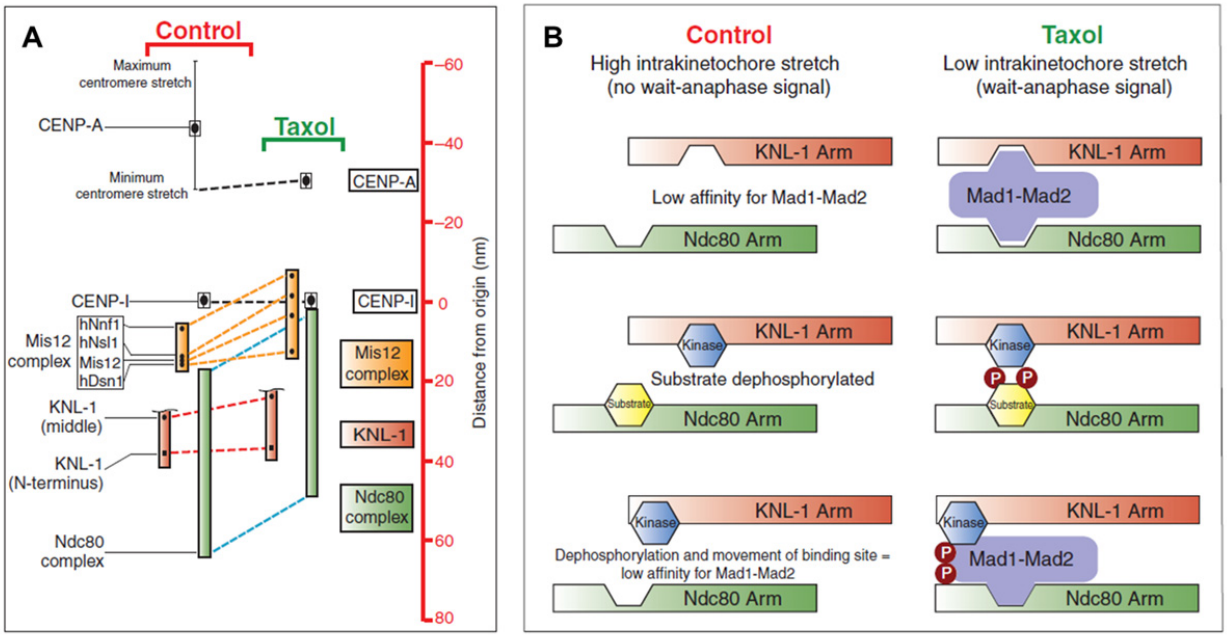

Figure 6. Relative movements of mechanical elements within KTs and their impact on SAC signaling. (A) High-resolution map of the KT reveals two mechanical arms within the KT (KNL-1 arm and Ndc80 arm) that move relative to each other in the presence or absence of MT-mediated intra-KT stretch (Control and Taxol, respectively) (Wan et al, 2009). **(B)** The geometrical arrangement of the two arms could affect SAC signaling by regulating the localization and/or phosphorylation of checkpoint components. Illustration adapted from (Maresca & Salmon, 2010).

of one additional metazoan specific ternary complex, called RZZ that is also required for Mad1/Mad2 KT recruitment (Kops et al, 2005). These data suggest that the KMN network is not sufficient for Mad1/Mad2 binding in higher cells and there is an additional requirement for the RZZ complex. In normal circumstances KTs bind either MTs or Mad1/Mad2 and the KMN network accounts for both interaction, suggesting a simple model in which KMN components bind either MTs or Mad1/Mad2 in a mutually exclusive fashion due to steric hindrance (discussed in Burke & Stukenberg, 2008). However, recent studies have demonstrated that KT-MT attachment triggers a KT structural deformation leading to intra KMN stretch that intimately correlates with SAC activation and Mad1/Mad2 KT recruitment (reviewed in Maresca & Salmon, 2010) (Fig.

6A). It is therefore likely that the KT (and particularly KMN) structural deformation triggers the relative movement of KT-components, possibly moving apart proteins that would otherwise contribute to the generation of the Mad1/Mad2 KT receptor (Fig. 6B).

Finally, recent studies have demonstrated that manipulation of the SAC kinase Mps1 at KTs can uncouple KT-MT attachment from the removal of Mad1/Mad2 from KTs (Jelluma et al, 2010; Kemmler et al, 2009), challenging therefore the notion of mutual exclusivity and suggesting that Mps1 participates in promoting the binding of Mad1/Mad2 to KTs by phosphorylating Mad1 itself and/or KMN components (Fig. 6B).

The anaphase promoting complex or cyclosome, the SAC target

Cyclin protein abundances vary throughout the cell cycle, determining changes in the activity of cyclin dependent kinases (CDKs) and therefore driving the alternation of S and M phase. States of low and high CDK activities are imposed by a cullin-RING finger E3 ubiquitin ligase, called anaphase promoting complex or cyclosome (APC/C), that targets cyclins for 26S proteasomal degradation. The APC/C is composed of 15-17 subunits, depending on the organism, most of which have been conserved through eukaryotic evolution (reviewed in Peters, 2006; Pines, 2011). The APC/C can be subdivided into two subcomplexes, one made of the catalytic subunit APC2 (homologous to cullin) and APC11 (the RING-finger protein), the other one made of several proteins containing tetratricopeptide repeats (TPRs) that serve as binding sites for establishing protein-protein interactions. The two subcomplexes are held together by the largest subunit, APC1 (Fig. 7A). APC/C dependent ubiquitination requires the presence of one WD40 repeat containing activator, either Cdc20 or Cdh1. Structural and biochemical data suggest that both the APC/C subunit APC10 together with Cdh1 confer substrate specificity by forming the receptor for one type destruction signals

present in substrates (the so called D-boxes) (Buschhorn et al, 2011; da Fonseca et al, 2011) (Fig. 7A-B). Biochemical evidence supports the notion that Cdc20 binds the APC/C to form a D-box degron receptor similarly to Cdh1 (Izawa & Pines, 2011), but structural evidence is missing.

The APC/C is responsible for degradation of a variety of cell cycle regulators that has to occur in a tightly controlled fashion (Fig. 7C). Unlike other E3 ligases that recognize their substrates only following pre-phosphorylation by regulatory kinases, the APC/C recognizes the vast majority of its substrates regardless of their phosphorylation status. This implicates that the APC/C activity itself is cell cycle regulated and that its substrate specificity changes throughout the cell cycle (Fig. 7C). Before mitotic entry, the APC/C is devoid of Cdk1 dependent phosphorylation that is triggered upon NEBD (Kraft et al, 2003). Mitotic Cdk1 firing will on one hand promote the association between the APC/C and its activator Cdc20 (Kraft et al, 2003; Rudner & Murray, 2000) and on the other hand functionally neutralize the other APC/C activator, Cdh1 (Cross, 2003).

Whereas APC/C^{Cdc20} dependent degradation of Cyclin A (and Nek2a) commences upon NEBD, the SAC imposes a delay in the poly-ubiquitination of the APC/C^{Cdc20} crucial substrates such as Cyclin B1 and Securin, coupling therefore chromosome bi-orientation with anaphase onset (Di Fiore & Pines, 2010; reviewed in Pines, 2011). The target of the SAC is Cdc20 and several SAC proteins associates with it in a cytoplasmic quaternary complex comprising Cdc20 itself, Mad2, BubR1 and Bub3, also called mitotic checkpoint complex (MCC)(Sudakin et al, 2001). Both Mad2 and BubR1 can bind Cdc20 directly and inhibit the APC^{Cdc20} *in vitro* (Fang, 2002; Fang et al, 1998; Tang et al, 2001), but recent evidence suggests that, upon SAC activation,

Mad2 binds Cdc20 first, thereby priming it for subsequent binding of BubR1:Bub3 (Kulukian et al, 2009; Nilsson et al, 2008). How can the latter complex prevent Cyclin B1 and Securin degradation is an active field of investigation and two models have been recently proposed: BubR1 (or Mad3 in *S. cerevisiae*) can on one hand act as a pseudosubstrate inhibitor of APC/C^{Cdc20} (Burton & Solomon, 2007) and on the other hand promote Cdc20 degradative autoubiquitination by the APC/C during SAC signaling, reducing therefore the APC/C^{Cdc20} activity towards other substrates (King et al, 2007; Nilsson et al, 2008; Pan & Chen, 2004). However, the role of Cdc20 autoubiquitination is controversial since other studies have proposed that it is required for MCC disassembly upon SAC silencing at metaphase (Reddy et al, 2007; Stegmeier et al, 2007). Whether these possibilities are mutually exclusive will have to be clarified, but recent evidence suggests that different MCC pools (bound and unbound to the APC/C) display differential dependencies on proteolysis for their disassembly (Ma & Poon, 2011), suggesting that degradative and non degradative ubiquitination might co-exist in the cell. Degradative ubiquitination of Cdc20 by the APC/C depends on the SAC and is crucial for cell cycle arrest. SAC dependent Cdc20 degradation requires the APC/C subunit APC15, that is otherwise dispensable for APC/C activity in the absence of the checkpoint (Mansfeld et al, 2011).

How the SAC directs the APC/C activity towards a subset of substrates while inhibiting degradation of others is only beginning to emerge. Recent evidence suggests that incorporation of Cdc20 into the MCC forces it to associate with a specific APC/C subunit during prometaphase (APC8). When the SAC is silenced in metaphase the Cdc20 association with the APC/C will also require APC3 (Izawa & Pines, 2011).

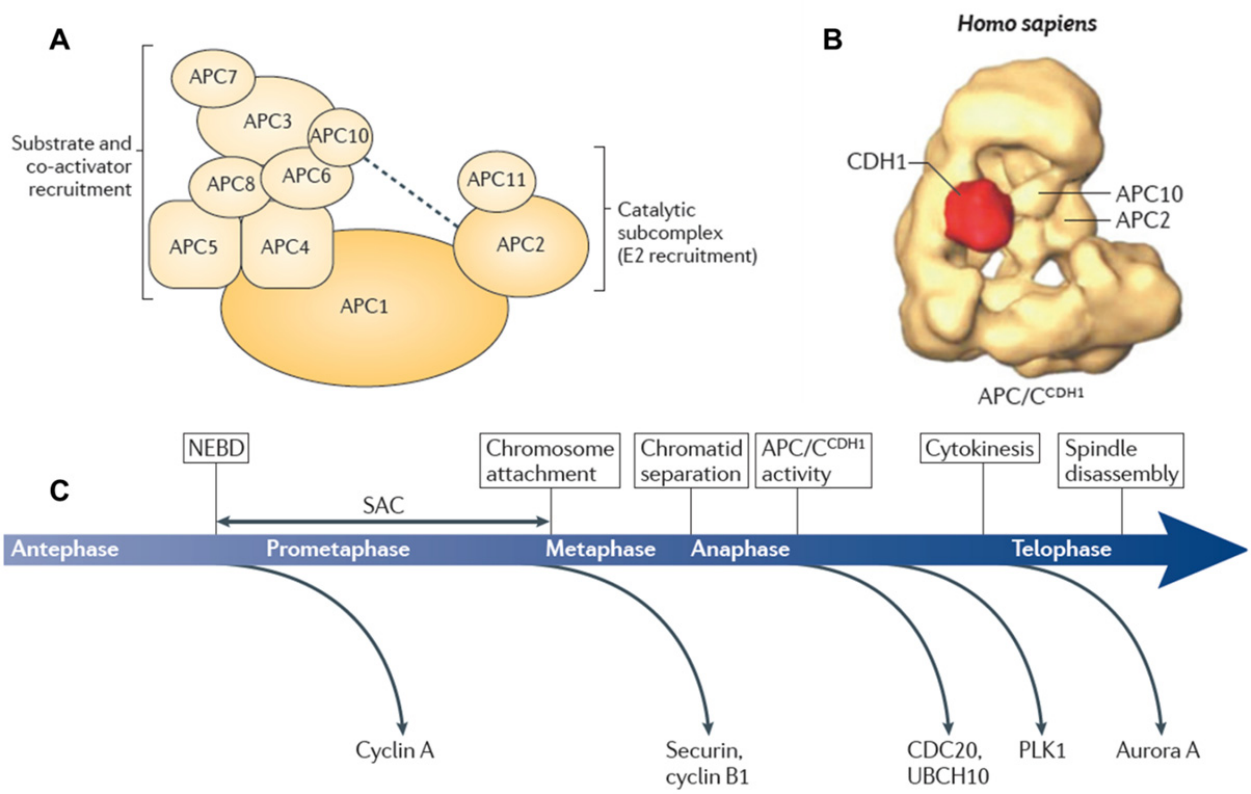

Figure 7. APC/C structure and function. (A) Schematic of the APC/C subunits. The APC/C can be subdivided in two subcomplexes that are connected by a scaffolding subunit (APC1). One subcomplex is catalytic and comprises APC2 and APC11 (which recruit the E2). The other subcomplex is composed of tetratricopeptide repeat (TPR)-containing proteins (APC3, APC6, APC7 and APC8) and binds substrates, APC10 and the co-activator (Cdc20 or Cdh1). APC10 seems to interact with both APC3 and APC2 (indicated by a dashed line). **(B)** Structure of the human APC/Cs derived from an electron microscopy single particle three-dimensional reconstruction study (Buschhorn et al, 2011). The APC/C appears as a pyramidal shape, with a central cavity in which the co-activator, Cdc20 or Cdh1, binds next to the APC10 subunit to form the destruction box (D box) degron receptor. **(C)** As cells progress through mitosis, specific proteins are degraded at distinct time points; these are depicted below the arrow. The timing of their destruction is determined by their sensitivity to the SAC (Cyclin A vs. Securin and Cyclin B1) and by whether they can be recognized before (Cyclin A, Securin and Cyclin B1) or after anaphase (Cdc20, UBCH10, Plk1 and Aurora A). Illustrations adapted from (Pines, 2011).

The Mad2 template model for SAC signaling and silencing

While the SAC control of the APC/C substrate specificity awaits structural clarification, our understanding of the role of Mad2 in SAC signaling has greatly benefited from structural analysis (Luo et al, 2002; Luo et al, 2004; Mapelli et al, 2007; Sironi et al, 2002). The Mad2 protein can in fact adopt two distinct natively folded states: "Open" (or "N1") and "Closed" (or "N2") (O and C-Mad2, respectively). The two conformers differ in the orientation of a C-terminal beta-sheet that in the Closed conformation surrounds the polypeptide chain of a Mad2-interaction partner (or "ligand") in a structure reminiscent of a safety belt (Sironi et al, 2002) (Fig. 8A). Best-known ligands of Closed-Mad2 are Mad1 (a SAC component) and Cdc20 (the SAC target). Mad1 is crucial for KT recruitment of Mad2, whereas Cdc20 is a cytoplasmic Mad2 target upon SAC activation. A prevailing model for SAC signaling, the so-called 'template model', can readily explain how Mad2 can relay a signal from the KT to APC/C^{Cdc20} in the cytoplasm. Central to the model is the ability of Mad2 to dimerize asymmetrically, i.e. O-Mad2 can bind C-Mad2 (Fig. 8B) (De Antoni et al, 2005; Mapelli et al, 2006; Mapelli et al, 2007). Moreover, reconstitution experiments have shown that a complex of Mad1:C-Mad2 can, through Mad2 asymmetric dimerization, enhance the ability of O-Mad2 to bind Cdc20, thereby generating a structurally equivalent C-Mad2:Cdc20 complex (De Antoni et al, 2005; Kulukian et al, 2009; Lad et al, 2009; Nasmyth, 2005; Vink et al, 2006), utilizing a prion-like mechanism of propagation of the closed conformer of Mad2 (Skinner et al, 2008) (Fig. 8C). Some aspects of this template model find experimental support also in the cellular environment: Mad1 clearly is the KT receptor of Mad2 (Chen et al, 1998; Luo et al, 2002; Martin-Lluesma et al, 2002) and interfering with Mad1 affects the ability of Mad2 to bind Cdc20 (Fraschini et al, 2001;

Hardwick et al, 2000; Hwang et al, 1998). Furthermore, FRAP experiments performed in mammalian cells revealed a biphasic recovery after photobleaching of KT-associated Mad2, indicating the existence of two distinct Mad2 populations (Shah et al, 2004). While one population showed a slow turnover reminiscent of the recovery kinetics of Mad1 (Shah et al, 2004), the other Mad2 population turned over much faster, similar to the behavior of Cdc20 at KTs (Howell et al, 2004). The template model has been supported by several lines of evidence, but direct experimental proof for its operation within cells was lacking.

Chromosome bi-orientation leads to SAC silencing and this in turn allows anaphase onset. While several pathways involved in SAC silencing have been described, two are thought to be crucial in mammalian cells. The first is based on the dynein dependent “stripping” from KTs of SAC components and other proteins, notably Spindly, upon MT attachment (Gassmann et al, 2010; Howell et al, 2001). This pathway accounts for the removal of the KT source of SAC signaling, but does not contribute directly to the disassembly of cytoplasmic complexes that should be rapidly promoted upon SAC inactivation. The second pathway is based on a binding partner of Mad2, known as p31comet, which associates selectively with the dimerization interface of C-Mad2 *in vitro*, suggesting that p31comet might act as a competitive inhibitor for Mad2 dimerization (Mapelli et al, 2007; Xia et al, 2004; Yang et al, 2007) (Fig. 8D). Depletion of p31comet from cells interferes with efficient recovery from a SAC dependent arrest and extends the duration of unperturbed mitosis (delaying the cytoplasmic disassembly of the MCC), whereas overexpression of p31comet causes a SAC override (Habu et al, 2002; Jia et al, 2011; Xia et al, 2004; Yang et al, 2007). Although these data strongly

implicate p31comet in SAC silencing, it is unknown how the p31comet:Mad2 interaction is regulated in time and space *in vivo*.

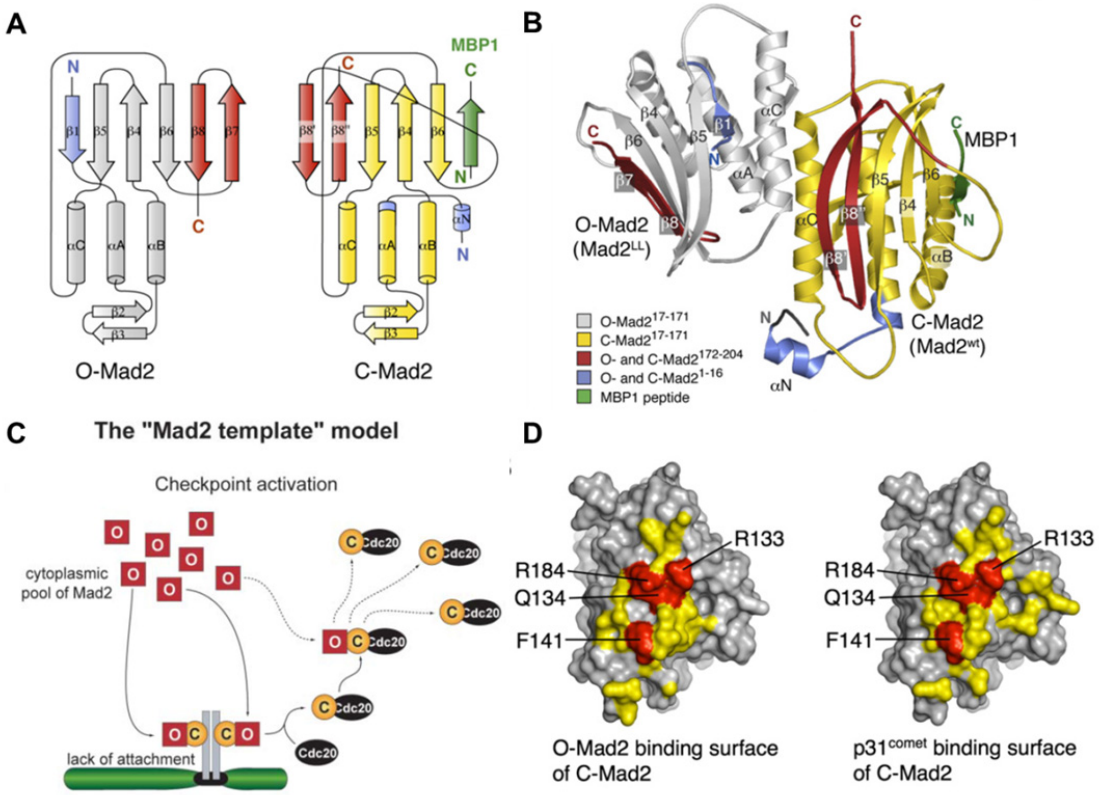

Figure 8. The Mad2 'template model' for SAC signaling. (A) Topology diagram of O-Mad2 and C-Mad2. In C-Mad2, the two strands β8'–β8'' are extensions in opposite directions of the β8 strand of O-Mad2. MBP1 = 12-residue Mad2 binding peptide 1. **(B)** Ribbon model of the Mad2 conformational dimer composed of $Mad2^{LL}$ (loop less, adopting the open conformation) and $Mad2^{wt}$–MBP1 (C-Mad2 binding MBP1) according to the crystal structure of the complex. **(C)** The Mad2 'template model': encounter of O-Mad2 with C-Mad2 bound to Mad1 starts the SAC. The Mad1/Mad2 core complex recruits O-Mad2 to KTs, and O-Mad2 is converted into C-Mad2 bound to Cdc20. Mad2/Cdc20 is a structural copy of Mad1/Mad2 because Mad1 and Cdc20 share a Mad2 binding motif and Mad2 adopts the same C-Mad2 conformation in these complexes. The C-Mad2/Cdc20 complex dissociates from the Mad1/Mad2 core complex. In the cytosol, Mad2/Cdc20 acts as a structural equivalent of Mad1/Mad2 to convert more O-Mad2 into Cdc20 bound C-Mad2. Signal amplification occurs because Mad2/Cdc20 converts O-Mad2 to Cdc20 bound C-Mad2. **(D)** A surface representation to show that C-Mad2 uses a similar surface for the binding of p31comet or O-Mad2. The p31comet-binding residues of C-Mad2 are colored yellow, and the four key interacting residues, R133, Q134, R184 and F141, are colored red. The O-Mad2-binding residues of C-Mad2 are colored yellow. The same four residues R133, Q134, R184, and F141 (red) that are important for p31comet binding are also involved in O-Mad2 binding. Illustrations adapted from (De Antoni et al, 2005; Mapelli et al, 2007; Yang et al, 2007).

Control of mitotic timing, clock or domino?

The circumstances in which SAC genes were discovered in *S. cerevisiae* defined their pathway as a genuine checkpoint: a non-essential surveillance mechanism that becomes active (and crucial) only upon malfunctions (Hoyt et al, 1991; Li & Murray, 1991). Later work has shown that the SAC genes are conserved in mammals, clarifying that they exert a similar checkpoint function (see for example Jin et al, 1998; Li & Benezra, 1996). Careful live cell imaging combined with antibody microinjection showed that functional neutralization of Mad2 and BubR1 in mammalian cells triggers a drastic anticipation of anaphase onset when compared to cells traversing mitosis in the absence of spindle defects (Gorbsky et al, 1998; Shannon et al, 2002). This suggested in turn that the SAC in mammals is more crucial than other checkpoints, as it becomes activated every cell cycle and contributes to the timing, and therefore faithful chromosome segregation, in all somatic cell divisions. Consistent with this idea, homozygous deletions of several SAC genes are embryonic lethal in mice (Dobles et al, 2000; Iwanaga et al, 2007; Wang et al, 2004). One explanation for the observed divergence between the SAC function in yeast and human might be extrinsic to the SAC signaling itself but rather depend on differences in KT-MT attachment. In other words, unattached KTs that are physiologically arising in every mammalian prometaphase might rarely occur in yeast, due to the fact that KT-MT attachment is established prior to mitotic entry in this organism. Consistent with this notion, Mad1 and Mad2 localize to KTs in every mammalian prometaphase, whereas the same localization is observed only upon spindle damage in budding yeast (Gillett et al, 2004). This view also readily explains observations made in flies, where KT-MT attachments are achieved very rapidly and the SAC is not essential for viability and fertility (Buffin et al, 2007). In this

perspective, the SAC remains a genuine checkpoint -or domino- with a sensor, a signal transduction cascade and an effector, but with the peculiarity that the 'defect' being sensed (unattached KTs) arises physiologically every cell cycle in certain organisms. This simple view has been challenged by one study that characterized the phenotypes of siRNA-mediated depletions of SAC components in human somatic cells (Meraldi et al, 2004). This study showed that siRNA of all SAC components tested (Mad1, Mad2, Bub3 and BubR1) compromised the ability of the cells to respond to spindle disruption by nocodazole, but only depletion of a subset of the same SAC components (Mad2 and BubR1), could trigger an acceleration of the traverse of mitosis. Importantly, depletions of Mad1 and Bub3 were shown to be sufficient to delocalize Mad2 and BubR1 from KTs, respectively, but this was nevertheless not sufficient to trigger the mitotic acceleration observed upon Mad2 and BubR1 direct depletion. This prompted Meraldi and colleagues to propose that Mad2 and BubR1 control mitotic timing independently of their KT localization and therefore the SAC. In this perspective, Mad2 and BubR1 would be part, in addtion to their contribution to the SAC, of a timer mechanism -or clock-, that acts in the cytoplasm.

The timer function of Mad2 does not readily find a mechanistic explanation in the template model, but the fact that Mad2 could influence the timing of Cyclin B1 degradation independently of Mad1 suggests that cytoplasmic O-Mad2 can form a C-Mad2:Cdc20 complex in a non-catalyzed fashion.

The nuclear envelope and the control of cell division

During mitosis the cell undergoes major structural rearrangements. Among the structures affected, the nuclear envelope (NE) is of special importance as it constitutes the defining boundary between the nuclear components and the cytoplasm. The NE can

be seen as an extended sheet of the endoplasmic reticulum that covers the chromatin. It is formed by two juxtaposed membranes, the outer and inner nuclear membrane. The NE surrounds the chromatin but does not form a continuous isolating layer since the outer and the inner membrane fuse forming holes that are occupied by large protein assemblies, called nuclear pore complexes (NPCs, Fig. 9A). NPCs serve as both molecular sieves and transport hubs during interphase. Higher eukaryotes undergoing an open mitosis form a cytoplasmic mitotic spindle, which requires NEBD to allow access of spindle MTs to KTs. NEBD not only involves the removal of NE membranes, but also the disassembly of large protein complexes, such as NPCs and the network of intermediate filament that composes the lamina (reviewed in Guttinger et al, 2009). An initial event of NEBD is the dispersal of soluble nucleoporins, many of which are released from the NE as mitotically stable nucleoporin subcomplexes. NPC disassembly occurs within minutes and affects multiple nucleoporins synchronously, with the exception of Nup98 that dissociates from NE slightly before other components (Dultz et al, 2008). NE disassembly continues with the lamina depolymerization. NPC disassembly and lamina depolymerization depend on the activation of mitotic kinases, which directly contribute to the phosphorylation of NE proteins, with CDK1 displaying a major role in NEBD (Heald & McKeon, 1990; Peter et al, 1991). Furthermore, CDK1 might also be directly involved in NPC disassembly as many nucleoporins are phosphorylated on CDK1 sites during mitosis, but additional kinases are known to contribute to NEBD in various species, including protein kinase C (PKC) (Goss et al, 1994), Aurora A (Hachet et al, 2007; Portier et al, 2007), NIMA-related kinases (Laurell et al, 2011) and polo like kinase 1 (PlK1). Particularly, a lack of PlK1 activity delays

NEBD in *C. elegans* and human somatic cells (Chase et al, 2000; Lenart et al, 2007) and a phosphoproteomic screen has recently identified several nucleoporins as likely Plk1 substrates (Santamaria et al, 2010).

Although the NE does not exist as a functional unit during mitosis, some of its components have key roles in the regulation of different mitotic processes after NEBD. Such processes include 1) spindle formation, 2) KT-MT attachment, 3) direct regulation of the APC/C and 4) indirect regulation of the APC/C through the SAC (reviewed in Guttinger et al, 2009). One nucleoporin that has been implicated in spindle assembly is RNA export 1 (RAE1). RAE1 forms a complex with NuP98. In mitosis, RAE1 binds to MTs and is required for spindle formation *in vitro* and *in vivo* (Blower et al, 2005). In addition, RAE1 has been shown to share sequence homology with the SAC protein Bub3 and *Rae1*$^{+/-}$ mice were shown to be unable to arrest in mitosis after the induction of spindle damage (Babu et al, 2003). Furthermore RAE1, in complex with its partner NuP98, interacts with a Cdh1-associated fraction of APC/C during prometaphase (Jeganathan et al, 2005), possibly playing an additional role in APC/C^{Cdh1} inhibition, beside CDK1 direct phosphorylation. Conversely, the NuP107-160 complex has a prominent role at KTs, where it promotes stable KT-MT attachment and recruits additional nucleoporins.

Interestingly, the SAC proteins Mad1 and Mad2 localize to the nuclear envelope during interphase in various organisms including *S. cerevisiae*, *A. nidulas*, *D. melanogaster* and humans, strongly suggesting that this localization pattern has been conserved throughout eukaryotic evolution. The recruitment of Mad1/Mad2 to the NE depends on direct interactions between Mad1 (and Mad2 in humans) with the

nucleoporin Mlp/Megator/Tpr in fungi/flies/humans, respectively (hereafter referred exclusively as Tpr) (De Souza et al, 2009; Iouk et al, 2002; Lee et al, 2008; Lince-Faria et al, 2009; Scott et al, 2005). Tpr is the architectural element of the nucleoplamic basket of NPCs (Krull et al, 2004) (Fig. 9B). Whether the association of Mad1/Mad2 with Tpr at NPCs induces a functionally inactivated state of the SAC components has not been tested, but it became recently clear that depletion of Tpr compromizes the SAC functionality in mitosis of all organisms analyzed (De Souza et al, 2009; Iouk et al, 2002; Lee et al, 2008; Lince-Faria et al, 2009; Scott et al, 2005). Whereas biochemical approaches showed that the interaction between Mad1/Mad2 and Tpr is maintained throughout mitosis, the localization of Tpr to KTs positive for Mad1/Mad2 remains controversial for human cells (Lee et al, 2008; Lince-Faria et al, 2009). Therefore, the mitotic action of Tpr could be exerted at KTs or in the form of soluble cytoplasmic component in human cells (Lee et al, 2008; Lince-Faria et al, 2009), in the context of a spindle associated 'matrix' in fly cells (Lince-Faria et al, 2009) or at the level of the intact NPCs proximal to KTs in fungi undergoing a closed mitosis (De Souza et al, 2009; Iouk et al, 2002; Scott et al, 2005). One alternative option that has not yet been emphasized in the literature is that Tpr might act during prophase by initiating the SAC at NPCs, prior to the re-localization of SAC components to KTs. To this end, the mitotic kinases as Mps1 and Plk1 also localize at the NE during prophase (Tighe et al, 2008; A. Santamaria, unpublished) and both Tpr and Mad1 are likely to be substrates of both kinases (Santamaria et al, 2010; C. von Schubert, A. Baron and A. Santamaria, unpublished), suggesting therefore that Tpr might serve as a scaffold at NPCs, promoting phosphorylation of SAC components required for their KT function.

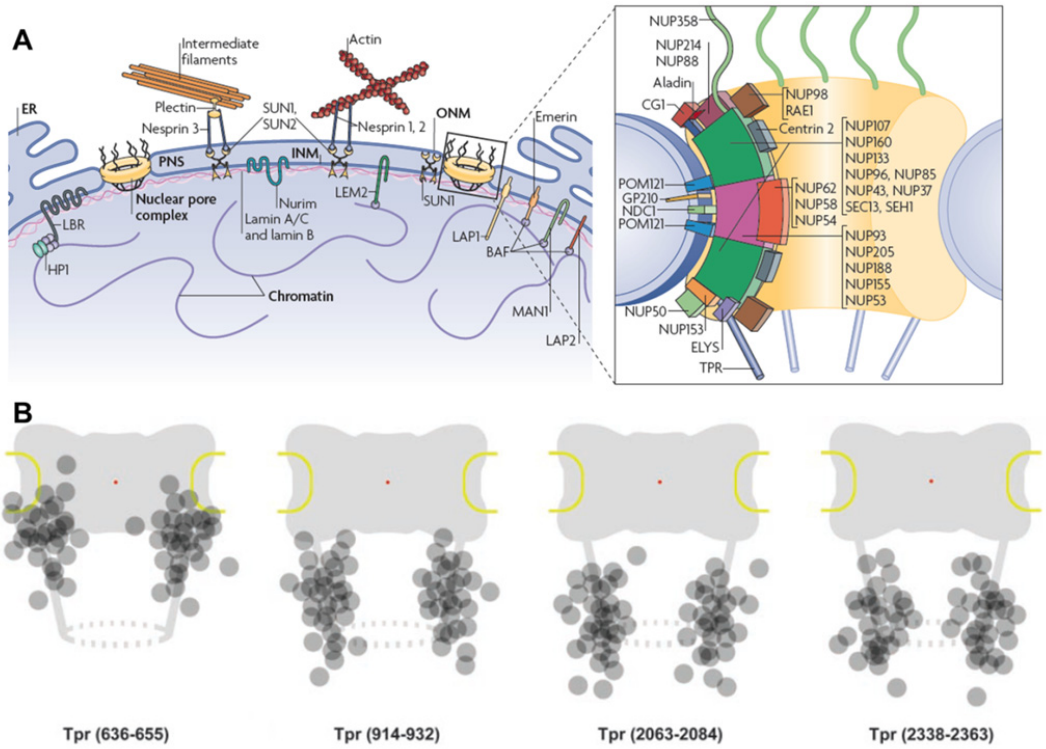

Figure 9 Structural features of the nuclear envelope and Tpr as architectural element of the NPC basket. (A) The inner and outer nuclear membranes (INM and ONM, respectively) are separated by the perinuclear space (PNS). The nuclear lamina underlies the nucleoplasmic face of the INM. INM proteins link the nuclear envelope (NE) membrane to chromatin and the lamina, whereas ONM proteins provide a connection from the nucleus to the cytoskeleton. NPCs are large macromolecular assemblies of 60–120 MDa that display eight‐fold rotational symmetry. They are built from ~30 different proteins, termed nucleoporins (Nups). Major architectural features of the NPC are cytoplasmic filaments and the nuclear basket. Illustration adapted from (Guttinger et al, 2009) **(B)** Evidence for Tpr constituting the central architectural element that forms the scaffold of the nuclear basket: distributions of gold grains relative to NPCs after immunogold labeling of different Tpr domains, as displayed in (Krull et al, 2004).

Aim

The Mad2 template model is supported by several lines of evidence, but direct experimental proof for its operation within cells was lacking. Although the model is central for our current understanding of the SAC signaling and is strongly supported by structural data (Luo & Yu, 2008; Mapelli & Musacchio, 2007), the lack of tools to discriminate between O-Mad2 and C-Mad2 has so far precluded the analysis of Mad2 conformation in a cellular context. Furthermore, some observations, particularly the purported Mad1-independent function of Mad2 in regulating mitotic timing (Meraldi et al, 2004), do not readily find a mechanistic explanation in the template model.

The general aim of this work has been to gather mechanistic insight on the action of Mad2 and on its regulation in the cellular context. To this end, we characterized a monoclonal antibody (mAb) raised against human Mad2 and demonstrate that it specifically recognizes the dimerization interface of the closed conformer of Mad2. This afforded a unique opportunity to test the template model in the cellular context. Specifically, we asked 1) whether Mad2 adopts two conformations in the cell, the open conformation for Mad2 devoid of ligands and the closed conformation when associated to those proteins, 2) whether the Mad2 template activity is controlled by the regulated 'capping' of C-Mad2 by p31comet, and 3) whether the conformational dimerization of Mad2 is required for SAC signaling. Furthermore, the combined used of mAbs recognizing Mad1 and C-Mad2 in microinjection experiments allowed us to test the controversial notion that Mad2 controls mitotic timing in the cytoplasm independently of Mad1 and the SAC. Finally, we aimed to shed mechanistic light on the action of

emerging regulators of Mad1:C-Mad2 activity at KTs, namely the kinases Mps1, Plk1 and the nucleoporin Tpr.

Results

Generation and characterization of antibodies to Mad1, p31comet and Mad2

With the aim of better defining the role of Mad1, Mad2 and p31comet in the SAC signaling of human cells, several antibodies recognizing specifically these key signaling molecules were generated. The availability of these reagents together with their detailed characterization reported below resulted in a toolbox for the study of the checkpoint signaling and constitutes the foundation of this thesis.

Mad1

To generate monoclonal antibodies to human Mad1, full length MBP (Maltose Binding Protein)-tagged Mad1 was expressed and purified from *E. coli* and used for immunization (see methods). Screening of positive supernatants of hybridoma clones performed by ELISA led to the identification of two clones producing antibodies reacting against the antigen, 117-468(-18) and 117-470(-19). The purified antibodies were further characterized, leading to a complementary and non-overlapping spectrum of functionality throughout the assays tested (Table 1), strongly suggesting that 117-468 recognizes a conformational epitope, whereas 117-470 recognizes a linear epitope. Use of a twelve-mere peptide array encompassing the entire sequence of human Mad1

Clone	Western blot	Linear epitope identified	Native immunoprecipitation	Immunofluorescence (formaldehyde)	Neutralizing in microinjection
117-468	No	No	Yes	Yes	Yes
117-470	Yes	Yes	No	No	No

Table 1. **Summary of the characterization of the two Mad1 mAbs used throughout this thesis.** The functionality of each clone is reported in several assays. One clone (117-468) was functional in assays that retained the three dimensional structure of the antigen and not functional on assays that compromised it, whereas the other clone (117-470) displayed the opposite behavior.

failed to reveal reactivity of 117-468 (consistent with its recognition of a conformational epitope), whereas 117-470 recognized two partly overlapping peptides, leading to the identification of the octamer Mad1$^{29\text{-}36}$ as the epitope of this mAb (Fig. 10).

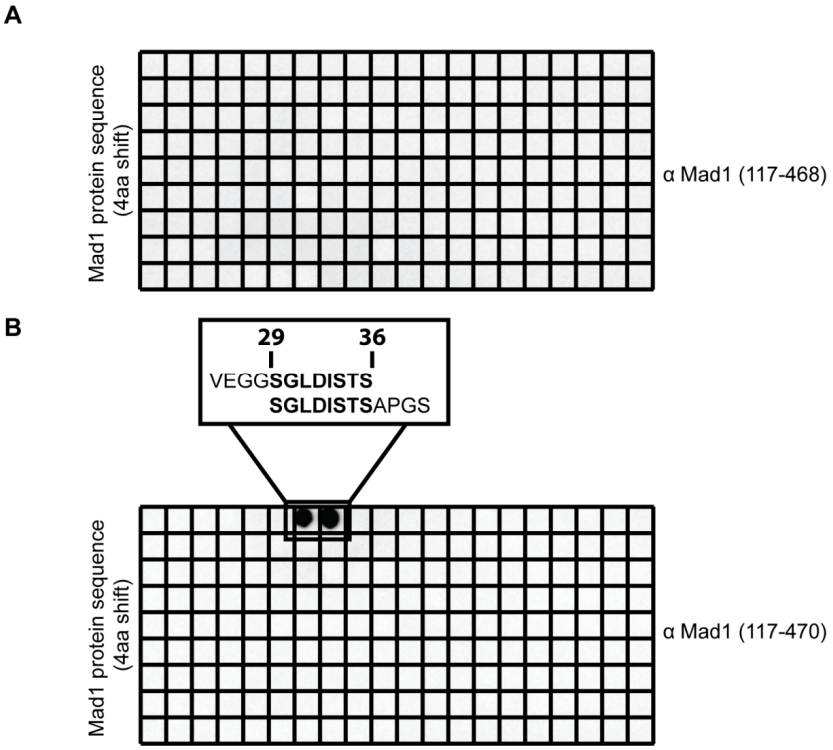

Figure 10. Epitope mapping of 117-470. A total of 178 12-mer peptides encompassing the entire Mad1 protein sequence (718 amino acids) with a 4 amino acid shift were spotted on nitrocellulose membranes in duplicates. Peptide arrays were constructed using standard F-moc chemistry on a MultiPep robotic spotter according to the manufacturer's directions (Intavis). Membranes were analyzed by Western blot with 117-468 **(A)** and 117-470 **(B)**. The reactivity of 117-470 towards two consecutive peptides (sequences are reported in the rectangle) highlights the SGLDISTS octamer (residues 29-36 of Mad1) as the minimal protein sequence sufficient for mAb recognition.

Mad1 structure comprises an extended coiled coil domain (aa 48-630) responsible for homodimerization that is just interrupted by an unstructured loop including the Mad2 binding motif (aa 531-549) and a C-terminal domain (aa 631-718) that should fold as a stable globular entity according to its resistance to limited proteolysis (Iwanaga et al, 2002; Sironi et al, 2002) (Fig. 11A). The conformational epitope of 117-468 within Mad1 could therefore arise at the level of the quaternary

structure within the coiled coil domain or within the tertiary structure of the C-terminal globular domain of the antigen. To discriminate between these possibilities, we overexpressed Myc-tagged truncations of Mad1 in HEK293T cells and assessed their ability to be immunoprecipitated by 117-468 (Fig. 11B). The results obtained are consistent with the notion that 117-468 recognizes a conformational epitope within the C-terminal globular domain of Mad1. Importantly, this domain includes determinants that are conserved from yeast to human and that are strictly required for Mad1 function in budding yeast (Chen et al, 1999; Sironi et al, 2002), consistent with the neutralizing power of this mAb in microinjection experiments (Table 1 and see below).

p31comet

To generate polyclonal antibodies to human p31comet, His-tagged full length human p31comet was expressed and purified from *E. coli* and used for immunization (see methods). Serum obtained from one rabbit (# 741212) was functional in Western blot and immunoprecipitation experiments, but could not recognize endogenous p31comet in immunofluorescence experiments (Fig. 12 and data not shown).

Mad2

To generate monoclonal antibodies to human Mad2, full length GST-tagged Mad1 was expressed and purified from *E. coli* and used for immunization (see methods). Screening of positive supernatants of hybridoma clones performed by ELISA led to the identification of one clone producing antibody reacting with the antigen, 107-276(-3). The purified antibody was characterized by immunofluorescence, microinjection, immunoprecipitation, Western blot and peptide binding experiments, displaying functionality exclusively in assays that retain the three dimensional structure of the

antigen (Fig. 13). This strongly suggested that 107-276 recognizes a conformational epitope on Mad2.

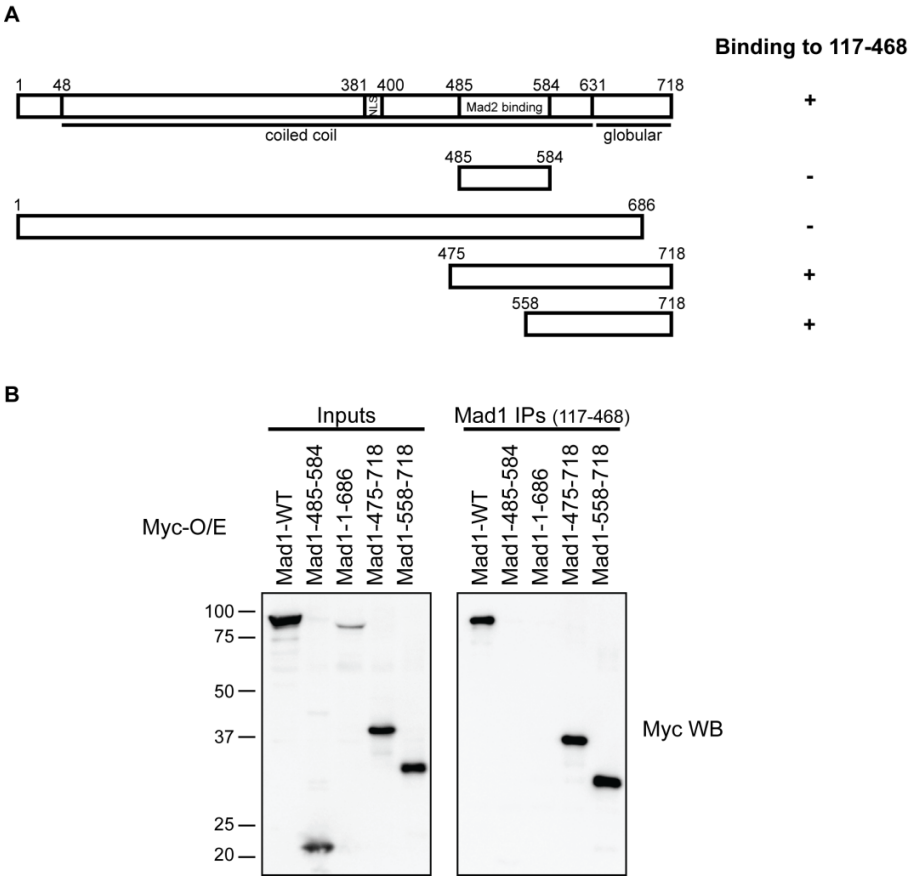

Figure 11. 117-468 recognizes the C-terminal globular domain of Mad1. (A) Schematic representation of the Mad1 domain structure. Mad1$^{48-630}$ constitutes a coiled coil domain interrupted exclusively in position 531-549 by the unstructured loop including the Mad2 binding motif, whereas Mad1$^{631-718}$ folds as a stable globular domain. Mad1$^{381-400}$ constitutes a nuclear localization signal (NLS) and Mad1$^{485-584}$ is the minimal region of Mad1 retaining dimerization and Mad2 binding. The presence/absence (+/-) of binding to 117-468 as shown in (B) is indicated for each truncation. **(B)** HEK293T cells were transfected with the indicated Myc-tagged constructs (Myc-O/E for Myc overexpression) for 36 h. Cells were lysed and immunoprecipitations (IPs) with Mad1 117-468 mAb were performed. Inputs and IPs were analyzed by SDS-PAGE and Western blot with Myc mAb.

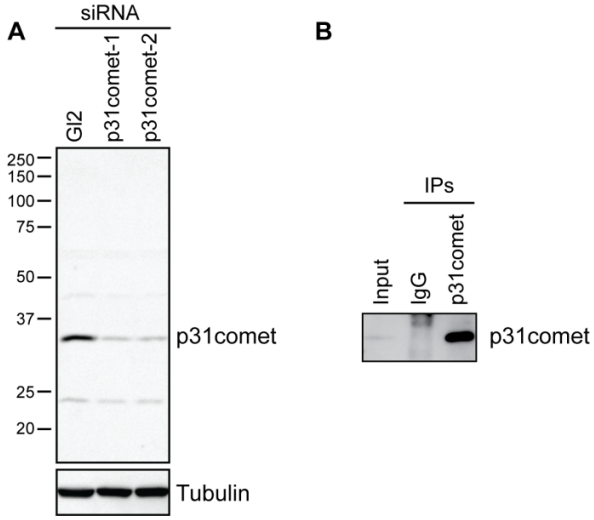

Figure 12. Basic characterization of 741212, rabbit polyclonal Ab to p31comet. (A) HeLaS3 cells were transfected with the indicated siRNA oligonucleotides for a total of 48 h, arrested with thymidine for 24 h, released for 10 h and harvested. Lysates were obtained and analyzed by Western blot with p31comet and α-tubulin antibodies. **(B)** IPs were performed from asynchronous HeLaS3 cells using rabbit unspecific IgGs (as control) and p31comet antibody. Input and IPs in were analyzed by Western blot using the p31comet antibody.

A

Clone	Western Blot	Linear epitope identified	Native immunoprecipitation	Immunofluorescence (formaldehyde)	Neutralizing in microinjection
107-276	No	No	Yes	Yes	Yes

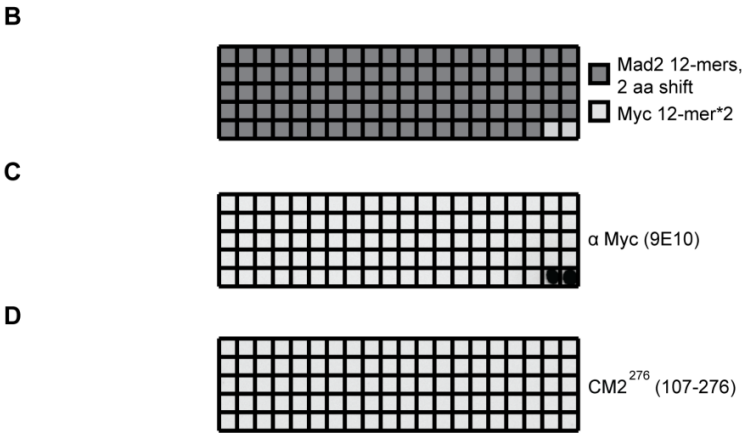

Figure 13. 107-276 recognizes a conformational epitope. (A) Table summarizing the characterization of the Mad2 mAb used throughout this thesis. The functionality of each clone is reported in several assays. 107-276 was functional in assays that retained the three dimensional structure of the antigen. **(B)** Scheme of the arrangement of 12-mer peptides on nitrocellulose. A total of 98 12-mer peptides encompassing the entire Mad2 sequence (205 amino acids) with 2 amino acid shifts were spotted in an ordered array. Peptide arrays were constructed using standard F-moc chemistry on a MultiPep robotic spotter according to the manufacturer's directions (Intavis). A c-Myc peptide (EEQKLISEEDLL) containing the epitope of the 9E10 mAb was spotted twice as positive control. The array described was spotted in duplicates. **(C and D)** Western blot on membranes described in (B) were performed with 9E10 or $CM2^{276}$ mAb, respectively.

Given the fact that Mad2 has two distinct native folded states (Luo et al, 2004), the possible selective recognition of the Open or Closed conformer was tested. To this end, His-tagged Mad2 was purified from *E. coli* in either its wild type form ($Mad2^{WT}$) or as mutants ($Mad2^{V193N}$ and $Mad2^{L13Q}$, respectively) that are known to mimic the two distinct conformers, O-Mad2 and C-Mad2 (Mapelli et al, 2007, see also Table 2 for a summary of the mutant´s characteristics). In IP, the mAb displayed increased reactivity towards C-Mad2 when compared to $Mad2^{WT}$ or O-Mad2 (Fig. 14). These results demonstrate that the mAb 107-276 is specific for the Closed conformer of Mad2; therefore, it will hereafter be referred to as "$CM2^{276}$" (Closed Mad2, clone 276). Note that a Mad2 polyclonal antibody that did not display preference for any Mad2 conformer in Western blot experiments (i.e. denaturing conditions, Fig. 14, lower panel) was used for all Western blot experiments throughout this thesis.

One additional monoclonal antibody against Mad2 (also recognizing C-Mad2 and named "$CM2^{2F12}$") was recently generated and its characterization is reported as Appendix.

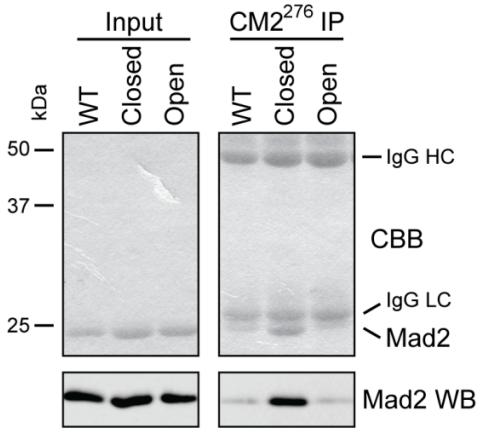

Figure 14. 107-276 ($CM2^{276}$) recognizes selectively C-Mad2. Purified $Mad2^{WT}$ (WT), $Mad2^{L13Q}$ (Closed) and $Mad2^{V193N}$ (Open) were immunoprecipitated (IP) with $CM2^{276}$. Inputs and IPs were analyzed by Coomassie Brilliant Blue staining (CBB) and Western blot (WB) using a rabbit polyclonal Mad2 antibody. IgG HC and LC indicate heavy and light IgG chains, respectively.

CM2^{276} recognizes C-Mad2 on the dimerization interface

A prediction arising from the selective recognition of C-Mad2 by CM2^{276} is that this mAb should be able to co-precipitate the known C-Mad2 interaction partners. Therefore, we asked whether the CM2^{276} can co-precipitate Mad1, Cdc20 and/or p31comet from a human cell lysate. Both Mad1 and Cdc20 were enriched in the immune complexes obtained after immunoprecipitating C-Mad2 from SAC-arrested HeLaS3 cells, whereas p31comet was not (Fig. 15A). Since the interaction of Mad2 with p31comet reportedly peaks upon SAC silencing (Xia et al, 2004), we also used CM2^{276} to immunoprecipitate C-Mad2 from a lysate of cells synchronized in metaphase by the proteasome inhibitor MG132 and having therefore an extinguished SAC. Again, p31comet was not detected in CM2^{276} immune complexes, although it was present in immunoprecipitates that were prepared using a polyclonal Mad2 antibody (Fig. 15B). These results demonstrate that CM2^{276} is unable to co-immunoprecipitate p31comet with Mad2, even though a Mad2:p31comet complex is present in metaphase-arrested cells. p31comet is known to

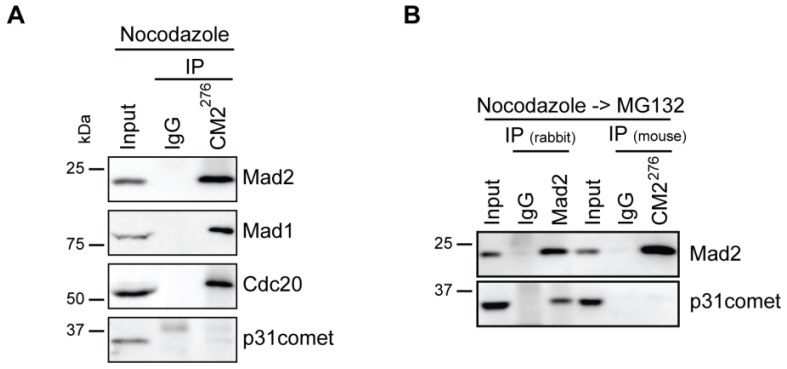

Figure 15. CM2^{276} can co-immunoprecipitate Mad1 and Cdc20 but not p31comet. (A) Immunoprecipitations (IPs) were performed with unspecific IgGs or CM2^{276} from HeLaS3 lysates obtained from cells arrested with nocodazole. **(B)** IPs were performed from HeLaS3 cells released from nocodazole for 2.5 h in the presence of MG132 using rabbit unspecific IgGs (as control) and a rabbit Mad2 antibody (IP (rabbit)) or with mouse unspecific IgGs (as control) and CM2^{276} (IP (mouse)). Input and IPs in (A) and (B) were analyzed by Western blot using the indicated antibodies.

interact with C-Mad2 through direct contact with the dimerization interface of Mad2 (Mapelli et al, 2006; Yang et al, 2007). Thus, we asked whether $CM2^{276}$ competes with p31comet for C-Mad2 binding. Specifically, we performed GST-pull down assays, using GST-$Cdc20^{111-138}$ that had been pre-adsorbed on glutathione-sepharose beads (GSH) and bound to His-tagged WT-Mad2 ($Mad2^{WT}$), thereby generating a C-Mad2:GST-$Cdc20^{111-138}$ complex (Mapelli et al, 2006). As expected, this complex readily pulled down both $CM2^{276}$ and His-tagged p31comet, provided that the two proteins were added separately (Fig. 16A, lanes 1 and 2). In striking contrast, co-incubation of $CM2^{276}$ with increasing concentrations of p31comet decreased the amount of $CM2^{276}$ that was bound by C-Mad2 (Fig. 16A, lanes 3-5), clearly demonstrating competition between p31comet and $CM2^{276}$ for binding to C-Mad2. Attesting to the specificity of this competition, increasing concentrations of the unrelated protein His-$hSpindly^{1-444}$ (Chan et al, 2009) did not affect the association of $CM2^{276}$ to C-Mad2 in this assay (Fig. 16B). One prediction of the observed competition between p31comet and $CM2^{276}$ is that the antibody should interfere with Mad2 conformational dimerization (Mapelli et al, 2006; Mapelli et al, 2007; Yang et al, 2007). Indeed, co-incubation of $CM2^{276}$ with $Mad2^{\Delta C}$, known to adopt the Open conformation (Table 2), also resulted in a competitive behavior in that $CM2^{276}$ abolished the ability of $Mad2^{\Delta C}$ to bind to C-Mad2:GST-$Cdc20^{111-138}$ (Fig. 16C, lanes 3-5). In contrast, equal concentrations of a Mad1 mAb did not interfere with the binding between $Mad2^{\Delta C}$ and C-Mad2, demonstrating specificity of this competition (Fig. 16D).

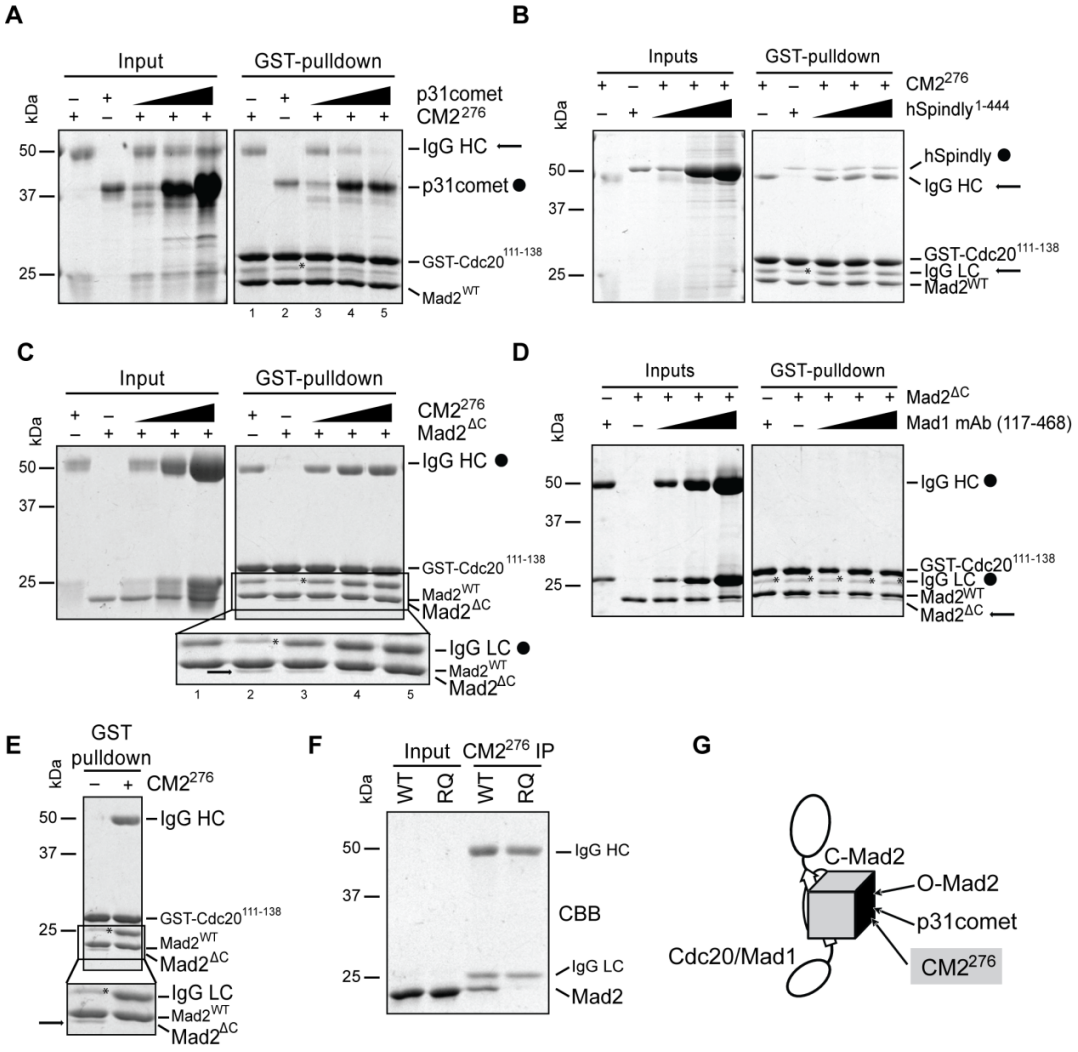

Figure 16. CM2^{276} recognizes the dimerization interface of C-Mad2. (A) Purified CM2^{276}, p31comet or a mixture of constant amount of Mad2 mAb with increasing concentrations of p31comet were incubated with Mad2:GST-Cdc20$^{111-138}$ complex preadsorbed on GSH beads. Inputs and GST pulldowns were analyzed by Coomassie Brilliant Blue staining. **(B)** Purified CM2^{276}, hSpindly$^{1-444}$ or a mixture of constant amounts of CM2^{276} with increasing concentrations of hSpindly$^{1-444}$ were treated as described in (A). **(C)** Purified CM2^{276}, Mad2$^{\Delta C}$ or a mixture of Mad2$^{\Delta C}$ with increasing concentrations of CM2^{276}, were treated as described in (A). **(D)** Purified Mad1 mAb (117-468), Mad2$^{\Delta C}$, or a mixture of Mad2$^{\Delta C}$ with increasing concentrations of Mad1 mAb were treated as described in (A). Asterisks in (A-D) indicate a contaminant of the GST-Cdc20$^{111-138}$ preparation with electrophoretic mobility similar to the IgG light chain. The arrow and the circle in (A-D) mark the species used at constant or increasing concentrations, respectively. **(E)** Purified Mad2$^{\Delta C}$ was added to Mad2:GST-Cdc20$^{111-138}$ complex adsorbed on GSH beads, following pre-incubation with buffer (-) or CM2^{276} (+). GST pull downs were analyzed by Coomassie Brilliant Blue staining. The arrow marks Mad2$^{\Delta C}$. **(F)** Purified Mad2^{WT} (WT) and Mad2^{RQ} (R133E-Q134A) were immunoprecipitated with CM2^{276}. Inputs and IPs were analyzed by Coomassie Brilliant Blue staining. **(G)** Schematic representation of the CM2^{276} epitope.

Binding of $Mad2^{\Delta C}$ was also prevented upon prior adsorption of $CM2^{276}$ to C-Mad2:GST-$Cdc20^{111-138}$ beads (Fig. 16E). To further demonstrate that $CM2^{276}$ binds to the C-Mad2 dimerization interface, we also tested its ability to recognize a Mad2 protein that carries the double mutation R133E-Q134A ($Mad2^{RQ}$), which is known to affect residues crucial for Mad2 dimerization and p31comet binding (De Antoni et al, 2005; Yang et al, 2007) (Fig. 16F). As shown in Fig. 10G, $Mad2^{RQ}$ was barely able to bind to $CM2^{276}$ when compared to $Mad2^{WT}$. The most likely interpretation of these data is that $CM2^{276}$ recognizes a conformational epitope on the dimerization interface of C-Mad2 and that this epitope is critical for both conformational dimerization and p31comet binding (Fig. 16G).

Abbreviation	Mutation	Conformation	Dimerization	p31comet binding	Reference
$Mad2^{WT}$	wild type	O/C	Yes	Yes	De Antoni et al., 2005
$Mad2^{L13Q}$	L13Q	C	Yes (with O)	Yes	Mapelli et al., 2007
$Mad2^{V193N}$	V193N	O	Yes (with C)	No	Mapelli et al., 2007
$Mad2^{RQ}$	R133E-Q134A	O/C	No	n.d.	De Antoni et al., 2005
$Mad2^{\Delta C}$	ΔC-term. 10 aa	O	Yes (with C)	No	De Antoni et al., 2005

Table 2 summarizes the features of the Mad2 mutants used throughout this thesis.

Only liganded Mad2 adopts the Closed conformation *in vivo*

Having established that $CM2^{276}$ recognizes selectively the Closed conformer of Mad2 that represents the "active" specie according to the "Mad2 template model" (De Antoni et al, 2005) afforded a unique opportunity for testing the prediction of the model in the cellular context. The template model predicts not only that Mad2 adopts two distinct conformations in the cell, Open and Closed, but also that O-Mad2 should freely diffuse in the cytoplasm and, by definition, be devoid of ligand, whereas C-Mad2 should tightly bind Mad1 and therefore be a resident component of unattached KTs. Furthermore, during SAC signaling the Mad1:C-Mad2 complex is predicted to exert a catalytic function by triggering the conversion (through asymmetric dimerization) of O-

Mad2 to C-Mad2 (with Cdc20 as ligand). Although this model is appealing and strongly supported by structural data (Luo & Yu, 2008; Mapelli & Musacchio, 2007), the lack of tools to discriminate between Open and Closed Mad2 has so far precluded the analysis of Mad2 conformation in a cellular context. To monitor the two state behavior of Mad2 in cells, we fractionated cell lysates by size exclusion chromatography (SEC) and analyzed each fraction for the presence of C-Mad2, using $CM2^{276}$ for IP (Fig. 17A). In order to analyze transitions between interphase and mitosis as well as cells with both an active and an inactive SAC, we synchronized HeLaS3 cells in G1/S phase, prometaphase and metaphase (by addition of thymidine, nocodazole and MG132, respectively; Fig. 17B). The use of a Superdex 200 column resulted in a Mad2 elution profile that showed two peaks of comparable intensity; these reflect Mad2 associated with its interaction partners (>440 kDa) and monomeric Mad2 (ca. 25 kDa), respectively (Fig. 17C, "TCAP" panels; see also Experimental Procedures). $CM2^{276}$ IP on all fractions invariably revealed the ability of this mAb to recognize Mad2 bound to its interaction partners, but not free Mad2 (Fig. 17C, "$CM2^{276}$ IP" panels). These data confirm that Mad2 adopts the Closed conformation when in complex with other proteins. Moreover, they indicate that free Mad2 adopts the Open conformation at all cell cycle stages examined. Theoretically, one could argue that the free Mad2 could actually be in the closed conformation but not be recognized by $CM2^{276}$, due to epitope masking by p31comet. However, this is clearly not the case as p31comet did not extensively co-migrate with free Mad2 (Fig. 17D). We also note that the elution profile of p31comet did not show major changes during the different cell cycle stages analyzed (Fig. 17D). The absence of

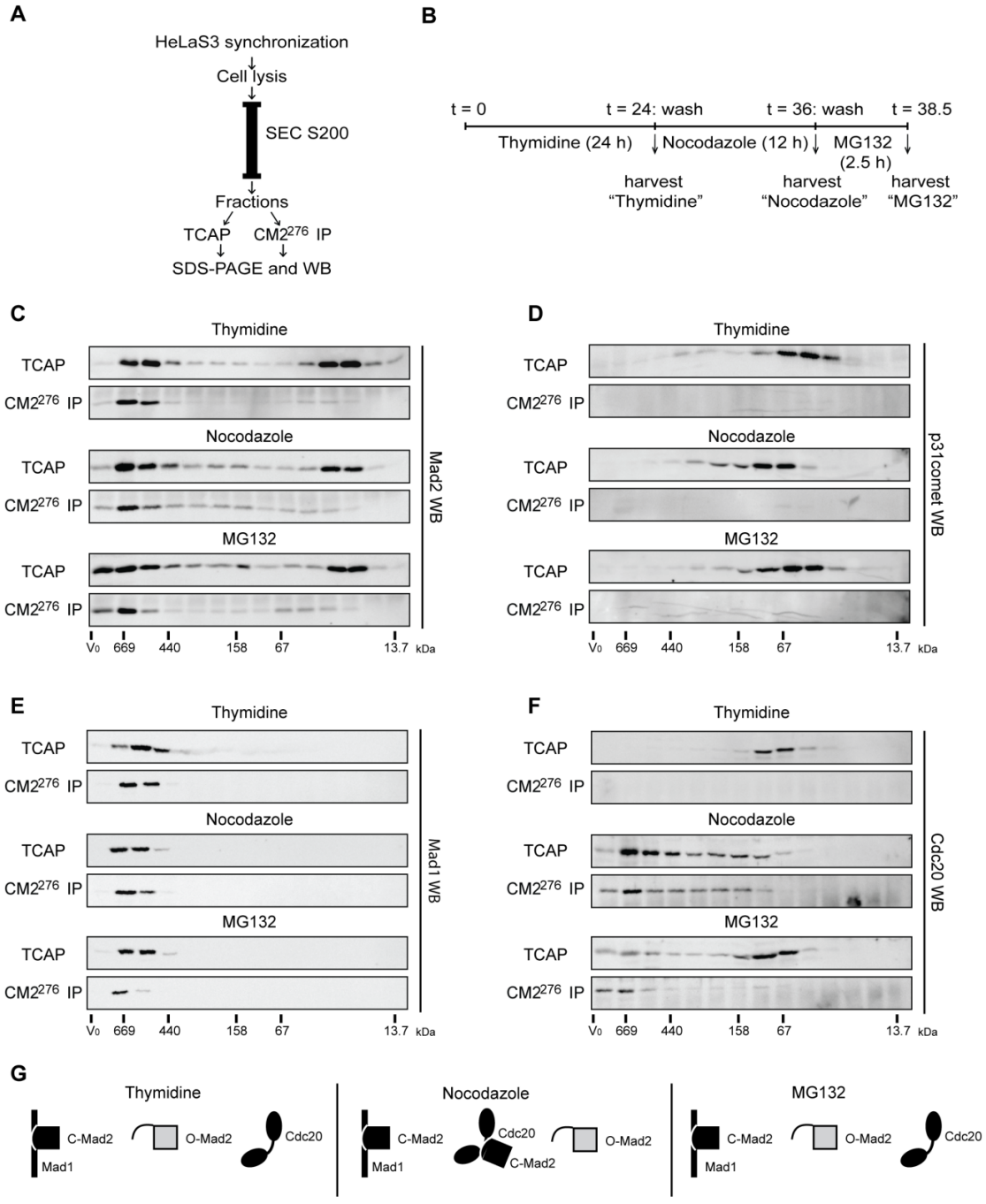

Figure 17. (A) Distribution of C-Mad2 among "free" and "bound" pools of the protein. (A) Schematic representation of the approach followed to study the distribution of C-Mad2. Synchronized HeLaS3 cells were lysed and fractionated by size exclusion chromatography (SEC). SEC was performed with a Superdex 200 16/60 column, followed by collection of 4 ml fractions through the 120 ml of elution volume. Fourteen fractions covering size ranges from the upper limit of the column to 13.7 kDa were further processed in parallel by TCA precipitation (TCAP) and $CM2^{276}$ IP. Resulting samples were analyzed by Western blot. **(B)** Timeline of the synchronization used for experiments shown in (C-E); "MG132" cells were first arrested in thymidine for 24 h and were incubated in the presence of nocodazole for 12 h after release, collected by mitotic shake off and released for 2.5 h in the presence of MG132.

"Thymidine" and "Nocodazole" cells were harvested following thymidine and nocodazole block, respectively. **(C-F)** Western blots on samples obtained from TCA precipitations (TCAP) and $CM2^{276}$ IP on fractions obtained as described in (A), following synchronization as described in (B). Western blots were performed with rabbit Mad2 polyclonal antibody (C), p31comet antibody (D), Mad1 mAb (E) and Cdc20 antibody (F). **(G)** Schematic summary of the results displayed in (C-F).

p31comet in the $CM2^{276}$ IPs is readily explained by antibody-competition for the p31comet binding site (see Fig. 16A and 7G) but it is more difficult to explain the absence of p31comet in the high molecular weight fractions of total cell lysates, especially in MG132 treated cells where we could clearly highlight the presence of a Mad2:p31comet complex (Fig. 15B). We interpret this to indicate that only a very minor fraction of the total cellular p31comet interacts with Mad1:C-Mad2 complexes at any given stage. In support of this conclusion, semi-quantitation of cellular protein levels indicates that p31comet is approximately twice as abundant as total Mad2 (Fig. 18).

Western blots for the other known Mad2 ligands revealed that Mad1 co-migrated with C-Mad2 and could be co-immunoprecipitated by $CM2^{276}$ throughout the cell cycle (Fig. 17E). In stark contrast, Cdc20 migrated as a monomeric species in interphase and did not display any interaction with C-Mad2 (Fig. 17F, upper panels), arguing against the existence of a sizeable pool of MCC during interphase. During SAC activation Cdc20 shifted to the higher molecular weight fractions, where it clearly interacted with C-Mad2 (Fig. 17F, middle panels). Upon SAC silencing, however, the bulk of Cdc20 was again released as a monomeric entity and only a minor population, still engaged in protein complexes, could be co-immunoprecipitated by $CM2^{276}$ (Fig. 17F, lower panels). Interestingly, the association of C-Mad2 with Cdc20 during prometaphase was not reflected in a major change in the overall elution profile of total Mad2 (Fig. 17C),

consistent with the emerging notion that the inhibitory action of Mad2 on Cdc20 is likely to be catalytic rather than stoichiometric (Kulukian et al, 2009; Nilsson et al, 2008).

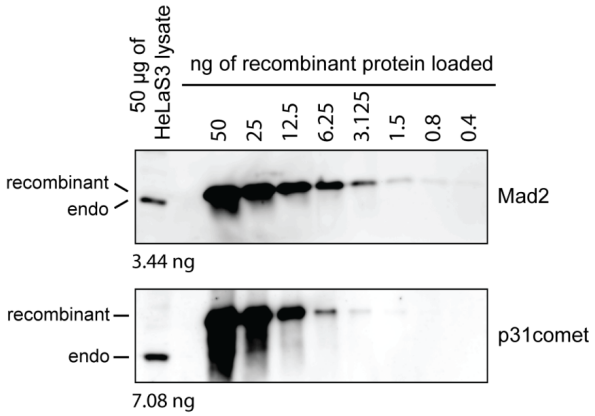

Figure 18. Estimate of Mad2 and p31comet protein abundances. 50 µg of an asynchronous HeLaS3 total cell lysate together with the indicated number of nanograms (ng) of recombinant 6His-Mad2 or 6His-p31comet (upper and lower panel, respectively), have been analyzed by SDS-PAGE and Western blot with the indicated antibodies. Bands corresponding to the recombinant and endogenous (endo) protein are indicated. Densitometry analysis of the bands was used to estimate the amount of endogenous protein loaded (estimate are shown below each gel).

Analytical fractionation of SAC components performed by size exclusion chromatography previously employing a Superose 6 matrix (Nilsson et al, 2008; Sudakin et al, 2001) could resolve different Mad2 subcomplexes, namely free-Mad2, Mad2 incorporated into the MCC complex (together with Cdc20 and BubR1:Bub3) and a Mad2 containing MCC that associates to the APC/C. Indeed, a similar experiment performed with a Superose 6 column also revealed the presence of Mad2 in both the MCC and the APC/C+MCC complexes (Fig. 19A). Downstream immunoprecipitation highlighted that Mad2 adopts the close conformation both in the MCC and APC/C+MCC fractions (Fig. 19B). Collectively, our results show that liganded Mad2 (i.e. bound to either Mad1 or Cdc20) adopts the Closed conformation in human cells, whereas free Mad2 remains in the Open conformation during the cell cycle.

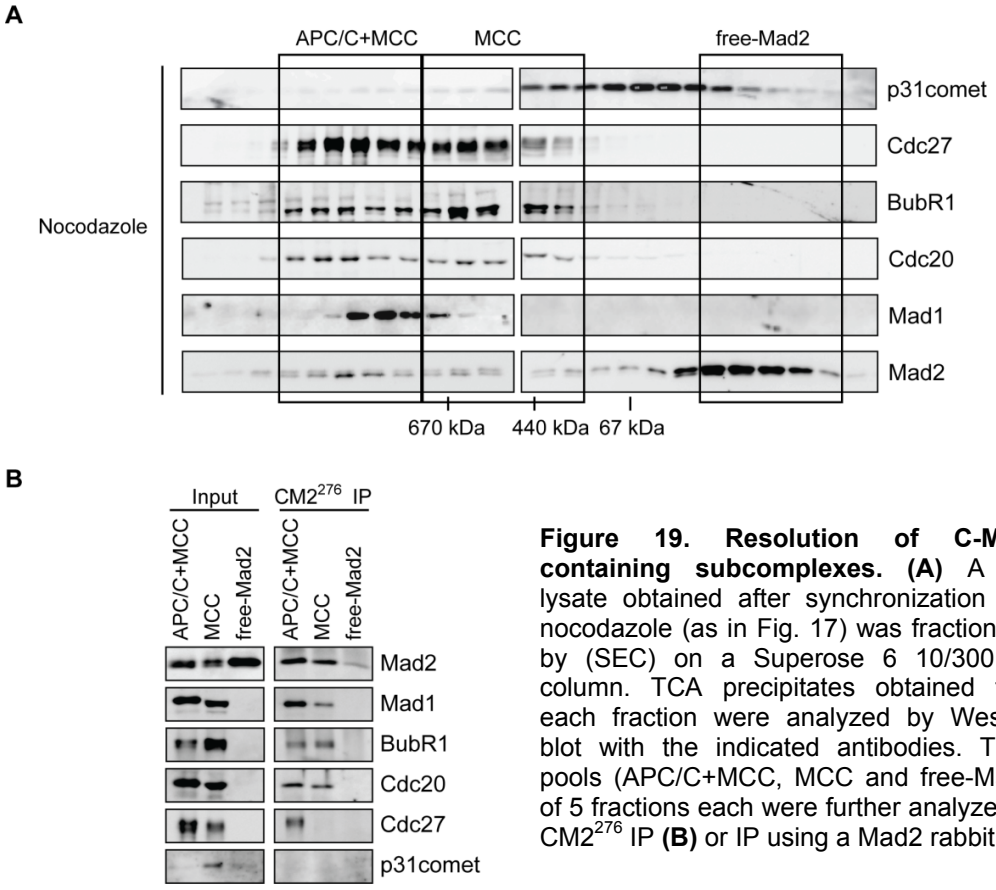

Figure 19. Resolution of C-Mad2 containing subcomplexes. (A) A cell lysate obtained after synchronization with nocodazole (as in Fig. 17) was fractionated by (SEC) on a Superose 6 10/300 GL column. TCA precipitates obtained from each fraction were analyzed by Western blot with the indicated antibodies. Three pools (APC/C+MCC, MCC and free-Mad2) of 5 fractions each were further analyzed by $CM2^{276}$ IP **(B)** or IP using a Mad2 rabbit Ab.

Mad1 is required for the formation of C-Mad2 in interphase

Our data show that, within cells, Mad1 is a constitutive ligand of C-Mad2, whereas Cdc20 is entrapped into Mad2´s safety belt only during checkpoint activation (Fig. 17 and 10). As C-Mad2 is the energetically favored conformer *in vitro* (Luo et al, 2004), we asked whether Mad2 can possibly adopt the Closed conformation *in vivo*, in the absence of any known ligand. To this end, we used siRNA to deplete Mad1 from interphase-arrested cells, in which Mad1 is the only established ligand of C-Mad2, before samples were analyzed using the assay described above. When compared to the Gl2 control, Mad1 siRNA caused a significant (albeit not complete) reduction in Mad1 protein levels (Fig. 20A-B and E). Under these conditions, a marked shift of Mad2

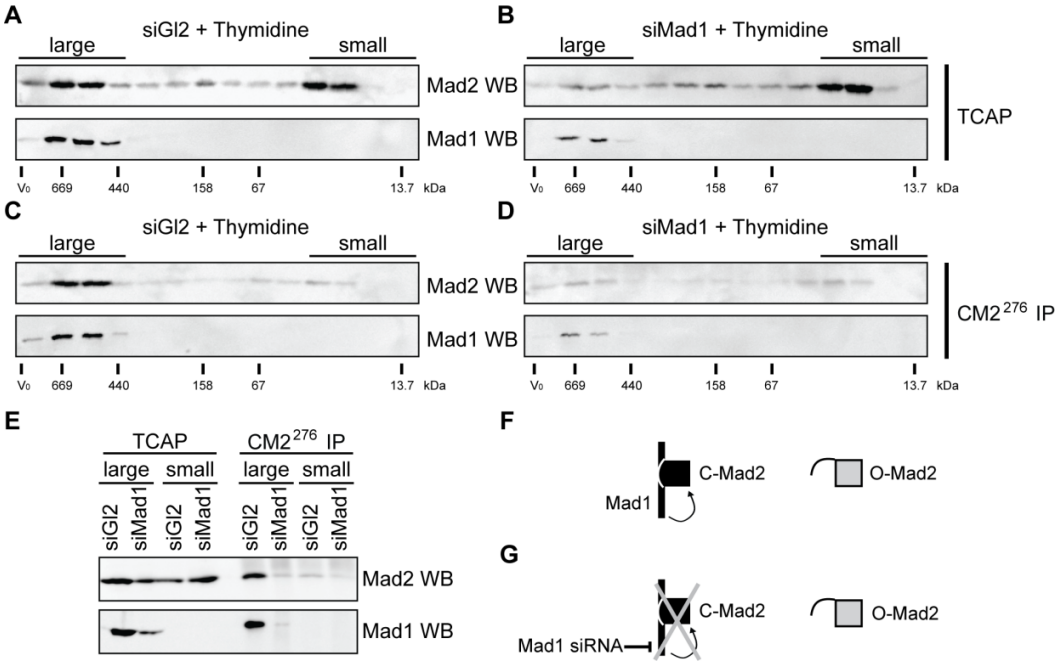

Figure 20. Requirement of Mad1 for C-Mad2 formation in interphase. (A) SEC analysis performed with a Superdex 200 16/60 column of a lysate obtained from HeLaS3 cells treated with Gl2 siRNA for 60 h and arrested with thymidine for 24 h. Samples were concentrated by TCA precipitation (TCAP). Western blots were performed with the indicated antibodies. **(B)** Samples obtained as in (A) but following Mad1 siRNA-mediated depletion. **(C, D)** Samples obtained by $CM2^{276}$ IP against the same fractions used in (A) and (B), respectively. Western blots were performed with indicated antibodies. **(E)** Fractions highlighted as large and small in (A-D) were pooled and Western blots were performed with the indicated antibodies. **(F)** Schematic representation of the Mad2 sub-complexes found in interphase: Mad2 is either bound to Mad1, adopting the Closed conformation or free, adopting the Open conformation. **(G)** In the absence of Mad1, Mad2 cannot adopt the Closed conformation during interphase, and the bulk is thereby released as Open free Mad2.

from the liganded population to the free population was observed (Fig. 20A-B and E), confirming that Mad1 is the major binding partner of Mad2 in interphase cells. Importantly, while $CM2^{276}$ was able to immunoprecipitate the Mad1:C-Mad2: complex, but not free Mad2, from Gl2 control cells (Fig. 20C-E), the amount of C-Mad2 that could be precipitated by $CM2^{276}$ from Mad1-depleted cells was decreased in proportion to the reduction in Mad1 levels, without a corresponding increase of free Mad2 in the $CM2^{276}$ IP (Fig. 20D-E). These data clearly demonstrate that the association with Mad1 is required for interphase Mad2 to adopt the Closed conformation; furthermore, they

suggest that, *in vivo*, C-Mad2 does not accumulate to significant levels in the absence of ligand (Fig. 20F-G).

The Mad1:C-Mad2 complex is required to initiate the SAC

The key prediction made by the template model is that C-Mad2 is required for the catalytic activation of a cytosolic pool of O-Mad2 and that this conversion is in turn indispensable for SAC signaling. The ability of $CM2^{276}$ to interfere with Mad2 conformational dimerization afforded a unique opportunity to test this model within the cellular context. In a series of experiments, monoclonal antibodies were microinjected into HeLaS3 stably expressing histone H2B-GFP and progression through mitosis was monitored by time lapse video microscopy. We first asked whether C-Mad2 is required to initiate SAC signaling. To this end, cells were injected in interphase and treated with nocodazole before progress through mitosis was monitored (Fig. 21A). As expected, the microinjection of a Myc mAb, used as negative control, did not interfere with the ability of HeLaS3 cells to respond to nocodazole, as all injected cells underwent mitotic arrest for at least 6 hours without signs of apoptosis (Fig. 21B-C). In stark contrast, the majority of the $CM2^{276}$ injected cells escaped the nocodazole block in less than 1 hour, resulting in cells with decondensed chromatin and aberrantly shaped nuclei, a phenotype typical of SAC override (Fig. 21B-C). Importantly, the microinjection phenotype caused by $CM2^{276}$ injection depended exclusively on C-Mad2 recognition, as coinjection of the antibody with $Mad2^{L13Q}$ but not $Mad2^{V193N}$ (mimicking C-and O-Mad2, respectively), abolished the observed phenotype (Fig. 22).

Having established that Mad1 is required for the formation of C-Mad2 in interphase, microinjection of cells with a neutralizing Mad1 antibody should lead to a

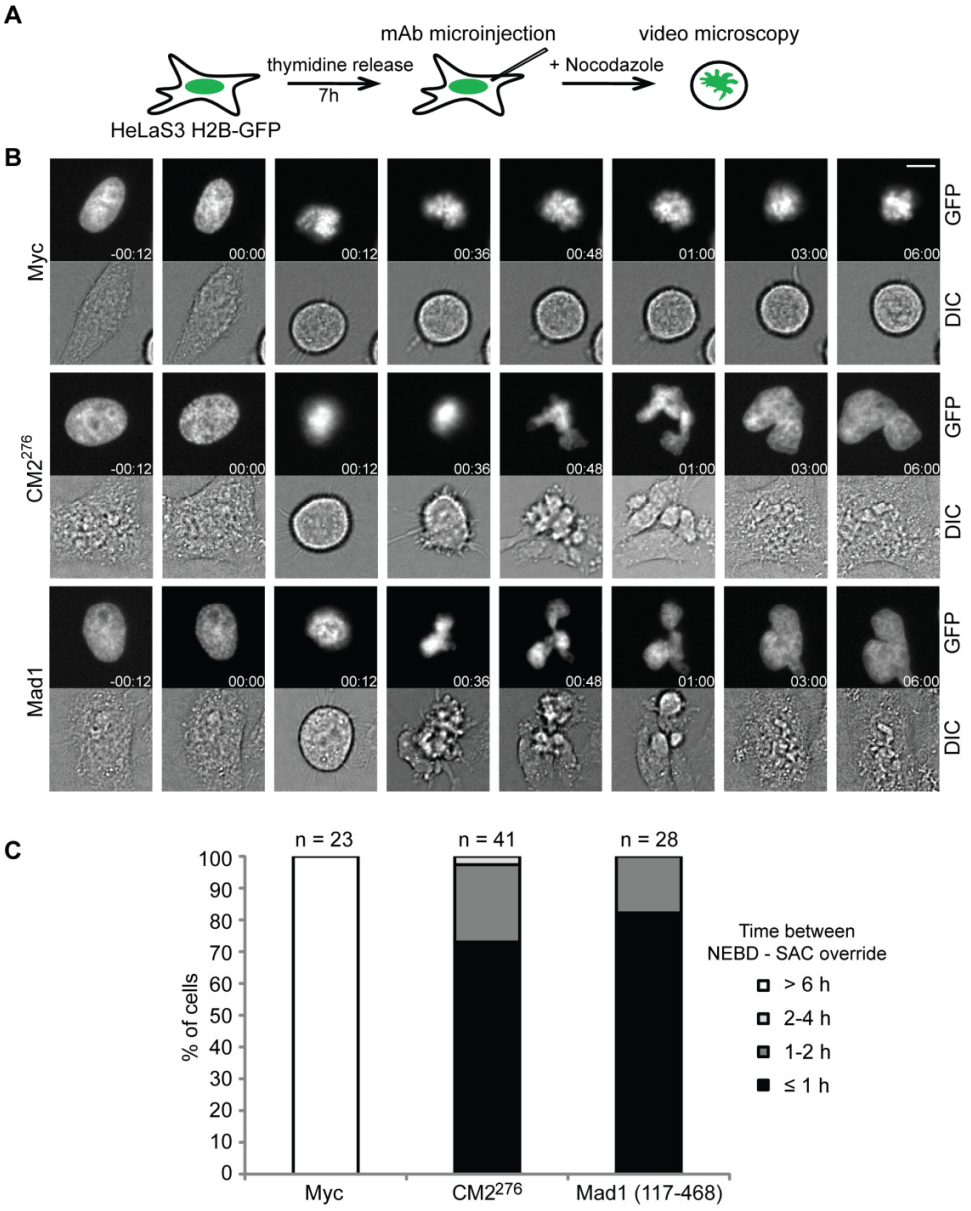

Figure 21. C-Mad2 is required for initiating and maintaining a SAC-dependent arrest. (A) Schematic representation of the microinjection protocol followed to assess the ability of cells to respond to nocodazole upon $CM2^{276}$ injection. Interphase HeLaS3 stably expressing histone H2B-GFP cells were subjected to microinjection 7 h after thymidine release and analyzed by time lapse video microscopy in the presence of nocodazole. **(B)** Movie stills from representative cells injected with the indicated mAbs. Time in h:min is indicated. T=0 was defined as the time point at which nuclear envelope breakdown (NEBD) became evident. Scale bars = 10 µm. **(C)** Histogram showing cells microinjected with the indicated mAbs, subdivided into the displayed categories according to the time elapsed between nuclear envelope breakdown (NEBD) and nocodazole override (SAC override). Percentage of cells is shown (n = total number of cells counted).

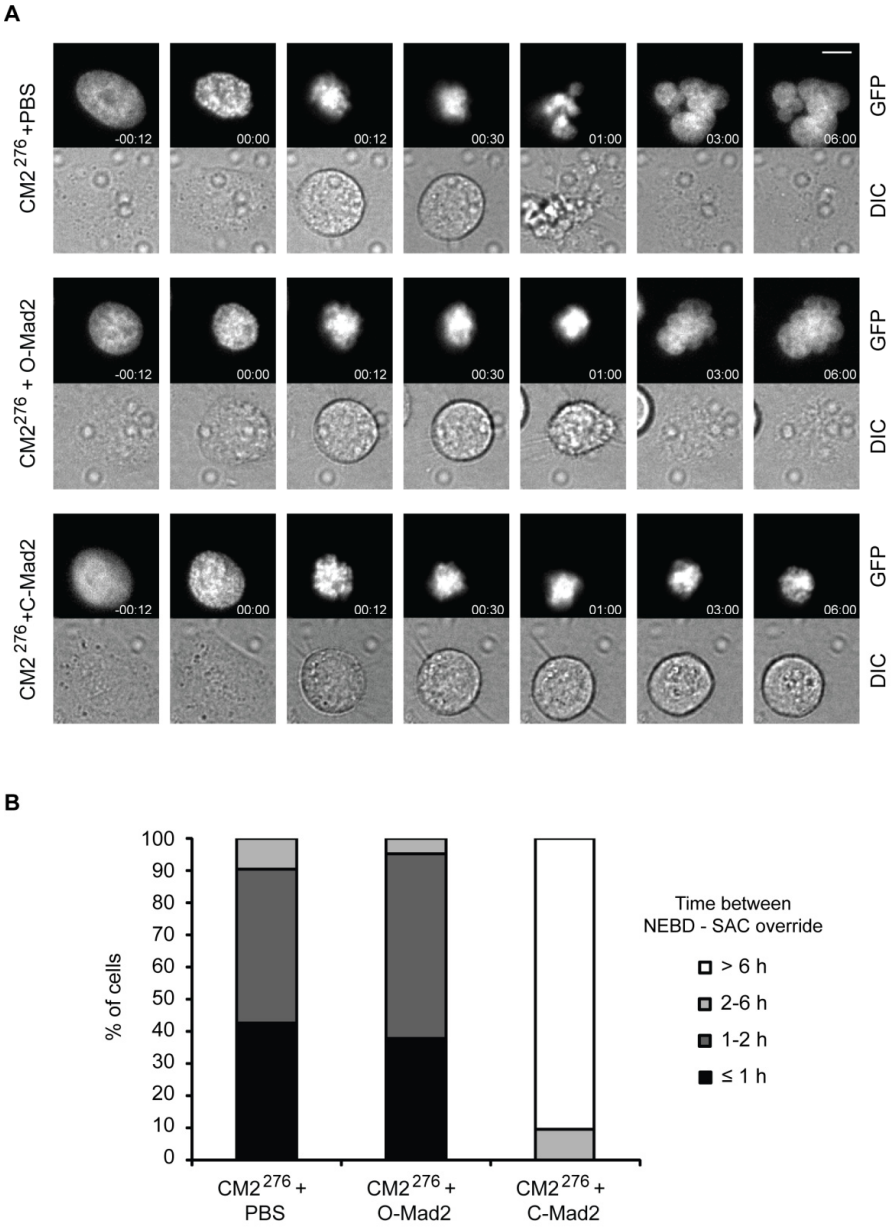

Figure 22. The microinjection phenotype of $CM2^{276}$ depends on reactivity towards C- but not O-Mad2. (A) Interphase HeLaS3 stably expressing histone H2B-GFP cells were subjected to microinjection 7 h after thymidine release and analyzed by time lapse video microscopy in the presence of nocodazole. Microinjection was performed with $CM2^{276}$ co-injected with PBS only ($CM2^{276}$ + PBS), 6His-$Mad2^{V193N}$ ($CM2^{276}$ + O-Mad2) or $Mad2^{L13Q}$ ($CM2^{276}$ + C-Mad2), utilizing a molar 1:2 ratio of antibody:recombinant Mad2. Movie stills from representative cells injected with the indicated mAbs. Time in h:min is indicated. T=0 was defined as the time point at which nuclear envelope breakdown (NEBD) became evident. Scale bar = 10 µm. **(B)** Histogram showing cells microinjected with the indicated mAbs, subdivided into the displayed categories according to the time elapsed between NEBD and nocodazole override (SAC override). Percentage of cells is shown (n = 21 cells per condition).

similar override. Indeed, Mad1 mAb injection (117-468), resulted in a nearly identical phenotype (Fig. 21B-C). These results strongly indicate that the conformational dimerization of Mad2 at the level of the Mad1:C-Mad2 complex is required for SAC signaling, as predicted by the template model and supported by experiments conducted in budding yeast (Nezi et al, 2006).

The Mad1:C-Mad2 complex is required to maintain the SAC

Next, we asked whether Mad2 conformational dimerization is also required to maintain an already established SAC arrest. This question was of particular interest, as several lines of recent evidence indicate that Mad2 acts epistatically upstream of BubR1/Mad3 (Burton & Solomon, 2007; Hardwick et al, 2000; King et al, 2007; Kulukian et al, 2009; Nilsson et al, 2008). To examine this issue, we injected $CM2^{276}$ into mitotic HeLaS3 cells in which the SAC had been activated by treatment with nocodazole and analyzed the injected cells 20, 40 and 60 minutes later by fluorescence microscopy (Fig. 21A). Already 20 minutes after $CM2^{276}$ injection, levels of Cyclin B1 were decreased to background levels in approximately half of the cells, and by 60 minutes all injected cells had overcome the nocodazole-induced arrest (Fig. 21B-C), while injection of Myc mAb for control did not trigger a SAC override, as expected (Fig. 21B-C). We have also analyzed the kinetics of SAC override in response to microinjection of the anti-Mad1 mAb. This antibody triggered an even faster SAC override than $CM2^{276}$ (Fig. 21B-C). These results demonstrate, first, that C-Mad2 (and hence conformational dimerization) is required to maintain an already established SAC-dependent arrest, supporting and extending previous data obtained with a polyclonal Mad2 antibody (Gorbsky et al, 1998).

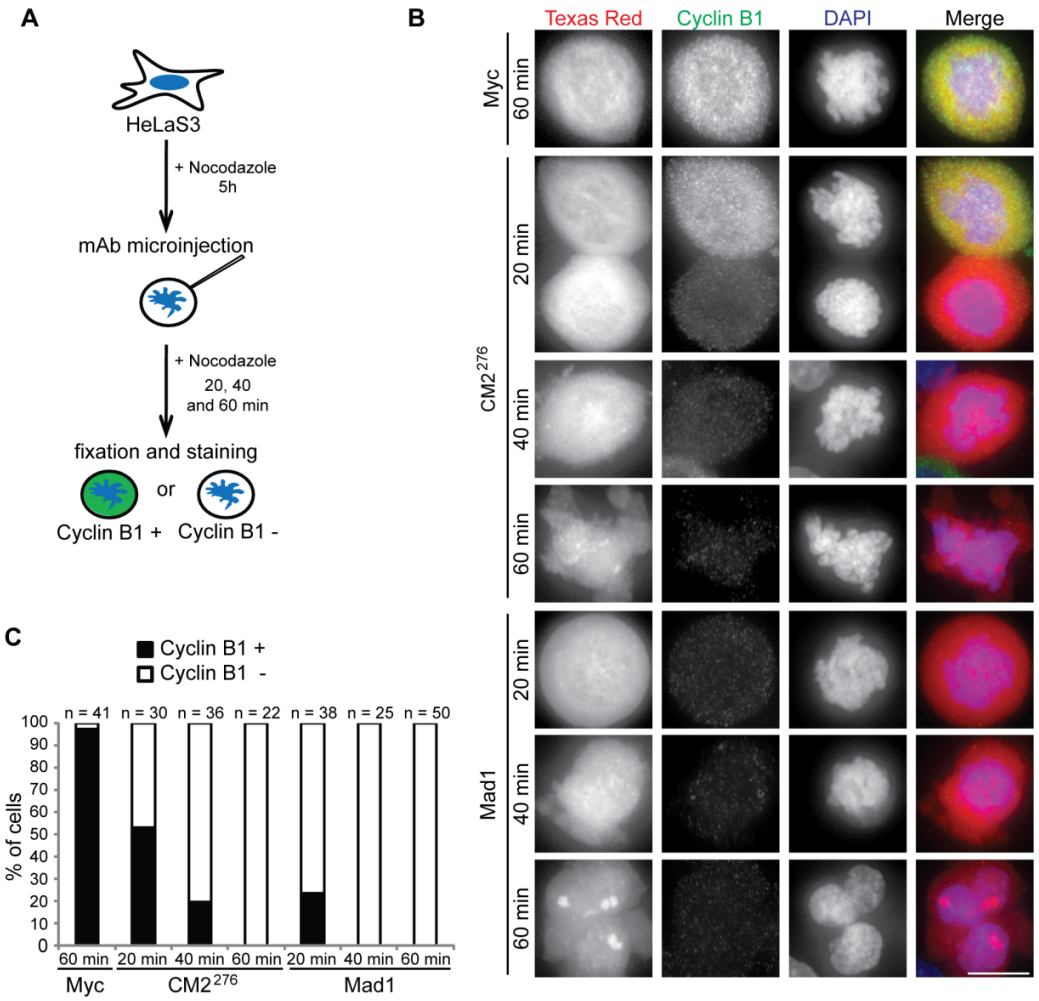

Figure 23. The Mad1:C-Mad2 complex is required for maintaining a SAC dependent arrest. (A) Schematic representation of the protocol followed to assess the capability of cells to maintain an already established SAC-dependent arrest upon microinjection of $CM2^{276}$ and Mad1 mAb. Asynchronous HeLaS3 cells were treated with nocodazole for 5 h and mitotic cells were selectively microinjected with the mAbs. After injection, cells were incubated for 20, 40 or 60 min in the presence of nocodazole and fixed with PTEMF. Cyclin B1 was stained with a mAb directly coupled to Alexa Fluor 488. **(B)** Representative cells treated as described in (A). Cyclin B1 (green), DNA was visualized with DAPI (blue) and the injection marker Texas Red dextran (red) are displayed. Scale bar = 10 µm. **(C)** Histogram showing cells microinjected with the indicated mAbs, subdivided into the displayed categories according to the absence (-) or presence (+) of Cyclin B1 staining. Percentage of cells is indicated (n = total number of cells counted). The microinjection procedure was established and performed by Manuel Kaulich.

Our data do not contradict an important role for BubR1 in APC/C^{Cdc20} inhibition, but demonstrate a continuous requirement for C-Mad2 for sustaining this inhibition. Second, they also bear on a model of SAC signaling that invokes a contribution of an autocatalytic loop based on cytosolic C-Mad2 (De Antoni et al, 2005). Specifically, our

side-by-side comparison of the consequences of anti-Mad1 mAb and $CM2^{276}$ injection argues that cytosolic C-Mad2 alone cannot provide sufficient C-Mad2:Cdc20 to maintain a SAC arrest.

The Mad1:C-Mad2 complex is required to regulate mitotic timing

In addition to being an essential component of the SAC, Mad2 has been proposed to constitute a key component of a mitotic timer operating in the cytosol (Meraldi et al, 2004). In support of this notion, the siRNA-mediated knockdown of Mad2 and BubR1 caused not only SAC silencing but also a striking acceleration of mitotic progression, whereas the knockdown of other Mad or Bub components was reported to abolish the SAC without accelerating the traverse of mitosis (Meraldi et al, 2004). A mechanistic understanding of the proposed KT-independent mitotic timer is presently elusive, but the fact that Mad1 was reportedly dispensable (Meraldi et al, 2004) suggested the non-catalytic generation of a C-Mad2:Cdc20 complex. To clarify the relationship between the proposed Mad2-dependent mitotic timer and the SAC in human cells, we took advantage of $CM2^{276}$ and asked whether interfering with conformational dimerization (and therefore C-Mad2 catalysis) would cause a similar mitotic acceleration, as the generalized Mad2 knockdown. We injected interphase HeLaS3 stably expressing histone H2B-GFP with either $CM2^{276}$ or Myc mAb, as control, and analyzed their progression through an unperturbed mitosis by time-lapse video microscopy (Figure 24A). Injection of Myc mAb (or buffer alone) caused a noticeable delay in the elapsed time between nuclear envelope breakdown (NEBD) and anaphase onset (54±8.1 and 69±6.1 min in average ± s.d., respectively), when compared with control non-injected cells (41.7±3.7 min) (Figure 24B and C), most likely reflecting the cellular stress caused by the microinjection procedure. More importantly, injection of

$CM2^{276}$ led to a drastic mitotic acceleration (22.4±1.5 min) (Figure 24B and C); in addition, $CM2^{276}$-injected cells invariably showed signs of chromosome missegregation, indicative of SAC abrogation (i.e. chromosome bridges and/or lagging chromosomes) (Figure 24B). These results clearly show that conformational dimerization of Mad2 is also involved in regulating mitotic timing. From the perspective of the proposed timer model, allegedly dependent on Mad2 but not Mad1, the above results create a conundrum. They imply that either C-Mad2 can be generated in a Mad1-independent manner or, alternatively, Mad1 is also part of the mitotic timer mechanism. To distinguish between these possibilities, we used the Mad1 mAb, which was able to neutralize the SAC (Figure 21), to carry out microinjection experiments. Remarkably, microinjection of this anti-Mad1 mAb led to a striking acceleration of unperturbed mitosis (19.1 ± 1.2 min), causing also a strong chromosome missegregation phenotype (Figure 24B and C), similar to the results obtained when injecting $CM2^{276}$. This indicates that Mad1 also contributes to mitotic timing regulation.

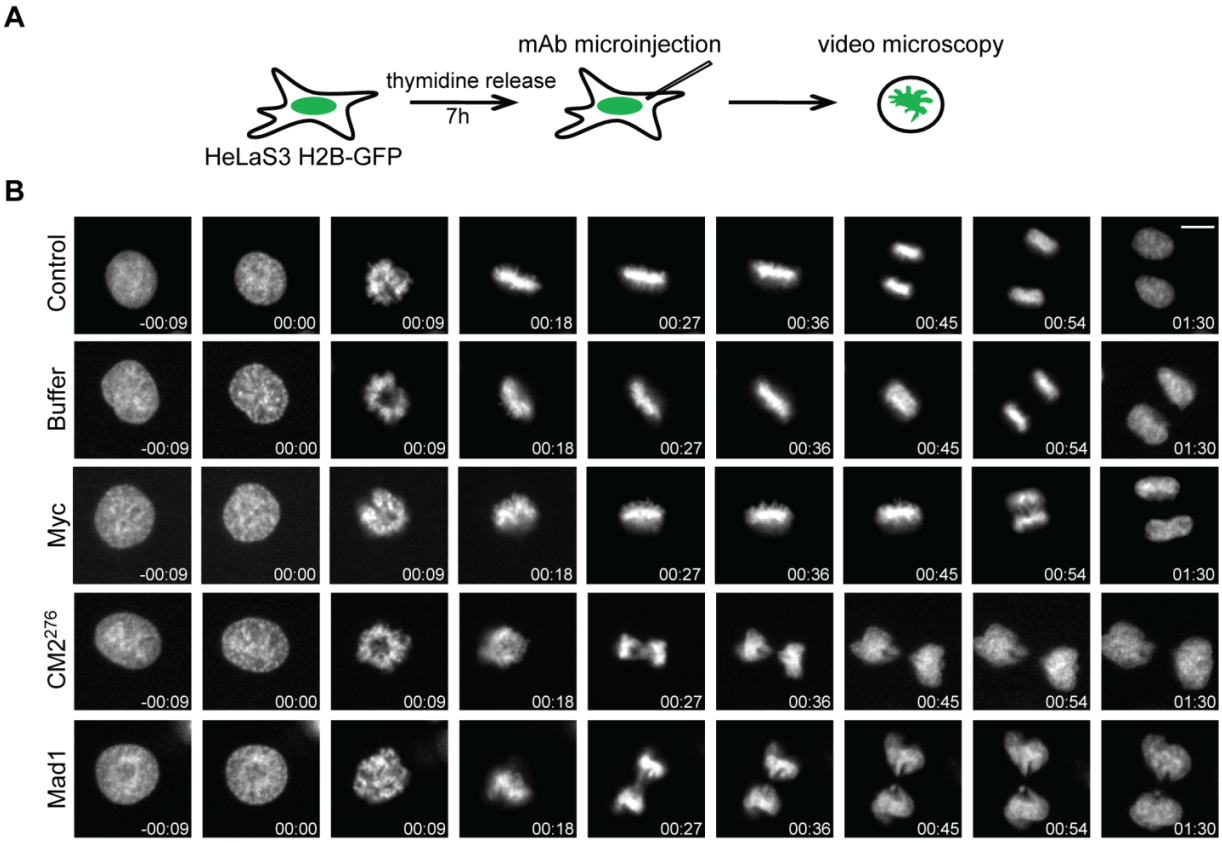

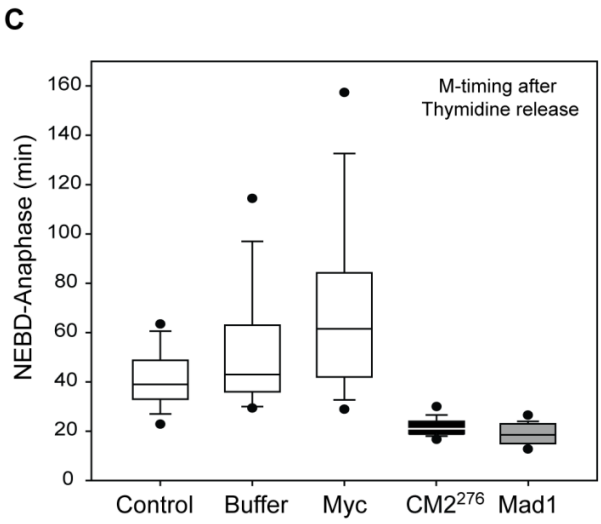

Figure 24. The Mad1:C-Mad2 complex is required for regulating mitotic timing. (A) Schematic representation of the microinjection protocol followed to analyze the progression through an unperturbed mitosis after mAb microinjection. Interphase HelaS3 stably expressing histone H2B-GFP cells were subjected to microinjection 7 h after thymidine release and analyzed by time lapse video microscopy. **(B)** Movie stills from representative cells injected with the indicated mAbs as described in (A). Control cells correspond to non-injected cells. Time in h:min is indicated. T=0 was defined as the time point at which NEBD became evident. Scale bar = 10 µm. **(C)** Box-and-whisker plot showing the elapsed time (min) between NEBD and anaphase onset for individual cells microinjected as described in (A). Analysis performed on > 40 cells per condition, from 3 independent experiments. Lower and upper whiskers in (C) represent 10th and 90th percentiles, respectively.

The SAC regulates mitotic timing operating intra-mitotically and not through a pre-assembled inhibitor

When the "timer model" has been originally proposed, it has been postulated that a timer mechanism would be necessary to keep the APC/C activity in check during prophase, while KTs are still assembling and are not yet fully mature and capable to generate a "wait anaphase" signal (Meraldi et al, 2004). In addition, a recent study proposed that the MCC assembles in the cytoplasm pre-mitotically in an Mps1-dependent manner, suggesting therefore that the MCC formed prior to mitosis corresponds to the "timer" (Maciejowski et al, 2010). In order to address to which extent the regulation of mitotic timing relies on the formation of an APC/C inhibitor during interphase, we undertook two different but complementary approaches. First, antibodies were microinjected into cells that had been arrested at the G2/M boundary with the Cdk1 inhibitor RO-3306 (Vassilev et al, 2006), and mitotic progression was then monitored following inhibitor wash out (Fig. 25A). The injection of either $CM2^{276}$ or the anti-Mad1 mAb caused a striking mitotic acceleration (NEBD-to-anaphase onset; 24.4 and 22.3 min on average, respectively) when compared with non-injected cells (68.5 min on average) (Fig. 25B-C). These data show that the pre-mitotic contribution of both C-Mad2 and Mad1 to mitotic timing regulation is minor if not absent. Second, we took advantage of the fact that the SAC kinase Mps1, required for Mad1:C-Mad2 loading to KTs, is amenable to chemical inhibition and has also been recently implicated in the regulation of mitotic timing (Hewitt et al, 2010; Maciejowski et al, 2010; Santaguida et al, 2010; Sliedrecht et al, 2010). Specifically, we monitored the timing of mitotic progression in cells that experienced an Mps1 inhibition already during S, G2 and M phase or only during M phase (Fig. 26A). Remarkably, Mps1 inhibition led to an

indistinguishable mitotic acceleration, regardless of the timing of inhibitor addition (Fig. 26B-C). These results lend no support to the idea that Mps1 affects the duration of mitosis acting independently of the SAC. Furthermore it did not escape our notice that first, we failed to observe a sizeable MCC during interphase (Fig. 17) and second,

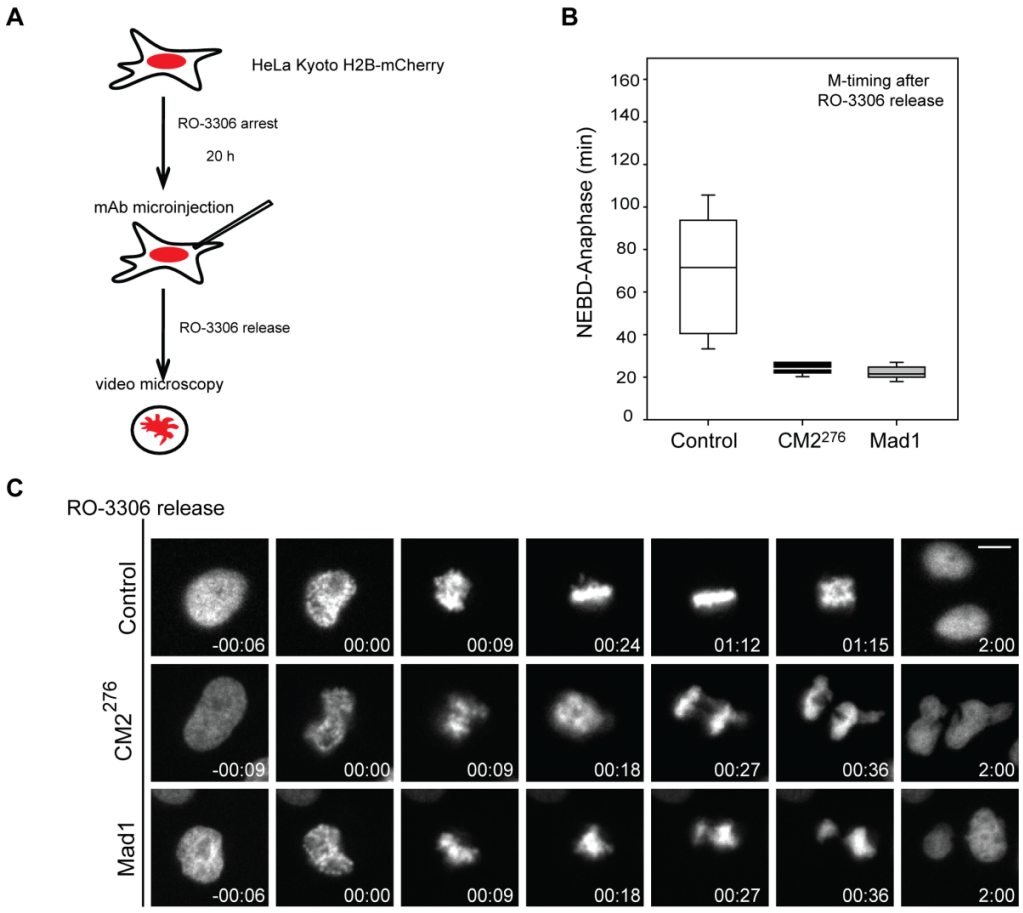

Figure 25. The Mad1:C-Mad2 complex controls mitotic timing acting after mitotic entry. (A) Schematic representation of the protocol followed to analyze the progression through mitosis when mAbs were microinjected at the G2/M boundary. HeLa Kyoto H2B-mCherry cells were microinjected after addition of RO-3306 for 20 h and mitotic progression was followed by time lapse video microscopy following RO-3306 release. Only cells that displayed nuclear envelope breakdown (NEBD) within 20 min after RO-3306 release were further analyzed. **(B)** Box-and-whisker plot showing the elapsed time (min) between NEBD and anaphase onset for individual cells microinjected as described in (A). Analysis performed on ≥ 10 cells. Lower and upper whiskers in (B) represent 10th and 90th percentiles, respectively. **(C)** Movie stills from representative cells injected with the indicated mAbs as described in (A). Control cells correspond to non-injected cells. Time in h:min is indicated. T=0 was defined as the time point at which NEBD became evident whereas the first still displayed corresponds to the first time point of the movie, concomitant to RO-3306 release. Scale bar = 10 μm.

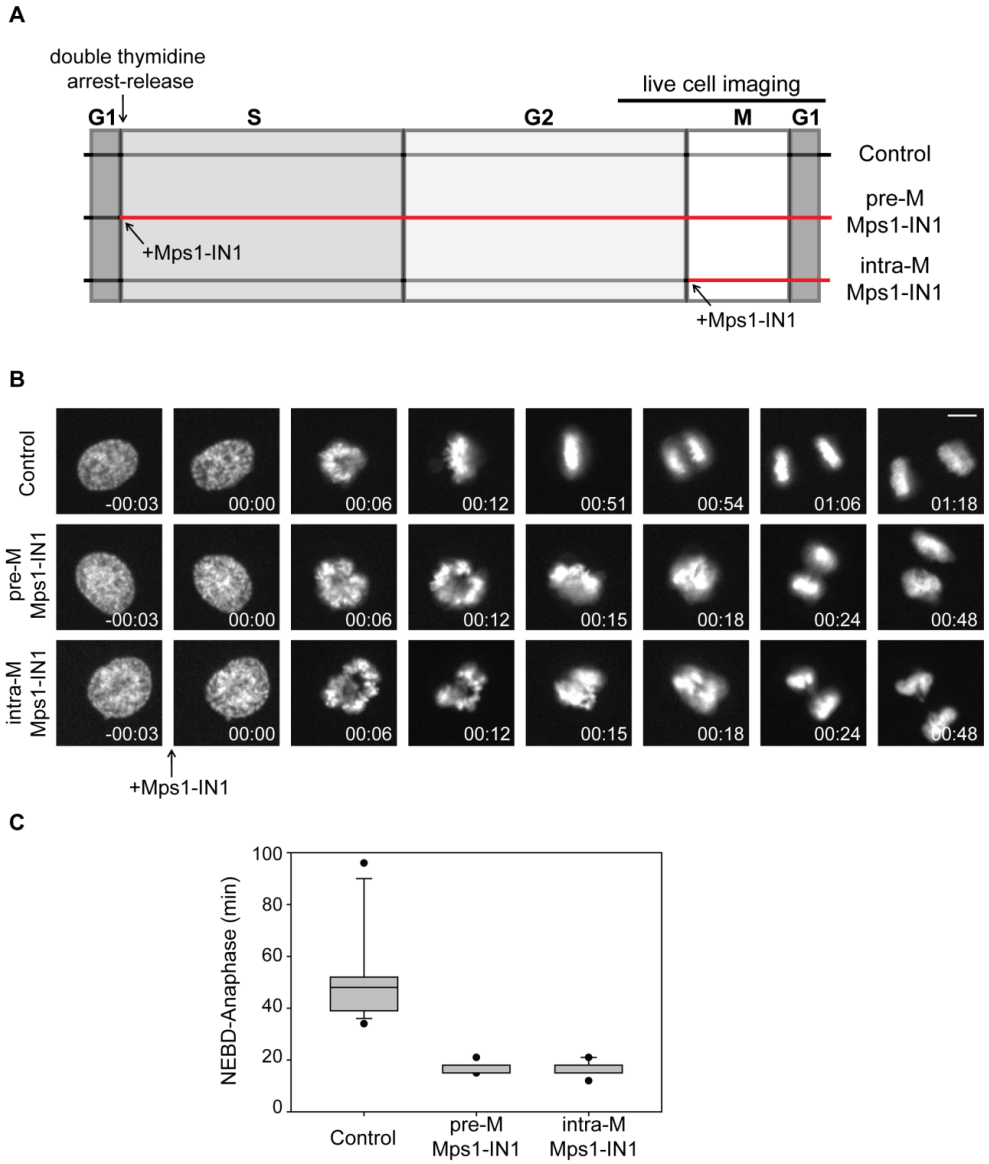

Figure 26. Mps1 control of mitotic timing (A) Schematic representation of the protocol followed to analyze the progression of cells through mitosis after Mps1 inhibition. HeLaS3 cells stably expressing histone H2B-GFP were synchronized by double thymidine arrest-release and their mitotic progression was monitored by time lapse video microscopy. Cells were either dividing in the absence of Mps1-IN1 (Control), following addition of Mps1-IN1 concomitant to the second thymidine release (pre-M Mps1-IN1) or with the addition of Mps1-IN1 concomitant to chromosome condensation (intra-M Mps1-IN1). **(B)** Movie stills from representative cells treated as described in (A). Time in h:min is indicated. T=0 was defined as the time point at which NEBD became evident and the time point of the addition of Mps1-IN1is indicated. **(C)** Box-and-whisker plot showing the elapsed time (min) between NEBD and anaphase onset for individual cells treated as described in (A). Twenty cells per condition were counted. Lower and upper whiskers in (C and D) represent 10^{th} and 90^{th} percentiles, respectively.

multiple KTs became Mad1:C-Mad2 positive before completion of nuclear envelope breakdown (see below). Taken together, the above data identify the KT Mad1:C-Mad2 complex as a prominent regulator of mitotic timing in human cells and they call for a reconsideration of the distinction between SAC and mitotic timer in human cells.

The Mad1:C-Mad2 complex undergoes p31comet dependent "capping"

Mad1 is known to form a constitutive protein complex with Mad2 throughout the cell cycle (Campbell et al, 2001; Chen et al, 1998; De Antoni et al, 2005). The two proteins also display identical localizations. They decorate the nucleoplasmic side of the nuclear pore complex (NPC) during interphase (Campbell et al, 2001) and then relocalize to KTs upon mitotic entry. Upon KT-MT attachment, they are "stripped" from KTs in a dynein and MT-dependent manner and transiently accumulate at spindle poles (Gorbsky et al, 1998; Howell et al, 2001; Li & Benezra, 1996). Here we used our newly generated mAbs to study the subcellular localization of Mad1 and the Closed conformer of Mad2. The known localization patterns were seen when endogenous Mad1 was stained with a mAb in HeLaS3 cells (Fig. 27A). However, contrary to expectation, co-staining of the same cells with $CM2^{276}$ revealed only partial co-localization with Mad1. Although $CM2^{276}$ staining revealed clear KT localization from prophase to prometaphase, C-Mad2 could barely be detected by this antibody at NPCs and spindle poles (Fig. 27A).

p31comet dependent capping of C-Mad2 at NPCs and spindle poles

One possible explanation for this result is that Mad2 adopts the Open conformation at NPCs and spindle poles. Alternatively, one or more proteins might mask the dimerization interface of C-Mad2 at NPCs and spindle poles. As p31comet

localizes to both NPCs (Tighe et al, 2008; A. Musacchio, personal communication) and the mitotic spindle (Habu et al, 2002) and we have previously demonstrated that

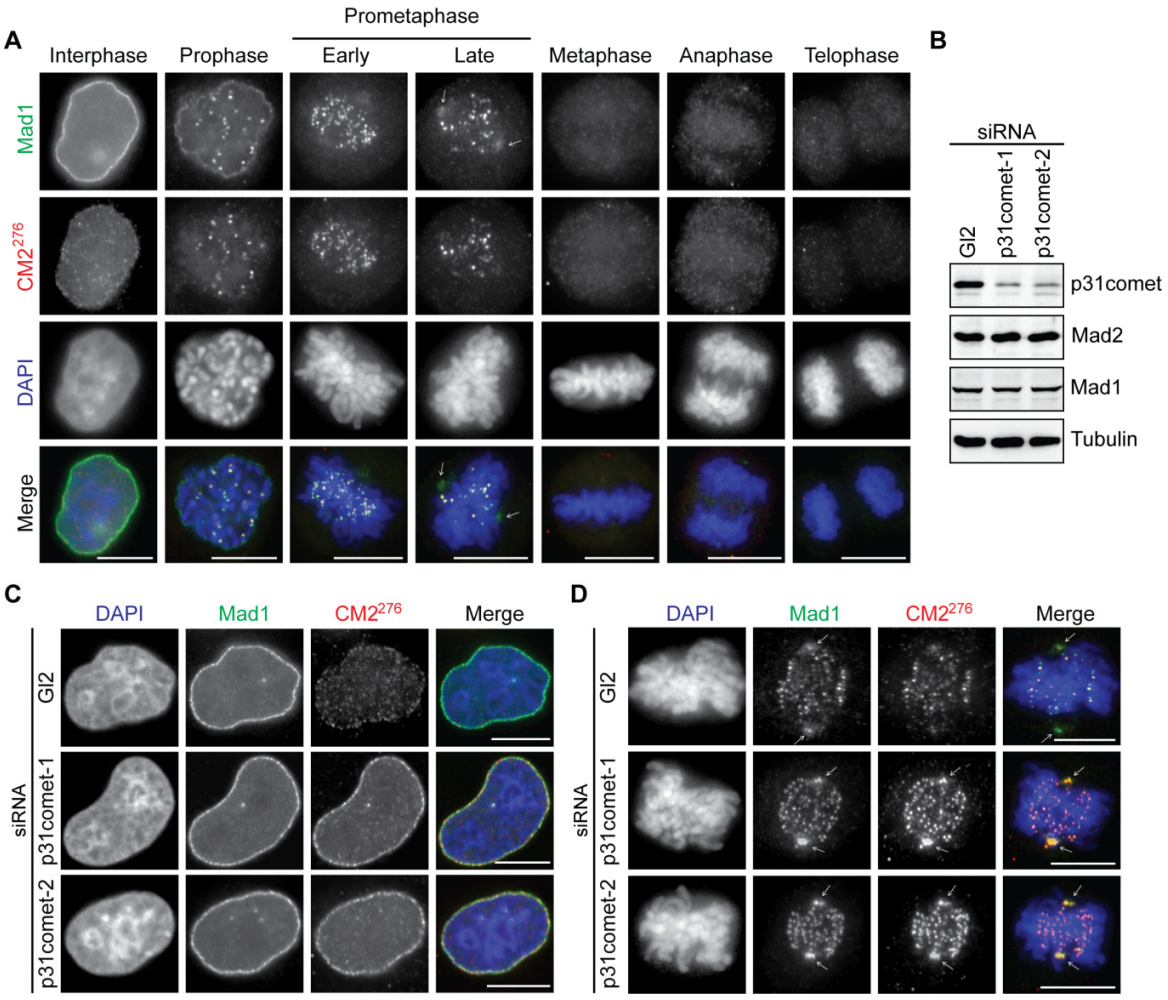

Figure 27. Subcellular localization of C-Mad2. (A) HeLaS3 cells arrested with thymidine for 24 h were released for 10 h and fixed with PTEMF. After fixation, C-Mad2 was stained with $CM2^{276}$, followed by secondary antibody incubation (red). After extensive washing, Mad1 was co-stained with a Mad1 mAb directly coupled to Alexa Fluor 488 (green), DNA was visualized with DAPI (blue). White arrows indicate spindle pole staining. **(B)** Cells were transfected with the indicated siRNA oligonucleotides for a total of 48 h, and synchronized as described in (A). Lysates were obtained and analyzed by Western blot with the indicated antibodies. **(C and D)** Cells transfected with the indicated siRNA oligonucleotides as in (B) were treated as described in (A). Scale bars = 10 μm.

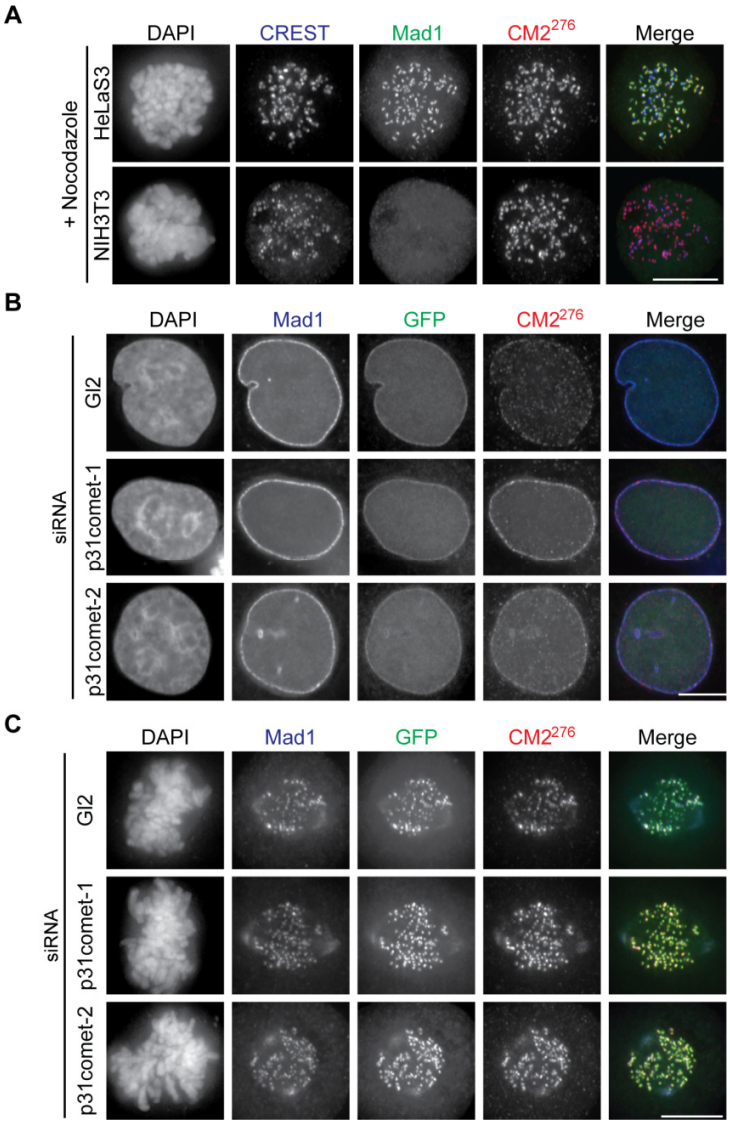

Figure 28. Localization of LAP^{GFP}-mouse-Mad2 upon p31comet siRNA (A) HeLaS3 and NIH3T3 cells were treated for 5 h with nocodazole and fixed with PTEMF. CM2^{276} antibody (red) and CREST serum (blue) incubations were followed by secondary antibody staining. After extensive washing, Mad1 was co-stained with Mad1 mAb (117-468) directly coupled to Alexa Fluor 488 (green), showing that whereas the Mad1 mAb cannot recognize mouse Mad1, CM2^{276} readily recognizes the mouse orthologue of Mad2. **(B and C)** HeLa Kyoto cells stably expressing LAP^{GFP}-mouse-Mad2 were transfected with the indicated siRNA oligonucleotides for a total of 48 h and synchronized as described in Figure 27. C-Mad2 was stained by CM2^{276} and subsequent secondary antibody incubation (red), Mad1 was directly coupled to Alexa Fluor 488 (blue) and LAP^{GFP}-mouse-Mad2 was visualized by direct GFP fluorescence (green). It is intriguing that depletion of p31comet resulted in an approximate doubling of GFP fluorescence selectively at KTs (but not at NPCs or spindle poles). This suggests that uncapping of C-Mad2 resulted in the selective recruitment of O-Mad2 only at KTs, hinting at a level of regulation of Mad2 heterodimer formation that is not presently understood. Scale bars = 10 µm.

p31comet can mask the $CM2^{276}$ epitope (Figure 16), we asked whether depletion of p31comet could restore the ability of $CM2^{276}$ to detect Mad2 at NPCs and spindle poles. Indeed, depletion of p31comet by two independent siRNA oligonucleotides readily allowed the detection of C-Mad2 by $CM2^{276}$ at both NPCs and spindle poles (Fig. 27C-D, respectively; for efficiency of p31comet depletion see Fig. 27B). To substantiate this conclusion, we also used a HeLa cell line expressing LAP^{GFP}-mouse-Mad2 (Hubner et al, 2010; Poser et al, 2008), which allowed us to study the localization of Mad2 through the monitoring of GFP fluorescence. As predicted, GFP-fluorescence at the nuclear envelope and at spindle pole staining was indistinguishable, regardless of the presence or absence of p31comet (Fig. 28A-C).

p31comet dependent capping of C-Mad2 at KTs

Most interestingly, we also observed that p31comet depletion caused a detectable increase in $CM2^{276}$ signal at KTs, without affecting the level of resident Mad1:C-Mad2 complex (Fig. 29A). Quantification (Fig. 29B) indicates that p31comet masks approximately 50 % of C-Mad2 at KTs. Furthermore, a significant increase in GFP signal at KTs could be observed in the cell line expressing LAP^{GFP}-mouse-Mad2 (Fig. 29C), suggesting that additional Mad2, almost certainly in the open conformation, had been recruited upon depletion of p31comet. Taken together, these data indicate that Mad2 can adopt the Closed conformation at multiple sub-cellular sites, but that the dimerization interface of Mad2 undergoes masking by p31comet at NPCs, spindle poles and, partially, also at KTs. The data also indicate that unmasking of C-Mad2 leads to recruitment of O-Mad2 selectively at KTs, implying that asymmetric dimer formation is differentially regulated at KTs, NPCs and spindle poles.

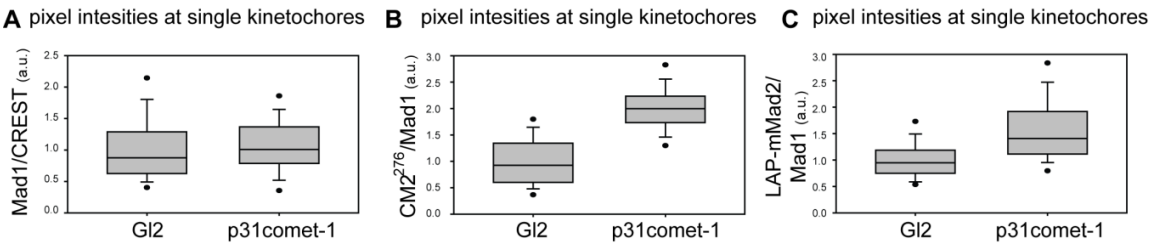

Figure 29. p31comet masks C-Mad2 at KTs. Box-and-whisker plots showing the average pixel intensities at single KTs expressed as the Mad1/CREST fluorescence ratio in **(A)**, the $CM2^{276}$/Mad1 ratio in **(B)** and the LAP^{GFP}-mouse-Mad2 (LAP-mMad2)/Mad1 ratio in **(C)** either in Gl2 or p31comet-1 siRNA-treated cells. a.u. = arbitrary units, n ≥ 80 KTs from four independent cells for **(A)** and **(B)** and n ≥ 180 KTs from eight independent cells for **(C)**. Lower and upper whiskers represent 10^{th} and 90^{th} percentiles, respectively.

p31comet localizes at KTs during an active SAC in a C-Mad2 dependent manner

The observation that a sizeable population of KT-associated C-Mad2 could be unmasked by depletion of p31comet predicts that p31comet associates with KTs already during prometaphase, when the SAC is active, and that this KT-association should depend on C-Mad2. To explore this point, we expressed Myc-p31comet in its wild type form or as a version carrying two point mutations (Q83A-F191A, abbreviated as $p31comet^{QAFA}$) that are known to abolish binding to C-Mad2 (Yang et al, 2007). Importantly, the use of a SV40 promoter allowed us to express p31comet at sub-endogenous levels (Fig. 30A). Following cytosolic pre-extraction, Myc-$p31comet^{WT}$, but not Myc-$p31comet^{QAFA}$, was readily visualized at C-Mad2 positive KTs (Fig. 30B). In addition, depletion of endogenous Mad2 by siRNA completely prevented Myc-$p31comet^{WT}$ to localize to KTs (Fig. 30C). Taken together, these data show that p31comet can localize at KTs during an active SAC and that the Mad1:C-Mad2 complex acts as its main KT receptor.

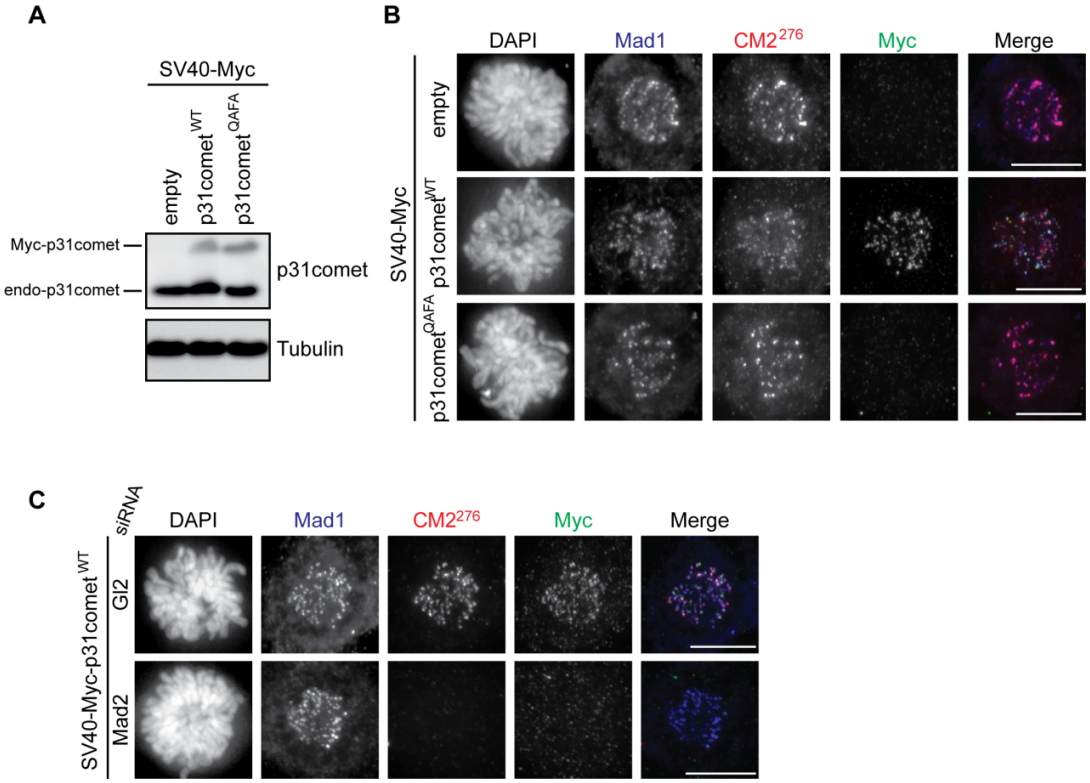

Figure 30. p31comet localizes at KTs in a Mad2 dependent manner. (A) HeLaS3 cells were transfected with the indicated SV40-Myc expression vectors for a total of 36 h. 12 h after transfection cells were arrested with thymidine for 14 h and subsequently released for 10 h. Lysates were obtained and analyzed by Western blot with the indicated antibodies. Bands corresponding to endogenous and ectopically expressed p31comet are indicated ("endo-p31comet" and "Myc-p31comet", respectively). **(B)** Cells transfected with the indicated expression vectors were treated as described in (A). $CM2^{276}$ and rabbit-Myc antibodies were detected by secondary antibody staining (red and green, respectively) whereas the Mad1 mAb was directly coupled to Alexa Fluor 647 (displayed in blue). **(C)** Cells transfected with either Gl2 or Mad2 siRNA for a total of 48 h were subsequently transfected with the SV40-Myc-$p31comet^{WT}$ construct, synchronized and treated as described in (B). Scale bars = 10 µm.

A role for Mps1 kinase activity in regulating p31comet dependent capping

siRNA mediated depletion of Mps1 had revealed its role in recruiting the Mad1:C-Mad2 complex (Martin-Lluesma et al, 2002), but additional layers of regulation could be only uncovered by the discovery of small molecule inhibitors of the kinase: whereas inhibition of Mps1 prior and during mitotic entry phenocopied the siRNA mediated depletion of the kinase (Hewitt et al, 2010; Kwiatkowski et al, 2010; Sliedrecht et al, 2010), a distinct function of Mps1 in promoting the Mad1:C-Mad2 template activity could

only be appreciated only when Mps1 is inhibited during mitosis (Hewitt et al, 2010). The data reported by Hewitt and colleagues are consistent with the notion that Mps1 promotes both the localization and the activity of the Mad1:C-Mad2 complex, but when the SAC signaling is initiated, Mps1 kinase activity is dispensable for the maintenance of Mad1:C-Mad2 at KTs but required for its sustained activity. To gather mechanistic insight into this regulation, we used $CM2^{276}$ to assess whether the dimerization interface of C-Mad2 undergoes p31comet-dependent capping upon intra-mitotic inhibition of Mps1. To this end, we synchronized cells by the simultaneous addition of nocodazole and MG132 (arresting cells either before mitotic entry or in prometaphase) and then inhibited Mps1 either with Reversine (Santaguida et al, 2010) or with Mps1-IN1 (Kwiatkowski et al, 2010)(Fig. 31A). Both inhibitors triggered a Mad1 de-localization from KTs, albeit not complete (Fig. 31B-C). One possible explanation is that Mps1 activity is not completely dispensable for the maintenance of Mad1:C-Mad2 during SAC signaling, in contrast to what had been previously reported (Hewitt et al, 2010). However, we noticed that the intra-mitotic Mps1 inhibition in a RPE-1 cell line expressing an analogue sensitive version of Mps1 (RPE-1-Mps1as) (Maciejowski et al, 2010) had a comparably minor impact on Mad1 KT maintenance (Conrad von Schubert, unpublished). This suggests that the observed differences might be explained by different genetic backgrounds and/or by the direct or indirect inhibition of Aurora B kinase activity by Reversine and Mps1-IN1 (Kwiatkowski et al, 2010; Santaguida et al, 2010), that is absent in RPE-1 cells expressing analogue sensitive Mps1(Maciejowski et al, 2010).

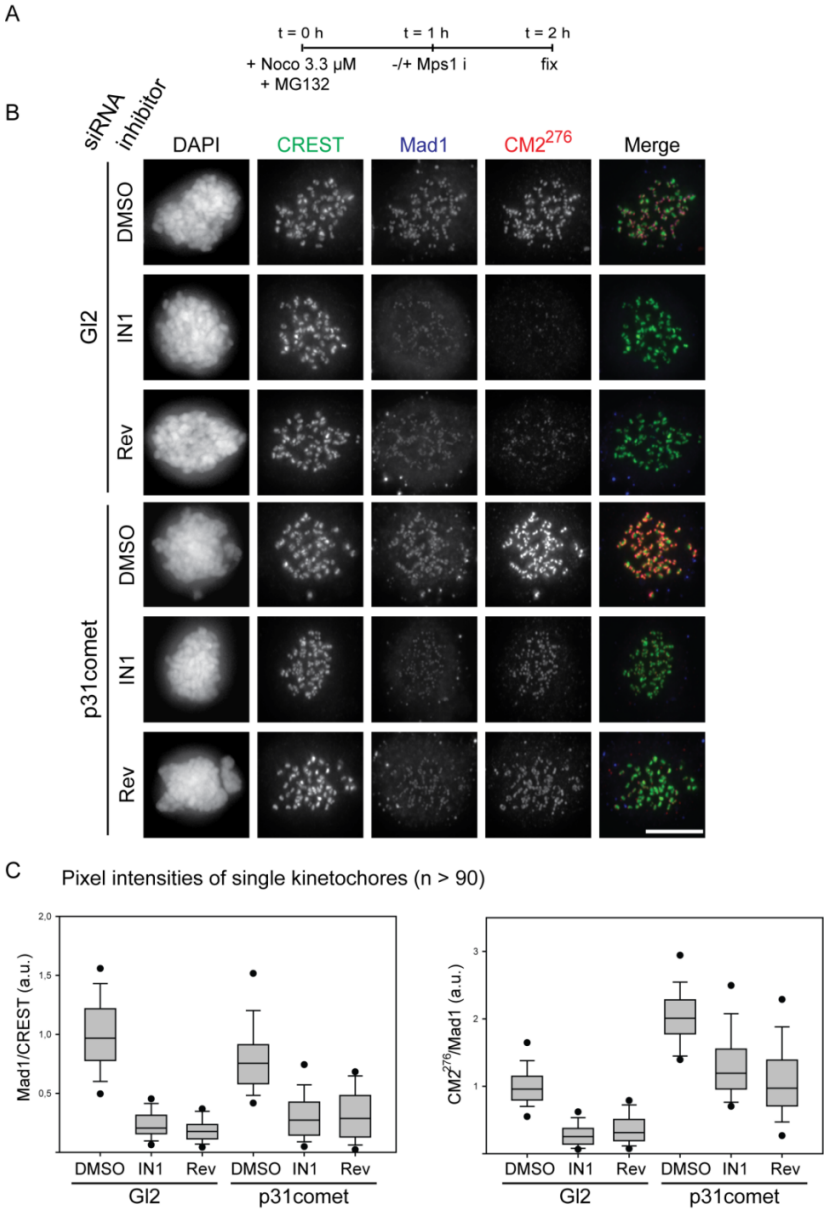

Figure 31 Mps1 regulates the availability of the C-Mad2 dimerization interface at KTs in a p31comet-dependent manner. (A) Schematic of the synchronization procedure used to assess the impact of Mps1 intra-mitotic inhibition on Mad1 and C-Mad2 detection at KTs. Briefly, nocodazole and MG132 were added at the same time for 1 h and followed by addition of Mps1 inhibitor (+) or DMSO (-) for one additional hour, followed by PTEMF fixation. **(B)** After fixation following either Gl2 or p31comet siRNA performed for 48h, $CM2^{276}$ and CREST primary antibody incubation were performed, followed by secondary antibody incubation (displayed in red and green). After extensive washing, Mad1 was co-stained with a Mad1 mAb directly coupled to Alexa Fluor 488 (displayed in blue), DNA was visualized with DAPI. Scale bar = 10 µm. **(C)** Box-and-whisker plots showing the average pixel intensities at single KTs expressed as the Mad1/CREST fluorescence ratio (left panel) or the $CM2^{276}$/Mad1 ratio (right panel), in both Gl2 or p31comet siRNA. n > 90 KTs from five independent cells. Lower and upper whiskers represent 10^{th} and 90^{th} percentiles, respectively.

Regardless of the effects of Mps1 intra-mitotic inhibition on Mad1 KT localization, fluorescence reflecting C-Mad2 detection by $CM2^{276}$ decreased more sharply than the Mad1 florescence, in HeLaS3 treated with either Reversine or Mps1-IN1 (Fig. 31B-C) and in RPE1-Mps1as cells treated with 3MB-PP1 (Conrad von Schubert, unpublished). These data indicate that Mps1 intra-mitotic inhibition leads to a reduction of the availability of the dimerization interface of Mad2. siRNA-mediated p31comet depletion led to a reversal of this phenomenon (Fig. 31B-C). This indicates that Mps1 kinase activity regulates the availability of C-Mad2 dimerization interface through a p31comet dependent mechanism. Intriguingly, p31comet has been also identified as a direct substrate of Mps1 *in vitro* assays (A. Musacchio, personal communication), suggesting that Mps1 might phosphorylate p31comet at KTs, therefore negatively regulating its interaction with C-Mad2.

A possible role for Tpr in regulating p31comet dependent capping

Several recent reports identified the nucleoporin Tpr as a conserved regulator of the SAC and interacting partner of Mad1/Mad2 (De Souza et al, 2009; Lee et al, 2008; Lince-Faria et al, 2009). Whereas there is consensus on the fact that Tpr directly interacts with both Mad1 and Mad2 at the NPCs during interphase and on the effects of its depletion leading to a SAC deficiency, its mechanistic action in SAC signaling remains elusive. According to Lee and colleagues (Lee et al, 2008), Tpr acts as a chaperon to promote binding of Mad2 to Mad1 at both the NPCs and KTs, but the presence of Tpr at KTs during prometaphase is questioned by Lince-Fraria and colleagues (Lince-Faria et al, 2009). We also failed to detect Tpr at KTs using two different antibodies that could detect Tpr during interphase at NPCs (data not shown). Although both studies have reported the absence of Mad2 from KTs following Tpr

depletion, the impact on Mad1 KT recruitment remains controversial. To rule out this controversy, we used our Mad1 and CM2^{276} antibodies to assess the effect of Tpr depletion on Mad1:C-Mad2 KT detection. Prometaphase cells that had been treated with Tpr RNAi for 72h displayed a normal recruitment of Mad1 to KTs, whereas C-Mad2 appeared nearly undetectable in the majority of the cells (Fig. 32).

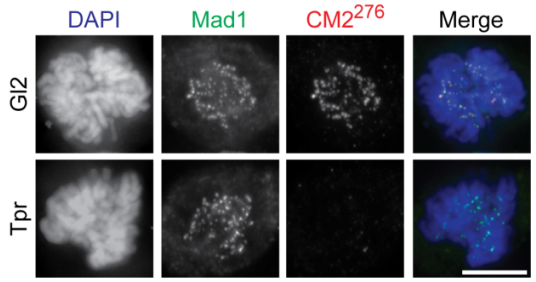

Figure 32 Tpr siRNA triggers a selective loss of C-Mad2 staining from KTs. HeLaS3 cells were transfected with the indicated siRNA oligonucleotides for a total of 72 h. Cells have been arrested with thymidine for 24 h were released for 10 h prior to PTEMF fixation. After fixation, C-Mad2 was stained with CM2^{276}, followed by secondary antibody incubation (red). Following extensive washing, Mad1 was co-stained with a Mad1 mAb directly coupled to Alexa Fluor 488 (green), DNA was visualized with DAPI (blue). Scale bar = 10 μm.

In order to assess whether the absence of C-Mad2 detection depended on p31comet, which would be consistent with an increased masking by the latter protein, we included in our analysis Tpr + p31comet depleted cells. As shown above, the single p31comet depletion doubled the fluorescence intensity of CM2^{276} at KTs (Fig 33A-C). Interestingly, the depletion of p31comet performed on the Tpr siRNA background restored the levels of C-Mad2 fluorescence intensity to levels intermediate to those displayed by control and single p31comet depleted cells (Fig 33A-C) (i.e.

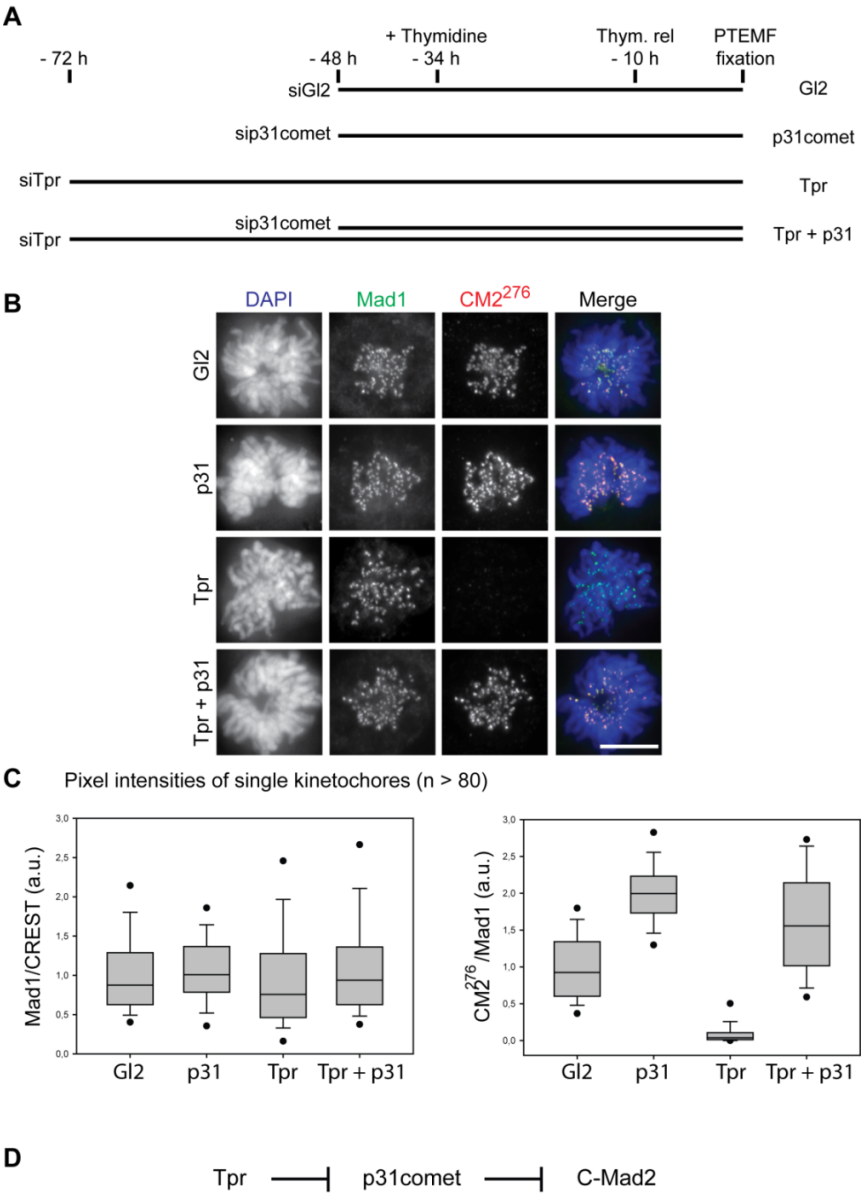

Figure 33 (A) Tpr controls the availability of the dimerization interface of C-Mad2 through p31comet. Schematic of the synchronization protocol employed to perform single and double depletions of p31comet (that could be depleted for maximally 48 h) and Tpr (that required a minimal depletion time of 72 h). **(B)** After fixation of HeLaS3 cells, C-Mad2 was stained with $CM2^{276}$, followed by secondary antibody incubation (red). After extensive washing, Mad1 was co-stained with a Mad1 mAb directly coupled to Alexa Fluor 488 (green), DNA was visualized with DAPI (blue). Scale bar = 10 µm. **(C)** Box-and-whisker plots showing the average pixel intensities at single KTs expressed as the Mad1/CREST fluorescence ratio (left panel) or the $CM2^{276}$/Mad1 ratio (right panel), in Gl2, p31comet, Tpr and p31comet + Tpr siRNA. n > 80 KTs from four independent cells. Lower and upper whiskers represent 10^{th} and 90^{th} percentiles, respectively. **(D)** Model describing the regulation of the availability of the C-Mad2 dimerization interface at KTs being regulated by Tpr through p31comet.

significantly higher than those observed in the single Tpr depletion), suggesting that Tpr positively sustains the SAC signaling in prometaphase by promoting the unmasking of the dimerization interface of C-Mad2 (Fig. 33D).

Since the increased masking of the dimerization interface at KTs observed upon Tpr depletion depended on p31comet, this raised the possibility that the described SAC regulation via Tpr depends on p31comet. In order to address this, we assessed the SAC functionality by monitoring the mitotic timing of HeLaS3 cells (stably expressing histone H2B-GFP) following single and double depletions as before. To this end we asked, first, whether the observed mitotic delay upon p31comet siRNA depended on Mad2, as proposed by others but never directly tested (Habu et al, 2002; Reddy et al, 2007; Vink et al, 2006; Xia et al, 2004). As expected, siRNA-mediated depletion of p31comet caused a metaphase arrest that depended on Mad2. This shows that the p31comet depletion phenotype depends on an hyperactivation of the SAC (almost certainly C-Mad2 itself) and not on a direct inhibition of the APC/C (Fig. 34A-C). Second, we analyzed the effect of the single Tpr depletion and in combination with p31comet: Tpr depletion alone resulted in a penetrant acceleration of the traverse of mitosis (Fig. 34D-F), consistent with the notion that Tpr is required to sustain the SAC (De Souza et al, 2009; Lee et al, 2008; Lince-Faria et al, 2009). The p31comet and Tpr co-depletion resulted in a mitotic timing that was significantly slower than the one observed upon single Tpr depletion and that resembled the timing observed in control cells (Fig. 34D-F). This observation is consistent with the notion that the removal of p31comet dependent masking of C-Mad2 at KTs observed in Tpr depleted cells (Fig. 33), is sufficient to restore a nearly physiological mitotic timing.

One of the caveats of extrapolating functional conclusions from double depletion experiments based on the siRNA technology is that different RNA duplexes have different potencies and their use in combination may results in competition phenomena, possibly through saturation of the RISC complex (Koller et al, 2006). We decided therefore to test whether the depletion efficiency of duplexes used in double siRNA transfections retained the efficiency displayed when used singly by Western blot. When Mad2 and p31comet were co-depleted, the p31comet depletion appeared unaffected by the presence/absence of the Mad2 siRNA (Fig. 35A), whereas Mad2 depletion efficiency was decreased in the absence of p31comet (Fig. 35A). This phenomenon could nevertheless be neglected in the functional analysis (Fig. 34A-C), as the reduction of Mad2 levels in the double depletion was sufficient to trigger the same mitotic acceleration observed in the single Mad2 depletion. This is consistent with the notion that even a minor reduction of Mad2 levels is sufficient to trigger a striking mitotic acceleration (Hubner et al, 2010).

When Tpr and p31comet were co-depleted, the depletion observed for each protein in single transfection experiments was retained (Fig. 35B). Surprisingly, Mad2 levels appeared downregulated in both Tpr and Tpr + p31comet depletions (Fig. 35B), indicating that this Tpr duplex leads to an unexpected Mad2 downregulation. Other Tpr siRNA duplexes led to a similar downregulation (data not shown) and the quantitation of Mad2 mRNA following Tpr siRNA suggested that the downregulation depends on altered protein stability rather than on a Mad2 mRNA reduction (H. Maiato, personal communication). This observation majorly complicates the interpretation of the

functional regulation of the SAC by Tpr through p31comet and it is discussed more in detail below (see Discussion).

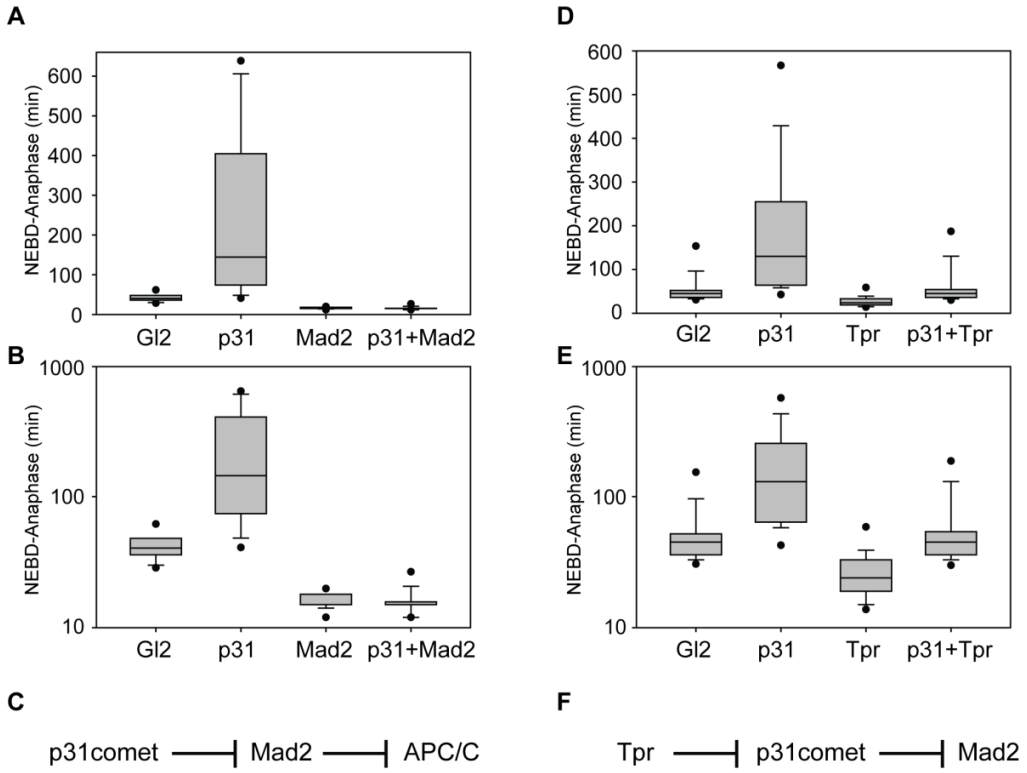

Figure 34 Tpr controls mitotic timing in a p31comet-dependent manner. (A) HelaS3 stably expressing histone H2B-GFP cells were transfected with the indicated siRNA duplexes for 48 h, treated with thymidine for 24h and analyzed by time lapse video microscopy 9 h after thymidine release. Box-and-whisker plot showing the elapsed time (min) between NEBD and anaphase onset/cell death for individual cells. Thirty cells per condition were counted. Mitotic cell death occurred exclusively in the p31comet siRNA sample in 6/30 cells. **(B)** The same dataset displayed in (A) appears plotted using a logarithmic scale. **(C)** Epistatic relationship between p31comet, Mad2 and the APC/C according to (B-C). **(D)** HelaS3 stably expressing histone H2B-GFP cells were transfected with the indicated siRNA duplexes and synchronized according to Fig. 33A. Nine hours following thymidine release they were analyzed by time lapse video microscopy. Box-and-whisker plot showing the elapsed time (min) between NEBD and anaphase onset/cell death for individual cells. Thirty cells per condition were counted. Mitotic cell death occurred exclusively in the p31comet siRNA sample in 4/30 cells. **(E)** The same dataset displayed in (D) appears plotted using a logarithmic scale. **(F)** Epistatic relationship between Tpr, p31comet and Mad2 according to (D-E). Lower and upper whiskers in (A-B and D-E) represent 10^{th} and 90^{th} percentiles, respectively.

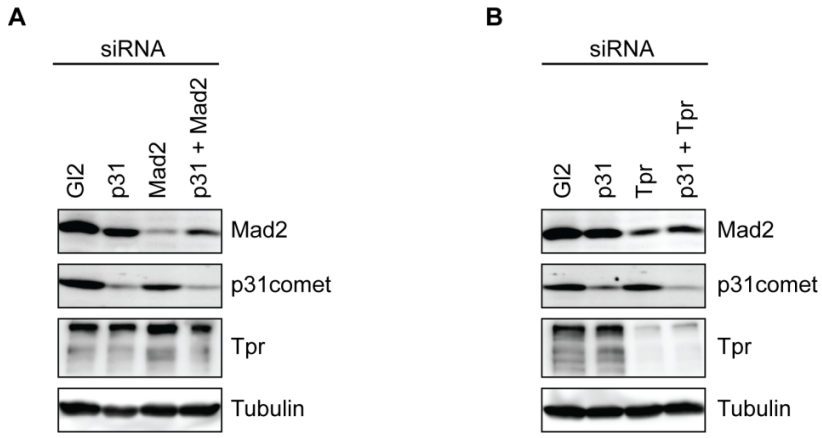

Figure 35 Efficiencies of p31comet, Mad2 and Tpr single and double depletions. (A) HeLaS3 cells were transfected with the indicated siRNA oligonucleotides for a total of 48 h and synchronized as for Fig. 34A-C. Lysates were obtained and analyzed by Western blot with the indicated antibodies. **(B)** HeLaS3 cells were transfected with the indicated siRNA oligonucleotides for a maximum of 72 h and synchronized as for Fig. 34D-F, i.e. following the protocol shown in Fig. 33A. Lysates were obtained and analyzed by Western blot with the indicated antibodies.

Analysis of the post-translational modifications and interaction partners of Mad1:C-Mad2

Given the availability of a monoclonal antibody that is capable of recognizing selectively C-Mad2, we set out to look for interacting partners of Mad2 and specifically of its closed conformer in an unbiased approach. To this end, we immunoprecipitated C-Mad2 from cells arrested in prometaphase by the addition of nocodazole and resolved the immune complexes by SDS-PAGE. All the Coomassie stained bands that were specifically appearing in the $CM2^{276}$ IP and that were absent in the IgG pre-cleared of the cell lysate were analyzed by triptic digestion followed by LC-MS/MS based peptide identification. In addition to Mad2 itself, Mad1 was found enriched in the immune complexes to a nearly 1:1 stoichiometric ratio (Fig. 36A). Additional proteins identified included the mitotic checkpoint complex (MCC) components BubR1 and Bub3. Cdc20 itself was not identified in this MS analysis due to the fact that the protein co-migrated

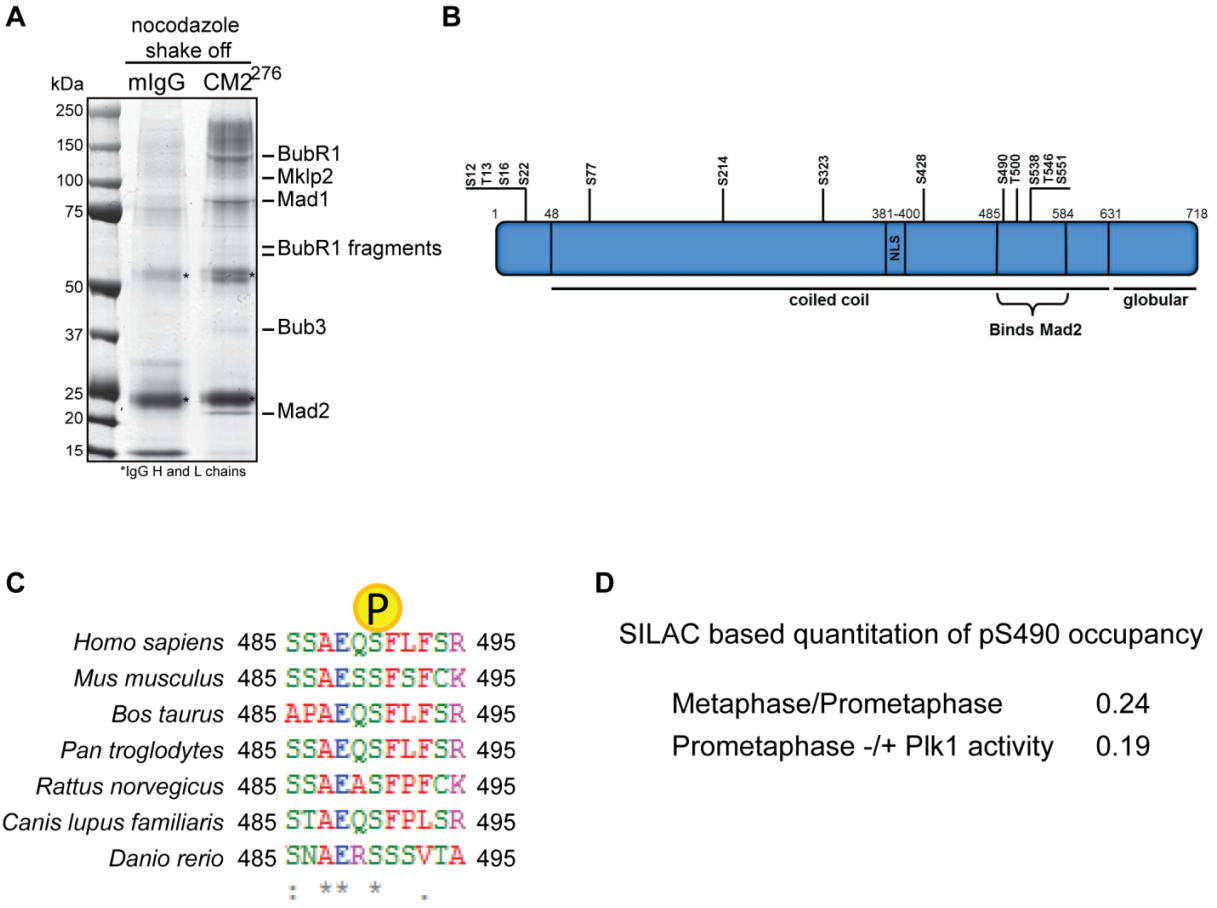

Figure 36 Interacting partners and phosphorylation sites of Mad1:C-Mad2. (A) Coomassie Brilliant Blue (CBB) staining of mouse unspecific IgGs (mIgG) and CM2^{276} immunoprecipites resolved on a 4–12% NuPAGE gel. About 15 mg mitotic HeLa S3 cell lysate was precleared by mIgGs followed by CM2^{276} IP. The indicated bands were excised, triptic in-gel digestion was performed followed by LC-MS/MS based identification. The first Mascot hit for each band is indicated. **(B)** Schematic showing Mad1 phosphorylation sites identified by mass spectrometry. **(C)** ClustalW alignment of residues 485-495 of human Mad1 and the orthologs of the indicated organisms. The "P" circled in yellow indicates the position of the identified phospho-site (pS490). **(D)** The relative phosphorylation levels, as identified by SILAC labeling and mass spectrometry, comparing Metaphase (nocodazole) with Prometaphase (MG132), both synchronizations performed as described in Fig. 17B or monopolar prometaphases -(TAL)/+(Monastrol) Plk1 activity.

with the antibody heavy chain and the corresponding band was not analyzed. Not surprisingly, these established interacting partners of Mad2 could be co-precipitated by CM2^{276} due to the fact that they were either ligands of C-Mad2 (Mad1 and Cdc20) or interacting partners of C-Mad2 through Cdc20 (BubR1 and Bub3). In addition, the mitotic kinesin-like protein 2 Mklp2 (Neef et al, 2003) was also found enriched in the

immune complexes. A recent study by Lee and co-workers has also described Mklp2 as an interacting partner of Mad2 and biochemical analyses described in the study are also consistent with the notion that Mklp2 interacts specifically with the closed conformer of Mad2 upon SAC activation (Lee et al, 2010). The two remaining gel slices analyzed by LC-MS/MS in the region between 50 and 75 kDa of the SDS-PAGE separation led to the identification of peptides of BubR1. Interestingly, BubR1 has been identified as a caspase substrate upon apoptosis (Kim et al, 2005; Mahrus et al, 2008). Our data is therefore consistent with the notion that a population of the cell sample used in this experiment was undergoing apoptosis at the harvest time (a possible consequence of the nocodazole arrest) and that BubR1 incorporated in the MCC underwent caspase-dependent cleavage. In solution digest of $CM2^{276}$ immunoprecipitates obtained in the same conditions led to the identification of one peptide of the 270 kDa protein Tpr (data not shown). As C-Mad2 binds to its ligands with strong affinity, further evidence would be required to support the notion that Tpr is a novel C-Mad2 ligand, but our data are consistent with the notion that Tpr can, directly or indirectly, bind the closed conformer of Mad2 in a dynamic fashion.

Since Mad2 has been described as phosphoprotein (Wassmann et al, 2003), we performed phosphopeptide enrichment on triptic digests of $CM2^{276}$ eluates in order to address whether the closed conformer of Mad2 undergoes phosphorylation. Despite repeated attempts, we failed to identify phosphopeptides of Mad2 in interphase, prometaphase and metaphase samples (synchronized as shown in Fig. 17B, data not shown). In support of this, recent work suggested that the phosphorylation of Mad2 stabilizes the open conformation (Kim et al, 2010). In striking contrast, Mad1 enriched in

$CM2^{276}$ eluates appeared heavily phosphorylated, with 13 phosphorylation sites being identified (Fig 36 B). Several of them clustered, in either the N-terminus or in the region comprised within 485-584 (Fig. 36B). Since these two regions are required for Mad1 KT-localization and Mad2 binding, respectively (Chung & Chen, 2002; Sironi et al, 2002), it is likely that Mad1 phosphorylation plays a crucial regulatory function. Mad1 has been described as an Mps1 substrate in yeast, where its phosphorylation correlates with SAC activation, suggesting that Mad1 is a key Mps1 substrate for SAC functionality (Hardwick et al, 1996). The fact that human Mps1 can phosphorylate Mad1 *in vitro* (Santaguida et al, 2010) and that Mps1 activity is required for Mad1 KT localization (Martin-Lluesma et al, 2002) suggests that Mad1 is a conserved substrate for Mps1 kinase, but a thorough analysis of a potential regulation of Mad1 by direct Mps1 phosphorylation is missing. In addition, Mad1 has been proposed to be a substrate of Plk1 (Chi et al, 2008; Santamaria et al, 2010) and both Mps1 and Plk1 kinases displayed a similar consensus for the target motif (Dou et al, 2011). In order to pinpoint the more relevant phosphorylation sites for Mad1 regulation, we performed a comparison of the phosphorylation site occupancy between prometaphase and metaphase. Among the sites identified, pS490 appeared to be strongly downregulated upon SAC silencing, displaying less than 25% of the occupancy observed in prometaphase (Fig. 36D). Importantly, this conserved phosphorylation site (Fig. 36C) required Plk1 activity to become phosphorylated, since S490 occupancy decreased to less than 20% in Plk1 inhibited samples (through the use of the small molecule inhibitor of Plk1 TAL (Santamaria et al, 2007)) when compared to samples were Eg5 was inhibited (through the use of monastrol (Mayer et al, 1999)) (Fig. 36D). These and other

data (Santamaria et al, 2010 and Santamaria, unpublished) are consistent with the notion that S490 undergoes SAC dependent phosphorylation by Plk1 and justified the generation of a phospho-specific antibody recognizing Mad1-pS490.

One serum appeared to recognize preferentially Mad1 when phosphorylated, both in WB and immunofluorescence (Fig. 37). S490 could be phosphorylated by Plk1 directly (Fig. 37A) and, consistent with our mass spectrometric analyses, Mad1 appeared phosphorylated at S490 during SAC activation (Fig. 37B-C). Interestingly, Mad1 appeared non-phosphorylated in interphase cells, it became phosphorylated at S490 at the NPCs concomitant with chromosome condensation in early prophase cells and remained phosphorylated till prometaphase while localizing at KTs (Fig. 37C). The inhibition of Plk1 in the above stages did not lead to a major Mad1 de-localization, but drastically reduced the phosphorylation of S490 (Fig. 37D). Our data are consistent with the notion that Mad1 undergoes direct phosphorylation by Plk1 at S490 at NPCs upon mitotic entry and this modification is maintained upon Mad1 re-localization at KTs during prometaphase. In metaphase, upon SAC silencing, S490 undergoes marked de-phosphorylation, indicating that this phosphorylation event correlates with SAC activation. At first glance, the fact that a drastic reduction of Mad1 phosphoryaltion by inhibition of Plk1 did not abolish the SAC functionality suggests that pS490 phosphorylation is dispensable for the SAC. It should nevertheless be noticed that only trace amounts of active Mad1 can support the SAC (see above) and that pS490 could potentially be phosphorylated -to a much lesser but yet sufficient extent- by residual Plk1 and/or Mps1 activity in TAL treated cells. To this end, similar analyses inhibiting Mps1 intra-mitotically (i.e. preserving Mad1 KT localization), revealed that Mps1 is also

required for *in vivo* phosphorylation of Mad1-S490 (Anna Baron, data not shown), suggesting Mad1 might be phosphorylated by both kinases on the same residue. Future work will have to strengthen this notion and to better define the relationship between Mps1 and Plk1 in KT SAC signaling.

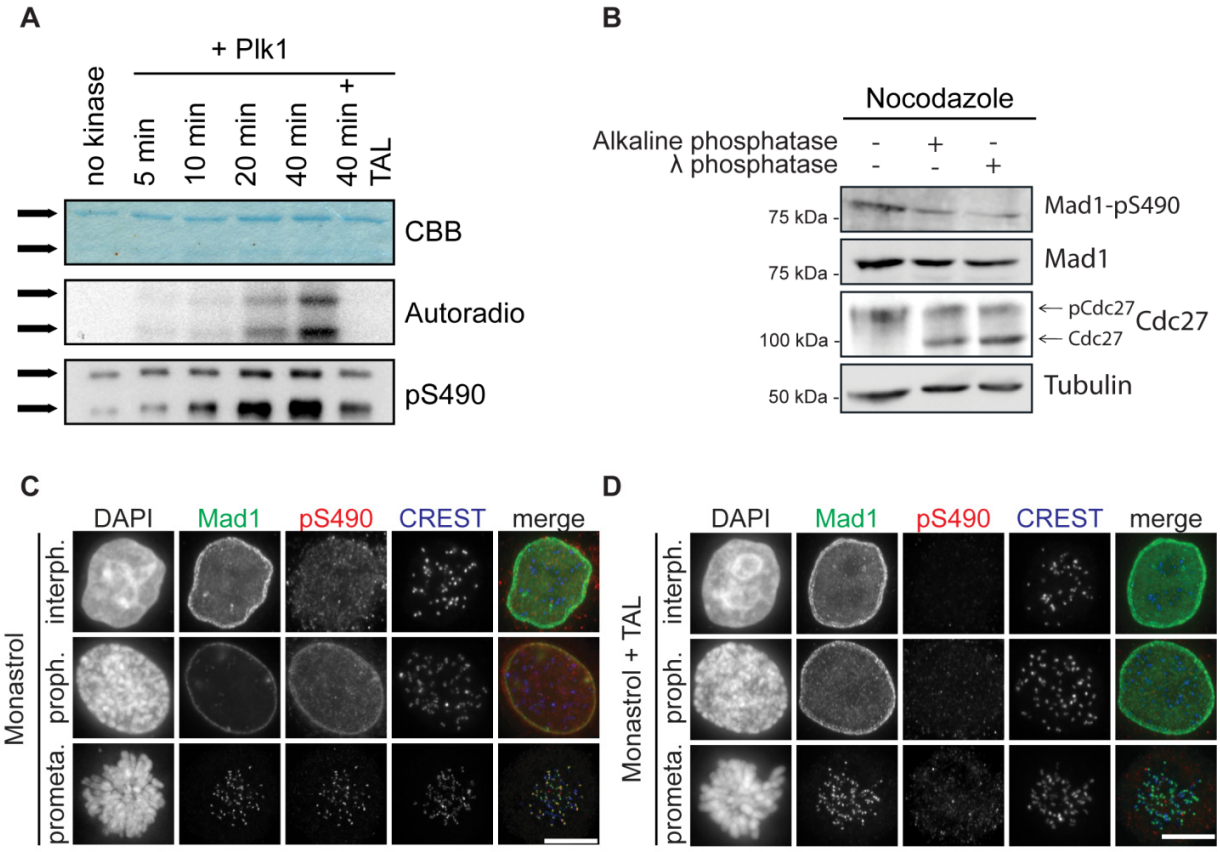

Figure 37 Direct phosphorylation of Mad1-S490 by Plk1 upon SAC activation. (A) In vitro phosphorylation of recombinant MBP-Mad1 in either kinase buffer alone, or by recombinant Plk1 for the indicated times with/without the Plk1 inhibitor TAL. The upper panel shows Coomassie Brilliant Blue staining (CBB) staining of the SDS-PAGE gel, the central panel shows the corresponding autoradiography and the lower panel shows WB analysis using pS490 antibody. The two arrows indicate the position of full length MBP-Mad1 and a degradation product for each panel. **(B**) HeLaS3 cells were arrested with nocodalole for 12 h and the obtained lysates were treated with either buffer alone or with the indicated recombinant phosphatases. Lysates were analyzed by WB with the indicated antibodies. **(C)** HeLaS3 cells arrested with thymidine for 24 h were released for 10 h in the presence of Monastrol and fixed with PTEMF. After fixation, Mad1, Mad1-pS490 and CREST were stained by primary and antibodies (green, red and blue, respectively), followed by secondary antibodies displayed in the indicated colors. **(D)** HeLaS3 cells were treated as described in (C) using both Monastrol and TAL. Scale bars = 10 µM. Experiments in B-D were performed by Anna Baron.

Discussion

In this thesis we have used a conformation-specific mAb ($CM2^{276}$) to study mechanistic aspects of SAC signaling in living human cells. We demonstrate that $CM2^{276}$ selectively recognizes one of the two Mad2 conformers, namely Closed-Mad2. This powerful tool provided a unique opportunity to probe Mad2 conformation and directly validate several aspects of the template model for SAC signaling in a cellular context. In particular the $CM2^{276}$ antibody allowed us to demonstrate that Mad1 is required for the generation of C-Mad2 *in vivo*, being therefore necessary for initiating and maintaining the SAC, thus providing strong support for the template model. We also demonstrate that mitotic timing depends on the Mad1:C-Mad2 template. This latter observation suggests that, from a mechanistic perspective, the SAC and the proposed mitotic timer are closely related if not identical. The $CM2^{276}$ antibody allowed us also to reveal a role for p31comet in capping C-Mad2 at particular subcellular locations and to implicate Mps1 and Tpr in the regulation of this process.

The two state behavior of Mad2 in the cell

The template model of SAC signaling hinges crucially on the existence and interconversion of two conformers of Mad2 (Luo & Yu, 2008; Mapelli & Musacchio, 2007). Using $CM2^{276}$ we have been able to directly visualize the proposed two state behavior of Mad2 within living cells. The fact that the C-Mad2 mAb could only immunoprecipitate Mad2 when bound to interaction partners strongly supports the concept that liganded but not free Mad2 adopts the Closed conformation and our data indicate that this conclusion holds true throughout the cell cycle. Importantly, structural analysis of Mad2 in complex with its ligands had been carried out using full length Mad2 bound to rather short truncations of either Mad1 or Cdc20 (99 out of 718 and 39 or less

out of 499 amino acids, respectively (Luo et al, 2000; Luo et al, 2002; Sironi et al, 2002). Importantly, later work has suggested that the binding of Mad2 to full length Cdc20 might differ concerning the affinity, dynamics and therefore binding mode (Kulukian et al, 2009; Nilsson et al, 2008). Our work supports the notion that the closed conformer of Mad2 -as it can be produced in *in vitro* reconstitutions- binds to its ligands Mad1 and Cdc20 in living human cells.

Concerning the equilibrium between the two conformers of free Mad2, most of Mad2 was released as a free moiety when Mad1 was depleted, and this free Mad2 existed in the Open conformation (as it was not recognized by $CM2^{276}$). Our data demonstrate that Mad1 is strictly required for Mad2 to adopt the Closed conformation *in vivo*. Previous work had already suggested that free Mad2 adopts the Open conformation in cells (Luo et al, 2004), and this important notion had been incorporated in the template model (De Antoni et al, 2005). However, a recent *in vitro* reconstitution study has also suggested that Mad1:C-Mad2 is able to generate unliganded C-Mad2, which then binds Cdc20 with higher efficiency than O-Mad2 (Yang et al, 2008). In our study, we did not detect significant levels of unliganded C-Mad2, suggesting that, *in vivo*, the life-time of this species must be short, if it exists at all. As C-Mad2 is the energetically favored conformer *in vitro* (Luo et al, 2004), this raises the question of why is C-Mad2 not accumulating as unliganded entity in the cell. Such an accumulation could, in the absence of a compensatory masking of the C-Mad2 dimerization interface, trigger the unscheduled activation of C-Mad2 dependent catalysis, which would be probably sufficient to promote unscheduled binding of Cdc20. Consistent with this notion, the microinjection of recombinant Mad2-L13Q (locked in the closed

conformation) triggered a metaphase arrest that was absent upon microinjection of Mad2-V193N (locked in the open conformation). Also, the p31comet depletion by siRNA was sufficient to trigger association of C-Mad2 with Cdc20 in thymidine (G1-S) arrested cells (data not shown). Our data support therefore the notion that the amounts of free C-Mad2 in the cell should be tightly controlled and raise the possibility that in the cytoplasm of living cells an as yet unknown mechanism actively promotes the Open conformation of unliganded Mad2. Interestingly, Mad2 is reportedly a phosphoprotein (Wassmann et al, 2003) and its phosphorylation affects equilibrium between the two conformers, stabilizing O-Mad2 (Kim et al, 2010). Mad2 phosphorylation might therefore represent one mechanism involved in the stabilization of free Mad2 in the open conformation.

Mad1:C-Mad2 initiating and maintaining the SAC

Several predictions of the template model find strong support in the microinjection experiments carried out in this thesis. The injection of $CM2^{276}$ abolished SAC activation, thus confirming the template model's prediction that pinpoints the dimerization interface as the active site of C-Mad2 catalysis (De Antoni et al, 2005; Kulukian et al, 2009; Lad et al, 2009; Simonetta et al, 2009). One interesting emerging view is that the C-Mad2:Cdc20 complex generated at KTs is not the final inhibitory component of the SAC, but that C-Mad2 acts catalytically - rather than stoichiometrically - to promote Cdc20 binding to BubR1 (Kulukian et al, 2009; Nilsson et al, 2008). From this perspective, it is interesting that interference with the Mad1:C-Mad2 KT template by injection of $CM2^{276}$ into cells in which the BubR1:Cdc20 complex was already functional, also caused an abrupt extinction of the SAC. This indicates that the continuous production of new C-Mad2:Cdc20 is required for maintaining a SAC-dependent arrest,

even after BubR1 had been loaded onto Cdc20. This in turn suggests that Mad2 is required for SAC maintenance by exerting a BubR1-independent inhibitory action on Cdc20 and/or by continuously replenishing an intrinsically unstable BubR1:Cdc20 complex (Burton & Solomon, 2007; King et al, 2007; Nilsson et al, 2008).

One interesting hypothesis in the SAC field is that cytoplasmic C-Mad2:Cdc20 can promote its own formation through an autocatalytic loop (De Antoni et al, 2005). This idea finds experimental support through *in vitro* experiments (Lad et al, 2009; Simonetta et al, 2009), but the *in vivo* contribution of a cytosolic branch of Mad2 template activity remains to be tested. From this perspective, it is interesting that microinjection (into nocodazole arrested cells) of an anti-Mad1 mAb (targeting exclusively the Mad1:C-Mad2 complex) was at least as efficient in causing a SAC override as injection of $CM2^{276}$ (targeting both KT-associated Mad1:C-Mad2 and cytosolic C-Mad2:Cdc20 complexes). Although these quantitative differences may well reflect a difference in the function-neutralizing potency of the injected antibodies, our observation clearly argues that a C-Mad2:Cdc20 autocatalytic loop is not in itself sufficient to maintain a SAC arrest. Interestingly, an *in silico* model of the SAC that accounts for key features of it and is based on measured biophysical parameters, excluded the possibility of a cytoplasmic amplification of the cell cycle inhibitor through an autocatalytic loop, as the activity of the inhibitor would become self-sustained and therefore impossible to be extinguished (see Ciliberto & Shah, 2009 for review; Doncic et al, 2005).

KT-dependent control of mitotic timing

Careful live cell studies in siRNA-treated human cells have led to the proposal that anaphase onset depends on a mitotic timer that involves Mad2 and BubR1, but not

Mad1 (Meraldi et al., 2004). Genetic analyses in *Drosophila* are consistent with such a timer model in that null mutants for Mad2 and BubR1 accelerate the traverse of mitosis to a slightly bigger extent than abrogation of Mad1 function (Buffin et al, 2007; Emre et al, 2011; Rahmani et al, 2009). It should also be noted that the contributions of Mad2 and BubR1 to mitotic timing in flies appear to be minor and, remarkably, the SAC is not strictly required for undisturbed mitoses in this organism (Buffin et al, 2007), suggesting that there is no need to extend the mitotic duration beyond the duration of APC/C activation in the absence of the SAC in this organism.

In the present thesis, injection of cells with antibodies directed at either C-Mad2 or Mad1 triggered a striking mitotic acceleration. These results cannot readily be reconciled with the proposal that Mad2 (together with BubR1) is part of a “cytoplasmic mitotic timer”, which works independently of the SAC (Meraldi et al, 2004). Although we cannot formally exclude that functional neutralization by mAb microinjection triggers a different (and even stronger) phenotype than the reduction of the corresponding proteins by siRNA-mediated depletion, we suspect that the reported differences in the phenotypes observed after siRNA-mediated depletion of Mad1 or Mad2 (Meraldi et al, 2004; our unpublished data) reflect differences in the functionality of residual protein levels. In particular, Mad2 depletion simultaneously affects both the KT-associated Mad1-bound Mad2 population (C-Mad2) and the cytoplasmic pool of Mad2 that awaits catalytic conversion (O-Mad2). Hence, even partial reduction of Mad2 readily causes acceleration of traverse through mitosis (Hubner et al, 2010). Conversely, Mad1 depletion affects exclusively the catalyst (the Mad1:C-Mad2 complex) and, therefore, minor amounts of residual Mad1 might be sufficient to partly support the checkpoint,

thus preventing mitotic acceleration. A possible caveat of the study by Meraldi and colleagues is that SAC and “timer” functionalities have been assessed using two different assays; on one hand cells have been challenged with nocodazole and the mitotic index has been counted at an end point. In this case Mad1 depletion resulted in a lower mitotic index when compared to control samples. On the other hand, live cell imaging experiments were carried out to monitor mitotic timing. In the latter case, Mad1 depletion did not accelerate the mitotic traverse beyond traverse speed of the bulk of control cells. When we monitored the effect of nocodazole challenge in a live cell imaging based assay, neither the Mad1 siRNA duplex published by Meraldi and colleagues, nor the one described herein (that produces larger protein downregulation), triggered a complete SAC abolishment but just displayed enhanced mitotic slippage (i.e. cells maintained the mitotic status for 4-6 h, data not shown). Our data suggest therefore that none of the Mad1 siRNA duplexes tested (for up to 72 h, including double transfection protocols) triggered a complete SAC abrogation, easily explaining the lack of mitotic timing acceleration.

A recent study has also implicated the SAC kinase Mps1 in the regulation of mitotic timing suggesting that Mps1 is also required during interphase to form an anaphase inhibitor in a KT independent manner (Maciejowski et al, 2010). However, as our present data demonstrate that functional abrogation of Mad1:C-Mad2 also accelerates mitotic progression, we would predict that complete neutralization of any SAC component, including Mps1, will translate into faster progression through mitosis. Most importantly, the consequences of Mps1 inhibition were indistinguishable, regardless of whether the kinase was inhibited already during interphase or only during

mitosis. Thus, interphase activity of Mps1 does not significantly contribute to the timing of mitotic progression. Collectively, our results on the role of Mad1:C-Mad2 and Mps1 should prompt a reconsideration of the distinction between SAC and mitotic timer.

What determines then the mitotic duration in the absence of the SAC? Rise and fall of CDK1 activity drive eukaryotic cells in and out of mitosis. Delaying Cyclin B1 degradation prolongs CDK1 activity in an unscheduled fashion, leading to an extended mitotic duration (Wolf et al, 2006), whereas the premature inhibition of CDK1 activity triggers mitotic exit (Potapova et al, 2006). Crucial events triggered by firing of CDK1 are nuclear envelope breakdown and APC/C activation; live cell imaging analyses have shown that these two events are tightly coupled in a temporal fashion, as Cyclin A degradation commences upon NEBD (Di Fiore & Pines, 2010; Gavet & Pines, 2010a; Gavet & Pines, 2010b). Cyclin B1 and Cyclin A degradation at a single cell level display nearly identical degradation kinetics, with a variable time gap depending on completion of chromosome bi-orientation, provided by the SAC (Di Fiore & Pines, 2010 and J. Pines, unpublished data). Interestingly, the duration of mitotic traverse in the absence of the SAC and the time elapsed between disappearance of Mad2 signal from KTs and anaphase onset are nearly identical (Howell et al, 2000; Meraldi et al, 2004). In the absence of the SAC, the time gap between degradation of Cyclin A and B1 is abolished and the timing of anaphase onset might depend exclusively on the speed by which the APC/C can degrade Cyclin A and B1 following CDK1 firing.

Regulation of Mad1:C-Mad2 through p31comet dependent capping

Considering the central role of the Mad1:C-Mad2 complex in SAC signaling it is clearly important to understand its regulation in time and space. On the one hand, KTs provide an essential microenvironment for the activity of the Mad1:C-Mad2 complex, as

indicated by the observation that the complex is removed from KTs in a dynein-dependent manner upon SAC silencing (Howell et al, 2001) and interference with this removal generates a SAC-dependent arrest (Gassmann et al, 2010; Griffis et al, 2007). On the other hand, SAC signaling is known to be inhibited by p31comet (Habu et al, 2002; Xia et al, 2004). The work carried out during this thesis provides further insight into the role of this protein. Immunostaining with $CM2^{276}$ revealed that the accessibility of C-Mad2 is controlled by p31comet at multiple locations. In particular, our siRNA experiments show that the dimerization interface of C-Mad2 is masked by p31comet at NPCs and spindle poles. The facts that p31comet siRNA could lead to unscheduled formation of Mad2:Cdc20 complex in interphase and to a metaphase arrest in mitosis (data not shown and this work, respectively) are consistent with the notion that Mad1:C-Mad2 that accumulates at any subcellular structure is capable of catalysis and this has to be suppressed by reducing the availability of the C-Mad2 dimerization interface.

More surprisingly, p31comet could associate with Mad1:C-Mad2 also during the SAC at KTs. In support of this conclusion, p31comet could be detected at KTs (Habu et al, 2002; this study). This raises the question of why a protein implicated in silencing of the SAC associates with the catalytic source of the SAC signal already during prometaphase. One possible explanation is that p31comet begins to cap and functionally inactivate individual C-Mad2 proteins as soon as a threshold of bipolar MT attachment to KTs has been reached, perhaps in preparation for subsequent stripping of the Mad1:C-Mad2:p31comet complex from KTs. The fact that p31comet localization as well as p31comet dependent masking could be observed not only in unperturbed prometaphases, but also in nocodazole arrested cells (data not shown) seems to

exclude this possibility. Alternatively, it would be premature to exclude that p31comet may have not only an inhibitory but also an activating role in SAC signaling, similar to the dual role of securin in the regulation of separase (Hornig et al, 2002). Future studies will have to explore these possibilities.

In addition, it will be important to better understand the role of posttranslational modifications in the formation and activity of KT-associated complexes (Burke & Stukenberg, 2008; Hewitt et al, 2010).

Is there a Tpr-Mps1 axis controlling Mad1:C-Mad2?

We could show that the detectability of C-Mad2 by $CM2^{276}$ decreases more sharply upon Mps1 intra-mitotic inhibition compared to the decrease observed for Mad1. The facts that 1) depletion of p31comet by siRNA could revert this phenomenon (this work), 2) Mps1 sustains the SAC by promoting not only the localization but also the activity of Mad1:C-Mad2 at KTs (Hewitt et al, 2010) and 3) p31comet can be directly phosphorylated by Mps1 *in vitro* (A. Musacchio, personal communication), are consistent with the notion that Mps1 sustains the SAC by promoting the dissociation between Mad1:C-Mad2 and p31comet. This simple model is challenged by the observation that the sharp decrease of C-Mad2 detectability over Mad1 observed when using $CM2^{276}$ following Mps1 intra-mitotic inhibition, can also be reproduced using $CM2^{2F12}$ (recognizing C-Mad2 regardless of its binding to p31comet, see Appendix) in the same conditions (Conrad von Schubert). This raises the possibilities that abrogation of Mps1 activity is either promoting a local dissociation of C-Mad2 from Mad1 in a p31comet dependent manner or, most probably, promoting the assembly of an inhibitory complex comprising p31comet and other factors masking both the epitopes for both $CM2^{276}$ and $CM2^{2F12}$.

The KTs localization of both Mad1 and Mad2 has become widely accepted as a marker for the lack of KT-MT attachment (see Maresca & Salmon, 2010 for review). The two proteins also tightly interact with each other, resisting up to 4 M urea and 2 M NaCl (Sironi et al, 2001). Also, Mad1 is saturated with Mad2 in the cell (Chung & Chen, 2002; Shah et al, 2004). It is therefore not surprising that in most circumstances the presence of Mad1 at KTs determines the simultaneous presence of Mad2. Exceptions to this include siRNA depleted cells for the proteins PICH and Tao1 (Baumann et al, 2007; Draviam et al, 2007) and cells in which Mps1 activity has been inhibited following KT-recruitment of Mad1 and Mad2 (Hewitt et al, 2010). In the case of PICH and Tao1 siRNA, the selective loss of Mad2 but not Mad1 from KTs appeared to depend on a downregulation of Mad2 mRNA induced by a subset of the siRNA duplexes targeting PICH and Tao1 (Hubner et al, 2010; Westhorpe et al, 2010) and not on an induced dissociation between Mad1 and Mad2, as originally suggested (Baumann et al, 2007; Draviam et al, 2007). For the intra-mitotic inhibition of Mps1, the lack of KT detection of Mad2 by immunostaining has been shown to correlate with a selective loss of O-Mad2 but not of C-Mad2 from KTs, prompting the authors to propose that Mad2 antibody staining in their setting primarily recognized O-Mad2 (Hewitt et al, 2010). Using $CM2^{276}$ we could also observe a decrease in C-Mad2/Mad1 fluorescence in similar experiments. We reasoned that an abrogation of Mad2 conformational dimerization at KTs could depend on an increased masking of the C-Mad2 dimerization interface by p31comet. The fact that the observed decrease of $CM2^{276}$/Mad1 fluorescence could be reverted by p31comet siRNA lends strong support to this idea.

Another circumstance in which the KT localization of Mad1 and Mad2 could be uncoupled is the siRNA-mediated depletion of Tpr (Lince-Faria et al, 2009). Also in this case, the selective loss of Mad2 detection from KTs could be confirmed utilizing $CM2^{276}$ and could be reverted by co-depletion with p31comet, suggesting that Tpr siRNA may act on Mad1:C-Mad2 similarly to the Mps1 intra-mitotic inhibition, i.e. through p31comet. The idea that Tpr and Mps1 both act in promoting the sustained activity of Mad1:C-Mad2 in the same pathway finds experimental support in the observation that Mps1 appeared delocalized from KTs in fly cells depleted of Tpr (Lince-Faria et al, 2009). Whether this is the case also in human cells will have to be tested, but the observation that overexpression of catalytically inactive Mps1 led to a massive accumulation of Tpr at prometaphase KTs of human cells (that is usually undetectable at those structures, Helder Maiato´s group, in preparation) supports the notion that there is a functional interplay at KTs between Tpr and Mps1 that will require further investigation.

The body of evidence discussed circumstantiates the notion that Tpr promotes KT localization of Mps1 which in turn may be required for the inhibitory phosphorylation of p31comet leading to its dissociation from Mad1:C-Mad2. However, this analysis has so far neglected that the Tpr siRNA duplex employed for this work also affected the protein levels of Mad2. Unlikely PICH and Tao1 depletions, Tpr siRNA did not impact on Mad2 mRNA levels (H. Maiato, personal communication). Since Tpr binds Mad2 directly (Lee et al, 2008), it is possible that Mad2 will become less stable in the absence of its interacting partner Tpr and contribution of the latter to the SAC could therefore be pleiotropic. Even a minor decrease in Mad2 protein levels is sufficient to compromise SAC signaling and it would not be necessary to invoke further effects beside the Mad2

downregulation for explaining the SAC function of Tpr. Nevertheless, both the $CM2^{276}$ undetectability of C-Mad2 at KTs and the acceleration of mitotic timing observed upon Tpr siRNA could be partly rescued by co-depletion of p31comet and they could both be phenocopied by small molecule inhibition of Mps1 within minutes, situation in which the Mad2 protein downregulation is unlikely to play a role. Future approaches such as the identification of the different Tpr determinants responsible for the different functions (such as interaction with Mad2 and promotion of Mps1 KT localization) will allow better comprehending the role of Tpr in SAC signaling.

Materials and Methods

Cloning procedures

For cloning of p31comet (MAD2L1BP), a cDNA clone (IRAUp969G0825D) was obtained from the Deutsches Ressourcenzentrum für Genomforschung (RZPD). The p31 coding sequence was amplified with the following oligonucleotides: CGGGATCCGCGGCGCCGGAGGCGGA and CCGCTCGAGTCATTCACTCGCGGAAGCC. A BamHI/XhoI digest of the PCR product was cloned into a pET28a(+) vector (Novagen) and a pcDNA3.1 vector (Invitrogen) that had been modified replacing the CMV with the SV40 promoter, carrying N-terminal 6His and 3xmyc tags, respectively. p31comet^{QA-FA} (Q83A-F191A; Yang et al., 2007) was generated by using the following oligonucleotides (AAGCATATCATGTATGCACGCCAGCAGCTCCCT and TGTTTGCGCCGTCTCGCCCGAGCCATATTCATG with their reversed complements) with a QuickChange Site-Directed Mutagenesis kit (Stratagene). All other plasmids were described elsewhere or were generated with similar molecular cloning approaches by modifying existing plasmids that have been already described (Mapelli et al., 2006; Mapelli et al., 2007; Martin-Lluesma et al., 2002).

Production and purification of recombinant proteins and antibodies

A polyclonal antibody against p31comet (741212) was generated by immunization of rabbits (Charles River Laboratories) with 6His-p31comet expressed in *E. coli*. IMAC purification of p31comet was performed using a HisTrap HP column (GE Healthcare), following the manufacturer´s instructions. After purification, p31comet was dialyzed against 50 mM Tris-HCl pH 7.5, 300 mM NaCl, 10% Glycerol, 2 mM β-

mercaptoethanol. The p31comet Ab was purified by Affi-Prep protein A matrix (Bio-Rad Laboratories).

Anti-pS490 Mad1 polyclonal antibody was generated by Anna Santamaria by immunizing rabbits with a KLH-conjugated phosphopeptide (H-CSAEQpSFLFS-OH) and the serum (3rd "bleed" of rabbit 833976) was used for immunofluorescence and Western blot experiments.

CM2^{276} (clone 107-276) has been generated by Andreas Uldschmid. Briefly, CM2^{276} (IgG1k) was generated against GST-tagged full-length human Mad2 by repeated subcutaneous injection of 100 µg of antigen into Balb/c mice using aluminium hydroxide as an adjuvant. Spleen cells were fused with PAIB$_3$Ag81 mouse myeloma cells. Supernatant screening was performed by ELISA.

Mad1 monoclonal antibodies (117-468 and 117-470, both IgG1) were generated by Andreas Uldschmid against full-length recombinant MBP-Mad1 expressed in *E. coli*. MBP-Mad1 was purified using an MBPTrap HP column (GE Healthcare) and immunization of mice has been carried out as for CM2^{276}.

CM2^{2F12} has been generated against IMAC purified 6His-tagged full length human Mad2. Injection and supernatant primary screening (performed using GST-tagged full length human Mad2) were performed by Moravian Biotechnology. See Appendix I for characterization.

Myc mAb (9E10) (Evan et al., 1985) has been described previously. All mAbs were purified using HiTrap protein G HP columns (GE Healthcare).

6His-Mad2^{WT}, 6His-Mad2^{mutants} were expressed purified as follows: BL21-CodonPlus(DE3)-*RIL* (Novagen) were transformed with plasmids encoding 6His-

Mad2$^{WT/mutants}$ (Sironi et al., 2001, Mapelli et al., 2007) and grown in LB medium at 30°C until O.D.$_{600}$ = 0.5 was reached. Bacteria were grown further at 25 °C until O.D.$_{600}$ = 0.75 was reached. Induction was then performed by addition of 0.5 mM IPTG for 7h at 23 °C. Lysis and IMAC purification using a HisTrap HP column (GE Healthcare) were performed at 4°C. Recombinant proteins were stored at -80 °C in PBS. GST-Cdc20$^{111-138}$ was purified as described previously (Mapelli et al., 2006).

Competition assays

For GST-pulldown experiments, a complex between GST-Cdc20$^{111-138}$ and His-tagged Mad2^{WT} was generated on Glutathione Sepharose 4B beads (GE Healthcare) as described before (Mapelli et al, 2007). Competition in binding to C-Mad2 was assessed by adding CM2^{276} to the beads at 0.2 μM together with p31comet at 0.6, 3.6 or 9 μM. The corresponding negative control was performed by replacing p31comet with equal concentrations of hSpindly$^{1-444}$. For the CM2^{276} and Mad2$^{\Delta C}$ competition, Mad2$^{\Delta C}$ was added to the beads at a concentration of 0.35 μM together with CM2^{276} at concentrations of 0.15, 0.45 or 1.35 μM. The corresponding negative control was performed by replacing CM2^{276} with equal concentrations of Mad1 mAb (117-468). For the sequential absorption experiment, Mad2$^{\Delta C}$ and CM2^{276} were used at concentrations of 0.35 and 0.9 μM, respectively.

Peptide spots array synthesis and antibody binding assay

Peptide arrays were constructed using standard F-moc chemistry on a MultiPep robotic spotter according the manufacturer's instructions (Intavis). Antibody binding to candidate peptides was performed incubating primary antibodies in milk/PBST 5%, w/v, followed by HRP-secondary antibody detection as in normal Western blot experiments.

In vitro kinase assay

In vitro phosphorylation of Mad1 was carried out at 30°C using 500 ng of recombinant MBP-Mad1 and 100 ng of Plk1 kinase in a total volume of 30 µL of BRB80 kinase reaction buffer (80 mM Pipes pH 6.8, 1 mM $MgCl_2$, 1 mM EGTA). Reactions were supplemented with 10 µM ATP and 2 µCi γ-32P-ATP (Amersham Pharmacia Biosciences, Piscataway, NJ). Reactions were stopped by addition of sample buffer. Samples were then resolved by SDS-PAGE and visualized by autoradiography and Western blotting using Mad1-pS490 antibody.

Cell culture and synchronization

Cells were cultured at 37°C, in a 5% CO_2 atmosphere in DMEM (Gibco), supplemented with 10% heat-inactivated fetal calf serum (FCS) and penicillin/streptomycin (100 IU/ml and 100 µg/ml, respectively). For synchronization, thymidine (2 mM), nocodazole (50 ng/ml) (both Sigma Aldrich), MG132 (10 µM, Calbiochem), Mps1-IN1 (10 µM, kindly provided by N.S. Gray), RO-3306 (9 µM, Enzo Life Science), Monastrol (150 µM, Mayer et al, 1999) and TAL (1 µM, Santamaria et al, 2007) were used as described in the figure legends. RO-3306 was used on HeLa Kyoto mCherry-H2B cells due to a better reversibility of the CDK1 inhibition observed in this cell line.

SILAC labeling of cultured cells

For SILAC labeling, HeLaS3 cells were cultured in DMEM formulated with either unlabeled L-lysine and L-arginine or labeled $^{13}C_6$ $^{15}N_4$ –L-arginine and $^{13}C_6$ $^{15}N_2$-L-lysine (Cambridge Isotope Laboratories) at the concentration of 42 and 72 µg/ml respectively, and supplemented with 10% dialyzed fetal bovine serum, 100 units/ ml penicillin, and 100 µg/ml streptomycin. Unlabeled and labeled HeLaS3 cells were synchronized in

mitosis as described in the figure legends. For the assessment of the Plk1 responsiveness of phosphorylation sites, cells were pre-synchronized by single thymidine arrest and released in media containing either TAL or Monastrol for 14 hours.

Transient transfections of plasmid DNA and siRNA duplexes

Plasmid transfections were performed for 36 h using TransIT-LT1 reagent (Mirus Bio Corporation) according to the manufacturer's instructions. siRNA duplexes were transfected using Oligofectamine (Invitrogen) as described previously (Chan et al, 2009). The following siRNA duplexes were purchased from QIAGEN: Mad1-3´UTR-1 (CCACAGGGCAGCAGCAUGA) and Mad1-3´UTR-2 (CUGCUUGGCCUGACCUGCA); p31comet-1 (GAAGAUUGGUUUCGACCCA), p31comet-2 (AUUCAUGGCUGAUGCCUUU) were described previously as part of a SmartPool (Reddy et al, 2007) and used here independently. The Mad2 (Martin-Lluesma et al, 2002), Tpr (Lince-Faria et al, 2009) and control Gl2 duplexes (Elbashir et al, 2001) were described previously. Different siRNA transfections were performed for the following times: p31comet, 48 h; Mad2, 48 h; Tpr, 72 h. For Mad1 depletion that was performed by combining Mad1-3´UTR-1 with Mad1-3´UTR-2 duplexes, transfecting cells twice at 0 and 24 h for a total of 60 h.

Cell extracts, Western blots and immunoprecipitations

Cell lysates and Western blot analysis were performed as described using lysis buffer (20 mM Tris-HCl pH 7.4, 150 mM NaCl, 0.5% IGEPAL CA-630) containing 1 mM DTT, 30 µg/ml RNase A, 30 µg/ml DNase, protease (EDTA-free Tablet, Roche) and phosphatase (Sigma, cocktails 1 and 2) inhibitors. The lysis buffer was applied on dried cell pellets for 30 minutes on ice. Following vigorous pipetting, lysates were clarified by

10 minutes centrifugation at 20.000 g at 4°C and the supernatants were further processed.

Immunoprecipitations against purified Mad2 wild type and mutants were performed using 10 µl of solid Affi-Prep protein A matrix (Bio-Rad Laboratories) pre-coupled with 1 µg/µl of antibody per condition. 0.5 ml of Tris lysis buffer containing 20 or 80 µg of Mad2 (when comparing $Mad2^{WT}$ with $Mad2^{L13Q}$ and $Mad2^{V193N}$ or $Mad2^{WT}$ with $Mad2^{RQ}$, respectively) was added to the beads and incubated at 4°C for 45 min. Immunoprecipitations on cell lysates were performed using 20 µl of solid beads chemically crosslinked to 1 µg/µl of antibody against 2 mg of clarified cell lysate for 2 h at 4°C. The beads were washed three times with Tris lysis buffer and bound species were resolved by SDS–PAGE. The following antibodies were used for Western blot: rabbit anti Mad2 (Bethyl Laboratories, cat. N. A300-301A, 1 µg/ml), rabbit anti Cdc20 (Santa Cruz Biotechnology, cat. N. sc-8358, 1 µg/ml), rabbit anti p31comet (741212, 1 µg/ml), mouse anti Mad1 (clone 117-470, 2 µg/ml), mouse anti α-tubulin (Sigma-Aldrich, cat. N. T9026, 0.2 µg/ml), mouse anti BubR1 (clone 68-3-9 2 µg/ml, Elowe et al, 2007), mouse anti CDC27 (BD Transduction Laboratories, cat. 610454, 0.5 µg/ml), mouse anti Myc (clone 9E10, 1 µg/ml Evan et al, 1985), rabbit anti Tpr (Bethyl Laboratories, cat. N. A300-825A, 2 µg/ml), rabbit anti Mad1-pS490 (3rd "bleed" of rabbit 833976, dilution 1:500). Primary antibodies were detected using HRP-conjugated goat secondary antibodies (Bio Rad) and the ECL (Pierce) fluorescence was detected using a LAS-3000 scanner (Fujifilm).

Mass spectrometry

Mass spectrometry analysis was performed as described previously (Dou et al, 2011), with the assistance of Kalyan Dulla and Roman Körner. Briefly, $CM2^{276}$ IPs were

performed against 30 mg of pre-cleared (using mouse unspecific IgG IP) lysate using 200 µl of beads coupled to 1 µg/µl of antibody. Beads were washed three times in lysis buffer and resuspended in NuPAGE sample buffer (Invitrogen). samples were separated by a 4–12% NuPAGE gel (Invitrogen) and Coomassie Brilliant Blue (CBB)-stained protein bands were in-gel digested by trypsin (sequencing grade, Roche, Germany) as described (Shevchenko et al, 1996). Phosphorylated peptides were enriched using TiO_2 affinity purification with glycolic acid as a modifier (Jensen & Larsen, 2007). Subsequently, tryptic peptides were analyzed by nanoLC-MS/MS using a nanoACQUITY ultra performance liquid chromatography system (Waters, U.K.) coupled to an LTQOrbitrap (Thermo, Germany). Samples were injected onto a silica capillary column (New Objective, U.S.A.) packed with 3-mm ReproSil-Pur C18-AQ (Dr. Maisch GmbH, Germany). Peptides were separated by a stepwise 110-min gradient of 0–100% between buffer A (0.2% formic acid in water) and buffer B (0.2% formic acid in acetonitrile) at a flow rate of 200 nL/min. The mass spectrometer was operated in data dependent MS/MS mode to automatically switch between MS survey and MS/MS fragmentation scans of five most abundant precursor ions. Peak lists were generated using DTA supercharge (Schulze & Mann, 2004) and searched using the Mascot (Matrix Science, UK) software package against the human International Protein Index (IPI) database (http://www.ebi.ac.uk/IPI/IPIhelp.html) with carbamidomethyl cysteine as a fixed modification and oxidized methionine, phosphorylation (S,T,Y), $^{13}C_6$ $^{15}N_4$ -L-arginine, and $^{13}C_6$ $^{15}N_2$-L-lysine as variable modifications. Searches were performed with a precursor mass tolerance of 5 ppm and fragment ion tolerances of 0.7 Da and identified phosphorylation sites were further validated by visual inspection of MS/MS

spectra. For phosphopeptide quantification, the ratios between the monoisotopic peaks of labeled and unlabeled forms of phosphopeptides were calculated by MSQuant (Schulze & Mann, 2004).

Immunofluorescence microscopy and fluorescence intensity measurements

HeLaS3 cells were grown on coverslips, simultaneously fixed and permeabilized for 10 min at room temperature (RT) in PTEMF buffer, as described previously (Chan et al, 2009). For cytosolic pre-extraction, PTEMF buffer devoid of fomaldehyde was used for 60 sec., followed by normal PTEMF fixation. Mad1/C-Mad2 co-staining was performed as follows: C-Mad2 mAb (107-276, 4 µg/ml) was incubated on coverslips for 1 h at RT. Either a Cy3- or Cy5-conjugated donkey anti–mouse secondary antibody was used (Dianova, 1:1000). Myc-p31comet and Myc-Mad2$^{\Delta C}$ transfected cells have been identified through primary rabbit anti-c-Myc incubation (Santa Cruz Biotechnology, A-14, 1 µg/ml), followed by Cy2- or Cy5-conjugated donkey anti–rabbit (Dianova, 1:1000). Extensive washing was performed and mouse anti Mad1 (117-468), directly coupled to Alexa Fluor 488 (Invitrogen), was added (10 µg/ml) together with DAPI (2 µg/ml) for 1 h. Images were acquired using a DeltaVision Olympus IX71 microscope equipped with a 60x/1.42 oil objective. Collection and processing of acquired images was carried out using Softworx (Applied Precision, LLC). Samples were examined with optical sections acquired 0.4 µm apart in the z-axis, deconvolved and projected into a single plane image using the Softworx software (Applied Precision, LLC). Images were processed in Adobe Photoshop CS3 and figures were assembled using Adobe Illustrator CS4 (Adobe Systems).

After antibody microinjection, DNA and Cyclin B1 were stained with DAPI and Cyclin B1 mAb (clone GNS3, Millipore) directly coupled to Alexa Fluor 488 (10 µg/ml), respectively, for 1h.

When using the HeLa-Kyoto-LAP^{GFP}-mouse-Mad2 cell line (Hubner et al, 2010; Poser et al, 2008), the localization of LAP^{GFP}-mouse-Mad2 was monitored by visualizing the GFP flurescence directly, following PTEMF fixation.

In order to visualize Mad1 phosphorylation on S490 in intact cells, Mad1-pS490 antibody (3rd "bleed" of rabbit 833976, 1:500) was used in combination with Mad1 mAb (117-468, 1 µg/ml) and CREST antibodies (serum by Immunovision, 1:1000), followed by secondary antibody detection.

For quantitation of fluorescence intensities, at least 20 round "regions of interest (ROIs)" of equal size were selected around KTs in each cell using ImageJ. Average fluorescence intensities were measured for each ROI, the average background fluorescence was subtracted and the calculated fluorescence ratios were normalized to control and displayed in box-and-whisker plots using SigmaPlot.

Antibody microinjection

Antibody injection was performed using Femtotips II capillaries operated on a FemtoJet microinjector (Eppendorf). Antibodies were injected at a needle concentration of 1-2 mg/ml in PBS in the presence of 1.66 mg/ml Texas Red dextran or Alexa Fluor 488 dextran (both 10.000 MW, Invitrogen). Each injection was performed for 0.2-0.3 sec with injection and compensation pressures of 15 hPa. To assess the SAC functionality and effects on mitotic timing upon mAb microinjection, HeLaS3 H2B-GFP (Sillje et al, 2006) cells or HeLa Kyoto H2B-mCherry (Neumann et al, 2010) were seeded on 35 mm µ-Dishes or coverslips and synchronized as described in the corresponding figure

legends. Different mAbs were injected at different grid coordinates within the same plate or on different coverslips and phenotypes were analyzed by live cell imaging or immunofluorescence microscopy.

Time-lapse microscopy

Cells were imaged using a Nikon ECLIPSE Ti microscope equipped with a CoolLED pE-1 excitation system and a 20x/0.75 air Plan Apo objective (Nikon). Images were acquired at multiple positions every 3 min. GFP/mCherry fluorescence and DIC images were acquired at each time point with 20 msec and 2 msec exposure times, respectively. Texas Red/Alexa Fluor 488 fluorescence was imaged every 5 time points with a 40 msec exposure. MetaMorph 7.7 software (MDS Analytical Technologies) was used to collect and process data.

Size exclusion chromatography followed by immunoprecipitation

Synchronized HeLaS3 cells were lysed as described in the "Cell extracts, Western blots and immunoprecipitations" section. For Superdex 200 chromatography, 1 ml of clarified lysate containing 10 mg of total protein extract was loaded on a Superdex 200 16/60 column (GE) using an Äkta Explorer FPLC system (Amersham). An isocratic elution was performed at 4°C applying a constant flow of 1.1 ml/min of 20 mM Tris-HCl, pH 7.4, 150 mM NaCl. Fractions were collected every 4 ml; protease and phosphatase inhibitors were added to each fraction as to the lysis buffer. Each fraction was subdivided in a 1.3 ml part and a 2.7 ml part, destined to trichloroacetic acid (TCA) precipitation and IP, respectively. IP was performed for 2 hours at 4°C using 20 µl of solid protein A beads (BioRad), previously coupled and cross-linked to the $CM2^{276}$ at 1 µg/µl. Beads were washed 3 times with 0.5 ml of elution buffer and resuspended in 30

µl of Laemmli buffer. TCA precipitated protein pellets were resuspended in 80 µl of Laemmli buffer. 10 µl were further analyzed by SDS-PAGE and Western blot.

For Superose 6 chromatography, 300 µl of 10 mg/ml clarified HeLaS3 mitotic lysate (nocodazole) were loaded on a Superose 6 10/300 GL column and an isocratic elution was performed at 4°C applying a constant flow of 0.4 ml/min of 20 mM Tris-HCl, pH 7.4, 150 mM NaCl. Fractions of 650 µl were collected; protease and phosphatase inhibitors were added to each fraction as to the lysis buffer. Half of each fraction was destined to trichloroacetic acid (TCA) precipitation and half was, after pooling of relevant fractions, probed by IP with $CM2^{276}$ Ab. Samples were processed as for the Superdex 200 chromatography and 10 µl were further analyzed by SDS-PAGE and Western blot.

Appendix

Generation of additional antibodies to Mad2

Large part of this work is based on the serendipitous discovery of a monoclonal antibody recognizing selectively the closed conformer of Mad2. Despite the availability of several Mad2 antibodies (commercially or otherwise), none of them has been, to the best of our knowledge, thoroughly characterized for its preference for binding the open, closed or both conformers of Mad2 with the exception of $CM2^{276}$. One sheep polyclonal Mad2 antibody has been proposed to recognize selectively the open conformer of Mad2 based on immunofluorescence results, but this notion has not been directly tested in biochemical assays and the epitope(s) of this antibody remain unknown (Hewitt et al, 2010). Therefore we used our purified recombinant Mad2-WT protein to immunize rabbits and mice, in order to obtain additional polyclonal and monoclonal Mad2 antibodies, respectively. Whereas the rabbit injection protocol did not result in any serum capable of recognizing cellular endogenous Mad2, the hybridoma supernatant screening for Mad2 mAbs resulted in one positive hit, clone 2F12. The injection protocol was performed with His-tagged Mad2, whereas the screening was performed using GST-tagged Mad2 in a dot blot-based assay. Further characterization showed that the clone 2F12 (IgG1) can recognize endogenous Mad2 in both immunofluorescence and immunoprecipitation, but not in Western blot (see below). These data support the notion that mAb 2F12 recognizes a conformational rather than a linear epitope on Mad2. In immunoprecipitation experiments 2F12 was unable to recognize O-Mad2, showing therefore its specificity for Closed-Mad2. We named therefore this antibody $CM2^{2F12}$. Similarly to $CM2^{276}$, $CM2^{2F12}$ could not immunoprecipitate free Mad2 isolated obtained from a cell lysate by size

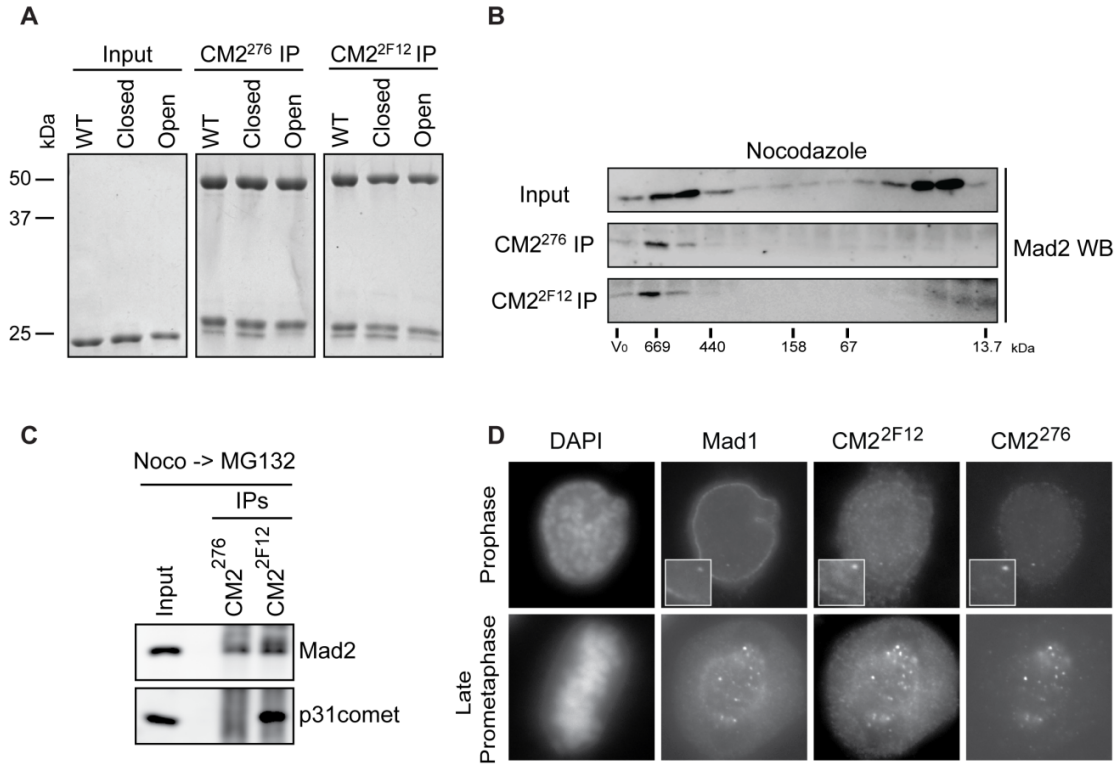

Figure 38. 2F12 ($CM2^{2F12}$) recognizes selectively C-Mad2. (A) Purified $Mad2^{WT}$ (WT), $Mad2^{L13Q}$ (Closed) and $Mad2^{V193N}$ (Open) were immunoprecipitated (IP) with $CM2^{276}$ or with $CM2^{2F12}$. Inputs and IPs were analyzed by Coomassie Brilliant Blue staining. **(B)** Western blots on samples obtained from TCA precipitations (Inputs), $CM2^{276}$ IP and $CM2^{2F12}$ IP on fractions obtained as described in Fig. 17A, following synchronization as described in Fig. 17B. Western blots were performed with rabbit Mad2 polyclonal antibody. **(C)** Immunoprecipitations (IPs) were performed with unspecific $CM2^{276}$ or $CM2^{2F12}$ from HeLaS3 lysate obtained from cells arrested with nocodazole. Input and IPs were analyzed by Western blot with the indicated antibodies. **(D)** HeLaS3 cells were fixed with PTEMF. After fixation, C-Mad2 was stained with $CM2^{276}$, followed by secondary antibody incubation. After extensive washing, co-staining with Mad1 mAb directly coupled to Alexa Fluor 488 and $CM2^{2F12}$ directly coupled to Alexa 647 was performed. DNA was visualized with DAPI (blue). Insets show enlarged views of a Mad1:C-Mad2 positive KT and the surrounding nuclear envelope.

exclusion chromatography, confirming that unliganded/free-Mad2 adopts the open conformation in living cells. In stark contrast to $CM2^{276}$, $CM2^{2F12}$ could readily co-immunoprecipitate p31comet from a human cell lysate, demonstrating that the epitope recognized by $CM2^{2F12}$ is not mapping on the dimerization interface (Fig. 38C). Interestingly, when used in immunofluorescence experiments, $Mad2^{2F12}$ could more readily recognize Mad2 at NPCs and spindle poles when compared to $CM2^{276}$ (Fig.

38D). These data support the notion that Mad2 adopts the closed conformation at any subcellular site and that the lack of its recognition by $CM2^{276}$ at NPCs and spindle poles depends on p31comet. Furthermore, the combined used of $CM2^{276}$ and $CM2^{2F12}$ will allow testing simultaneously the presence of C-Mad2 and its association to p31comet in immunofluorescence based assays.

List of generated plasmids

name	tag	gene	insert	vector	comment
LF 1	N-Myc	p31-comet	full-length	pCDNA3.1	Mammalian expression, full-length
LF 2	N-6His	p31-comet	full-length	pET28a(+)	Bacterial expression, full-length
LF 3	N-Flag	p31-comet	full-length	pCDNA3.1	Mammalian expression, full-length
LF 4	N-6His	p31-comet	aa121-274	pET28a(+)	Bacterial expression, C-term. High exp of unsoluble pr.
LF 5	GAL4-BD	p31-comet	full-length	pGBD-C(I)	Yeast two hybrid, BD-p31full length
LF 6	N-Myc	Mad1	aa485-584, R558H	pCDNA3.1	Mammalian expression, aa485-584, R558H
LF 7	N-Flag	Mad1	aa485-584, R558H	pCDNA3.1	Mammalian expression, aa485-584, R558H
LF 8	GAL4-BD	p31-comet	full-length	pFBT9'	Yeast two hybrid, BD-p31full length
LF 9	N-Myc	Mad1	full-length, R558H, S233A	pUNI10*p1226	Mammalian expression, full length, R558H, S233A
LF 10	N-Myc	Mad1	full-length, R558H, S233D	pUNI10*p1226	Mammalian expression, full length, R558H, S233D
LF 11	N-Myc	Mad1	full-length, R558H, S490A	pUNI10*p1226	Mammalian expression, full length, R558H, S490A
LF 12	N-Myc	Mad1	full-length, R558H, S490D	pUNI10*p1226	Mammalian expression, full length, R558H, S490D
LF 13	N-Myc	Mad1	aa485-584, R558H, S490A	pCDNA3.1	Mammalian expression, aa485-584, R558H, S490A
LF 14	N-Myc	Mad1	aa485-584, R558H, S490D	pCDNA3.1	Mammalian expression, aa485-584, R558H, S490D
LF 15	N-Flag	Mad1	aa485-584, R558H, S490A	pCDNA3.1	Mammalian expression, aa485-584, R558H, S490A
LF 16	N-Flag	Mad1	aa485-584, R558H, S490D	pCDNA3.1	Mammalian expression, aa485-584, R558H, S490D
LF017	mCherry	p31-comet	full length	pcDNA3.1mCherryC	mammalian expression
LF018	AD HA	INCENP	822-919	pACT2	Y2H
LF019	AD HA	INCENP	790-897	pACT2	Y2H
LF020	Myc	Mad1	full length wild-type	pcDNA3.1 3xmyc-C	mammalian expression
LF021	6-His	p31-comet	S102A	pET28a	bacterial expression
LF022	6-His	p31-comet	f.l. S236A	pET28a	bacterial expression
LF023	6-His	p31-comet	f.l T242A	pET28a	bacterial expression
LF024	6-His	p31-comet	a.a. 1-120	pET28a	bacterial expression
LF025	N-Myc	p31-comet	f.l. Q83A F191A	pCDNA3.1	Mammalian expression, full-length
LF026	6-His	Mad2	full-length	pET43	bacterial expression, gift from A. Musacchio
LF027	6-His	Mad2	f.l. L13Q	pET43	bacterial expression, gift from A. Musacchio
LF028	6-His	Mad2	f.l. V193N	pET43	bacterial expression, gift from A. Musacchio
LF029	6-His	Mad2	f.l. R133E Q134A	pET43	bacterial expression, gift from A. Musacchio
LF030	GST	p31-comet	full length	pGEX6p	bacterial expression, full length
LF031	GST	Mad2	full length	pGEX6p	bacterial expression, full length
LF032	6-His	Mad2	f.l. F141A	pET43	bacterial expression, gift from A. Musacchio
LF033	6-His	Mad2	DeltaC10	pET43	bacterial expression, gift from A. Musacchio. Mad missing the C-terminal 10 aa
LF034	6-His	p31-comet	f.l. Q83A F191A	pET28a(+)	bacterial expression, full length, deficient in the Mad2 binding
LF035	6-His	Mad2	f.l. R133A	pET43	bacterial expression, full length

name	tag	gene	insert	vector	comment
LF036	6-His	Mad2	f.l. R133A L153A	pET43	bacterial expression, full length
LF037	6-His	Mad2	f.l. R133A Y156A	pET43	bacterial expression, full length
LF038	N3*Myc	Mad2	full length	pcDNA3.1	mammalian expression, full length
LF039	N3*Myc	Mad2	f.l. L13Q	pcDNA3.1	mammalian expression, full length
LF040	N3*Myc	Mad2	f.l. V193N	pcDNA3.1	mammalian expression, full length
LF041	GST	Cdc20	111-138	pGEX6p	bacterial expression, Mad2 binding part
LF042	6-His	Mad2	f.l. L13Q R133A	pET43	bacterial expression, full length
LF043	6-His	Mad2	f.l. L13Q Q134A	pET43	bacterial expression, full length
LF044	6-His	Mad2	f.l. L13Q F141A	pET43	bacterial expression, full length
LF045	6-His	Mad2	f.l. L13Q R184A	pET43	bacterial expression, full length
LF046	N3*Myc	Mad2	f.l. R133A	pcDNA3.1	mammalian expression, full length
LF047	N3*Myc	Mad2	f.l. R133A L13Q	pcDNA3.1	mammalian expression, full length
LF048	N3*Myc	Mad2	f.l. R133A V193N	pcDNA3.1	mammalian expression, full length
LF049	N3*Myc	Mad2	WT siRNA resistant	pcDNA3.1	carrying 5 silent mutations conferring resistance to oligo #531
LF050	N3*Myc	Mad2	L13Q siRNA resistant	pcDNA3.1	carrying 5 silent mutations conferring resistance to oligo #531
LF051	N3*Myc	Mad2	V193N siRNA resistant	pcDNA3.1	carrying 5 silent mutations conferring resistance to oligo #531

References

Allshire RC, Karpen GH (2008) Epigenetic regulation of centromeric chromatin: old dogs, new tricks? *Nat Rev Genet* **9:** 923-937

Babu JR, Jeganathan KB, Baker DJ, Wu X, Kang-Decker N, van Deursen JM (2003) Rae1 is an essential mitotic checkpoint regulator that cooperates with Bub3 to prevent chromosome missegregation. *The Journal of cell biology* **160:** 341-353

Baumann C, Korner R, Hofmann K, Nigg EA (2007) PICH, a centromere-associated SNF2 family ATPase, is regulated by Plk1 and required for the spindle checkpoint. *Cell* **128:** 101-114

Blower MD, Nachury M, Heald R, Weis K (2005) A Rae1-containing ribonucleoprotein complex is required for mitotic spindle assembly. *Cell* **121:** 223-234

Blower MD, Sullivan BA, Karpen GH (2002) Conserved organization of centromeric chromatin in flies and humans. *Developmental cell* **2:** 319-330

Buffin E, Emre D, Karess RE (2007) Flies without a spindle checkpoint. *Nat Cell Biol* **9:** 565-572

Burke DJ, Stukenberg PT (2008) Linking kinetochore-microtubule binding to the spindle checkpoint. *Dev Cell* **14:** 474-479

Burton JL, Solomon MJ (2007) Mad3p, a pseudosubstrate inhibitor of APCCdc20 in the spindle assembly checkpoint. *Genes Dev* **21:** 655-667

Buschhorn BA, Petzold G, Galova M, Dube P, Kraft C, Herzog F, Stark H, Peters JM (2011) Substrate binding on the APC/C occurs between the coactivator Cdh1 and the processivity factor Doc1. *Nature structural & molecular biology* **18:** 6-13

Campbell MS, Chan GK, Yen TJ (2001) Mitotic checkpoint proteins HsMAD1 and HsMAD2 are associated with nuclear pore complexes in interphase. *J Cell Sci* **114:** 953-963

Chan YW, Fava LL, Uldschmid A, Schmitz MH, Gerlich DW, Nigg EA, Santamaria A (2009) Mitotic control of kinetochore-associated dynein and spindle orientation by human Spindly. *J Cell Biol* **185:** 859-874

Chase D, Serafinas C, Ashcroft N, Kosinski M, Longo D, Ferris DK, Golden A (2000) The polo-like kinase PLK-1 is required for nuclear envelope breakdown and the completion of meiosis in Caenorhabditis elegans. *Genesis* **26:** 26-41

Cheeseman IM, Desai A (2008) Molecular architecture of the kinetochore-microtubule interface. *Nature reviews Molecular cell biology* **9:** 33-46

Cheeseman IM, Niessen S, Anderson S, Hyndman F, Yates JR, 3rd, Oegema K, Desai A (2004) A conserved protein network controls assembly of the outer kinetochore and its ability to sustain tension. *Genes & development* **18:** 2255-2268

Chen RH, Brady DM, Smith D, Murray AW, Hardwick KG (1999) The spindle checkpoint of budding yeast depends on a tight complex between the Mad1 and Mad2 proteins. *Mol Biol Cell* **10:** 2607-2618

Chen RH, Shevchenko A, Mann M, Murray AW (1998) Spindle checkpoint protein Xmad1 recruits Xmad2 to unattached kinetochores. *J Cell Biol* **143:** 283-295

Chi YH, Haller K, Ward MD, Semmes OJ, Li Y, Jeang KT (2008) Requirements for protein phosphorylation and the kinase activity of polo-like kinase 1 (Plk1) for the kinetochore function of mitotic arrest deficiency protein 1 (Mad1). *J Biol Chem* **283:** 35834-35844

Chung E, Chen RH (2002) Spindle checkpoint requires Mad1-bound and Mad1-free Mad2. *Mol Biol Cell* **13:** 1501-1511

Ciliberto A, Shah JV (2009) A quantitative systems view of the spindle assembly checkpoint. *EMBO J* **28:** 2162-2173

Cleveland DW, Mao Y, Sullivan KF (2003) Centromeres and kinetochores: from epigenetics to mitotic checkpoint signaling. *Cell* **112:** 407-421

Cross FR (2003) Two redundant oscillatory mechanisms in the yeast cell cycle. *Developmental cell* **4:** 741-752

da Fonseca PC, Kong EH, Zhang Z, Schreiber A, Williams MA, Morris EP, Barford D (2011) Structures of APC/C(Cdh1) with substrates identify Cdh1 and Apc10 as the D-box co-receptor. *Nature* **470:** 274-278

De Antoni A, Pearson CG, Cimini D, Canman JC, Sala V, Nezi L, Mapelli M, Sironi L, Faretta M, Salmon ED, Musacchio A (2005) The Mad1/Mad2 complex as a template for Mad2 activation in the spindle assembly checkpoint. *Curr Biol* **15:** 214-225

De Souza CP, Hashmi SB, Nayak T, Oakley B, Osmani SA (2009) Mlp1 acts as a mitotic scaffold to spatially regulate spindle assembly checkpoint proteins in Aspergillus nidulans. *Molecular biology of the cell* **20:** 2146-2159

DeLuca JG, Dong Y, Hergert P, Strauss J, Hickey JM, Salmon ED, McEwen BF (2005) Hec1 and nuf2 are core components of the kinetochore outer plate essential for organizing microtubule attachment sites. *Molecular biology of the cell* **16:** 519-531

Di Fiore B, Pines J (2010) How cyclin A destruction escapes the spindle assembly checkpoint. *The Journal of cell biology* **190:** 501-509

Dobles M, Liberal V, Scott ML, Benezra R, Sorger PK (2000) Chromosome missegregation and apoptosis in mice lacking the mitotic checkpoint protein Mad2. *Cell* **101:** 635-645

Doncic A, Ben-Jacob E, Barkai N (2005) Evaluating putative mechanisms of the mitotic spindle checkpoint. *Proceedings of the National Academy of Sciences of the United States of America* **102:** 6332-6337

Dou Z, von Schubert C, Korner R, Santamaria A, Elowe S, Nigg EA (2011) Quantitative mass spectrometry analysis reveals similar substrate consensus motif for human Mps1 kinase and Plk1. *PloS one* **6:** e18793

Draviam VM, Stegmeier F, Nalepa G, Sowa ME, Chen J, Liang A, Hannon GJ, Sorger PK, Harper JW, Elledge SJ (2007) A functional genomic screen identifies a role for TAO1 kinase in spindle-checkpoint signalling. *Nat Cell Biol* **9:** 556-564

Dultz E, Zanin E, Wurzenberger C, Braun M, Rabut G, Sironi L, Ellenberg J (2008) Systematic kinetic analysis of mitotic dis- and reassembly of the nuclear pore in living cells. *The Journal of cell biology* **180:** 857-865

Elbashir SM, Harborth J, Lendeckel W, Yalcin A, Weber K, Tuschl T (2001) Duplexes of 21-nucleotide RNAs mediate RNA interference in cultured mammalian cells. *Nature* **411:** 494-498

Elowe S, Hummer S, Uldschmid A, Li X, Nigg EA (2007) Tension-sensitive Plk1 phosphorylation on BubR1 regulates the stability of kinetochore microtubule interactions. *Genes Dev* **21:** 2205-2219

Emre D, Terracol R, Poncet A, Rahmani Z, Karess RE (2011) A mitotic role for Mad1 beyond the spindle checkpoint. *J Cell Sci* **124:** 1664-1671

Evan GI, Lewis GK, Ramsay G, Bishop JM (1985) Isolation of monoclonal antibodies specific for human c-myc proto-oncogene product. *Mol Cell Biol* **5:** 3610-3616

Fang G (2002) Checkpoint protein BubR1 acts synergistically with Mad2 to inhibit anaphase-promoting complex. *Mol Biol Cell* **13:** 755-766

Fang G, Yu H, Kirschner MW (1998) The checkpoint protein MAD2 and the mitotic regulator CDC20 form a ternary complex with the anaphase-promoting complex to control anaphase initiation. *Genes Dev* **12:** 1871-1883

Fraschini R, Beretta A, Sironi L, Musacchio A, Lucchini G, Piatti S (2001) Bub3 interaction with Mad2, Mad3 and Cdc20 is mediated by WD40 repeats and does not require intact kinetochores. *EMBO J* **20:** 6648-6659

Gassmann R, Holland AJ, Varma D, Wan X, Civril F, Cleveland DW, Oegema K, Salmon ED, Desai A (2010) Removal of Spindly from microtubule-attached

kinetochores controls spindle checkpoint silencing in human cells. *Genes Dev* **24:** 957-971

Gavet O, Pines J (2010a) Activation of cyclin B1-Cdk1 synchronizes events in the nucleus and the cytoplasm at mitosis. *J Cell Biol* **189:** 247-259

Gavet O, Pines J (2010b) Progressive activation of CyclinB1-Cdk1 coordinates entry to mitosis. *Dev Cell* **18:** 533-543

Gillett ES, Espelin CW, Sorger PK (2004) Spindle checkpoint proteins and chromosome-microtubule attachment in budding yeast. *The Journal of cell biology* **164:** 535-546

Gorbsky GJ, Chen RH, Murray AW (1998) Microinjection of antibody to Mad2 protein into mammalian cells in mitosis induces premature anaphase. *J Cell Biol* **141:** 1193-1205

Goss VL, Hocevar BA, Thompson LJ, Stratton CA, Burns DJ, Fields AP (1994) Identification of nuclear beta II protein kinase C as a mitotic lamin kinase. *The Journal of biological chemistry* **269:** 19074-19080

Griffis ER, Stuurman N, Vale RD (2007) Spindly, a novel protein essential for silencing the spindle assembly checkpoint, recruits dynein to the kinetochore. *J Cell Biol* **177:** 1005-1015

Guttinger S, Laurell E, Kutay U (2009) Orchestrating nuclear envelope disassembly and reassembly during mitosis. *Nature reviews Molecular cell biology* **10:** 178-191

Habu T, Kim SH, Weinstein J, Matsumoto T (2002) Identification of a MAD2-binding protein, CMT2, and its role in mitosis. *EMBO J* **21:** 6419-6428

Hachet V, Canard C, Gonczy P (2007) Centrosomes promote timely mitotic entry in C. elegans embryos. *Developmental cell* **12:** 531-541

Hardwick KG, Johnston RC, Smith DL, Murray AW (2000) MAD3 encodes a novel component of the spindle checkpoint which interacts with Bub3p, Cdc20p, and Mad2p. *J Cell Biol* **148:** 871-882

Hardwick KG, Weiss E, Luca FC, Winey M, Murray AW (1996) Activation of the budding yeast spindle assembly checkpoint without mitotic spindle disruption. *Science* **273:** 953-956

Hartwell LH, Culotti J, Pringle JR, Reid BJ (1974) Genetic control of the cell division cycle in yeast. *Science* **183:** 46-51

Hartwell LH, Weinert TA (1989) Checkpoints: controls that ensure the order of cell cycle events. *Science* **246:** 629-634

Heald R, McKeon F (1990) Mutations of phosphorylation sites in lamin A that prevent nuclear lamina disassembly in mitosis. *Cell* **61:** 579-589

Hewitt L, Tighe A, Santaguida S, White AM, Jones CD, Musacchio A, Green S, Taylor SS (2010) Sustained Mps1 activity is required in mitosis to recruit O-Mad2 to the Mad1-C-Mad2 core complex. *J Cell Biol* **190:** 25-34

Hornig NC, Knowles PP, McDonald NQ, Uhlmann F (2002) The dual mechanism of separase regulation by securin. *Curr Biol* **12:** 973-982

Howell BJ, Hoffman DB, Fang G, Murray AW, Salmon ED (2000) Visualization of Mad2 dynamics at kinetochores, along spindle fibers, and at spindle poles in living cells. *J Cell Biol* **150:** 1233-1250

Howell BJ, McEwen BF, Canman JC, Hoffman DB, Farrar EM, Rieder CL, Salmon ED (2001) Cytoplasmic dynein/dynactin drives kinetochore protein transport to the spindle poles and has a role in mitotic spindle checkpoint inactivation. *J Cell Biol* **155:** 1159-1172

Howell BJ, Moree B, Farrar EM, Stewart S, Fang G, Salmon ED (2004) Spindle checkpoint protein dynamics at kinetochores in living cells. *Curr Biol* **14:** 953-964

Hoyt MA, Totis L, Roberts BT (1991) S. cerevisiae genes required for cell cycle arrest in response to loss of microtubule function. *Cell* **66:** 507-517

Hubner NC, Wang LH, Kaulich M, Descombes P, Poser I, Nigg EA (2010) Re-examination of siRNA specificity questions role of PICH and Tao1 in the spindle checkpoint and identifies Mad2 as a sensitive target for small RNAs. *Chromosoma* **119:** 149-165

Hwang LH, Lau LF, Smith DL, Mistrot CA, Hardwick KG, Hwang ES, Amon A, Murray AW (1998) Budding yeast Cdc20: a target of the spindle checkpoint. *Science* **279:** 1041-1044

Iouk T, Kerscher O, Scott RJ, Basrai MA, Wozniak RW (2002) The yeast nuclear pore complex functionally interacts with components of the spindle assembly checkpoint. *The Journal of cell biology* **159:** 807-819

Iwanaga Y, Chi YH, Miyazato A, Sheleg S, Haller K, Peloponese JM, Jr., Li Y, Ward JM, Benezra R, Jeang KT (2007) Heterozygous deletion of mitotic arrest-deficient protein 1 (MAD1) increases the incidence of tumors in mice. *Cancer Res* **67:** 160-166

Iwanaga Y, Kasai T, Kibler K, Jeang KT (2002) Characterization of regions in hsMAD1 needed for binding hsMAD2. A polymorphic change in an hsMAD1 leucine zipper affects MAD1-MAD2 interaction and spindle checkpoint function. *J Biol Chem* **277:** 31005-31013

Izawa D, Pines J (2011) How APC/C-Cdc20 changes its substrate specificity in mitosis. *Nature cell biology* **13:** 223-233

Jeganathan KB, Malureanu L, van Deursen JM (2005) The Rae1-Nup98 complex prevents aneuploidy by inhibiting securin degradation. *Nature* **438:** 1036-1039

Jelluma N, Dansen TB, Sliedrecht T, Kwiatkowski NP, Kops GJ (2010) Release of Mps1 from kinetochores is crucial for timely anaphase onset. *J Cell Biol* **191:** 281-290

Jensen SS, Larsen MR (2007) Evaluation of the impact of some experimental procedures on different phosphopeptide enrichment techniques. *Rapid communications in mass spectrometry : RCM* **21:** 3635-3645

Jia L, Li B, Warrington RT, Hao X, Wang S, Yu H (2011) Defining Pathways of Spindle Checkpoint Silencing: Functional Redundancy between Cdc20 Ubiquitination and p31comet. *Molecular biology of the cell*

Jin DY, Spencer F, Jeang KT (1998) Human T cell leukemia virus type 1 oncoprotein Tax targets the human mitotic checkpoint protein MAD1. *Cell* **93:** 81-91

Kemmler S, Stach M, Knapp M, Ortiz J, Pfannstiel J, Ruppert T, Lechner J (2009) Mimicking Ndc80 phosphorylation triggers spindle assembly checkpoint signalling. *The EMBO journal* **28:** 1099-1110

Kim M, Murphy K, Liu F, Parker SE, Dowling ML, Baff W, Kao GD (2005) Caspase-mediated specific cleavage of BubR1 is a determinant of mitotic progression. *Mol Cell Biol* **25:** 9232-9248

Kim S, Sun H, Ball HL, Wassmann K, Luo X, Yu H (2010) Phosphorylation of the spindle checkpoint protein Mad2 regulates its conformational transition. *Proc Natl Acad Sci U S A* **107:** 19772-19777

King EM, van der Sar SJ, Hardwick KG (2007) Mad3 KEN boxes mediate both Cdc20 and Mad3 turnover, and are critical for the spindle checkpoint. *PLoS One* **2:** e342

Kirschner M, Mitchison T (1986) Beyond self-assembly: from microtubules to morphogenesis. *Cell* **45:** 329-342

Koller E, Propp S, Murray H, Lima W, Bhat B, Prakash TP, Allerson CR, Swayze EE, Marcusson EG, Dean NM (2006) Competition for RISC binding predicts in vitro potency of siRNA. *Nucleic Acids Res* **34:** 4467-4476

Kops GJ, Kim Y, Weaver BA, Mao Y, McLeod I, Yates JR, 3rd, Tagaya M, Cleveland DW (2005) ZW10 links mitotic checkpoint signaling to the structural kinetochore. *The Journal of cell biology* **169:** 49-60

Kops GJ, van der Voet M, Manak MS, van Osch MH, Naini SM, Brear A, McLeod IX, Hentschel DM, Yates JR, 3rd, van den Heuvel S, Shah JV (2010) APC16 is a

conserved subunit of the anaphase-promoting complex/cyclosome. *J Cell Sci* **123:** 1623-1633

Kraft C, Herzog F, Gieffers C, Mechtler K, Hagting A, Pines J, Peters JM (2003) Mitotic regulation of the human anaphase-promoting complex by phosphorylation. *The EMBO journal* **22:** 6598-6609

Krull S, Thyberg J, Bjorkroth B, Rackwitz HR, Cordes VC (2004) Nucleoporins as components of the nuclear pore complex core structure and Tpr as the architectural element of the nuclear basket. *Molecular biology of the cell* **15:** 4261-4277

Kulukian A, Han JS, Cleveland DW (2009) Unattached kinetochores catalyze production of an anaphase inhibitor that requires a Mad2 template to prime Cdc20 for BubR1 binding. *Dev Cell* **16:** 105-117

Kwiatkowski N, Jelluma N, Filippakopoulos P, Soundararajan M, Manak MS, Kwon M, Choi HG, Sim T, Deveraux QL, Rottmann S, Pellman D, Shah JV, Kops GJ, Knapp S, Gray NS (2010) Small-molecule kinase inhibitors provide insight into Mps1 cell cycle function. *Nat Chem Biol* **6:** 359-368

Lad L, Lichtsteiner S, Hartman JJ, Wood KW, Sakowicz R (2009) Kinetic analysis of Mad2-Cdc20 formation: conformational changes in Mad2 are catalyzed by a C-Mad2-ligand complex. *Biochemistry* **48:** 9503-9515

Laurell E, Beck K, Krupina K, Theerthagiri G, Bodenmiller B, Horvath P, Aebersold R, Antonin W, Kutay U (2011) Phosphorylation of Nup98 by multiple kinases is crucial for NPC disassembly during mitotic entry. *Cell* **144:** 539-550

Lee SH, McCormick F, Saya H (2010) Mad2 inhibits the mitotic kinesin MKlp2. *The Journal of cell biology* **191:** 1069-1077

Lee SH, Sterling H, Burlingame A, McCormick F (2008) Tpr directly binds to Mad1 and Mad2 and is important for the Mad1-Mad2-mediated mitotic spindle checkpoint. *Genes Dev* **22:** 2926-2931

Lenart P, Petronczki M, Steegmaier M, Di Fiore B, Lipp JJ, Hoffmann M, Rettig WJ, Kraut N, Peters JM (2007) The small-molecule inhibitor BI 2536 reveals novel insights into mitotic roles of polo-like kinase 1. *Curr Biol* **17:** 304-315

Li R, Murray AW (1991) Feedback control of mitosis in budding yeast. *Cell* **66:** 519-531

Li Y, Benezra R (1996) Identification of a human mitotic checkpoint gene: hsMAD2. *Science* **274:** 246-248

Lince-Faria M, Maffini S, Orr B, Ding Y, Claudia F, Sunkel CE, Tavares A, Johansen J, Johansen KM, Maiato H (2009) Spatiotemporal control of mitosis by the conserved spindle matrix protein Megator. *J Cell Biol* **184:** 647-657

Luo X, Fang G, Coldiron M, Lin Y, Yu H, Kirschner MW, Wagner G (2000) Structure of the Mad2 spindle assembly checkpoint protein and its interaction with Cdc20. *Nat Struct Biol* **7:** 224-229

Luo X, Tang Z, Rizo J, Yu H (2002) The Mad2 spindle checkpoint protein undergoes similar major conformational changes upon binding to either Mad1 or Cdc20. *Mol Cell* **9:** 59-71

Luo X, Tang Z, Xia G, Wassmann K, Matsumoto T, Rizo J, Yu H (2004) The Mad2 spindle checkpoint protein has two distinct natively folded states. *Nat Struct Mol Biol* **11:** 338-345

Luo X, Yu H (2008) Protein metamorphosis: the two-state behavior of Mad2. *Structure* **16:** 1616-1625

Ma HT, Poon RY (2011) Orderly inactivation of the key checkpoint protein mitotic arrest deficient 2 (MAD2) during mitotic progression. *The Journal of biological chemistry* **286:** 13052-13059

Maciejowski J, George KA, Terret ME, Zhang C, Shokat KM, Jallepalli PV (2010) Mps1 directs the assembly of Cdc20 inhibitory complexes during interphase and mitosis to control M phase timing and spindle checkpoint signaling. *J Cell Biol* **190:** 89-100

Mahrus S, Trinidad JC, Barkan DT, Sali A, Burlingame AL, Wells JA (2008) Global sequencing of proteolytic cleavage sites in apoptosis by specific labeling of protein N termini. *Cell* **134:** 866-876

Mansfeld J, Collin P, Collins MO, Choudhary JS, Pines J (2011) APC15 drives the turnover of MCC-CDC20 to make the spindle assembly checkpoint responsive to kinetochore attachment. *Nature cell biology*

Mapelli M, Filipp FV, Rancati G, Massimiliano L, Nezi L, Stier G, Hagan RS, Confalonieri S, Piatti S, Sattler M, Musacchio A (2006) Determinants of conformational dimerization of Mad2 and its inhibition by p31comet. *EMBO J* **25:** 1273-1284

Mapelli M, Massimiliano L, Santaguida S, Musacchio A (2007) The Mad2 conformational dimer: structure and implications for the spindle assembly checkpoint. *Cell* **131:** 730-743

Mapelli M, Musacchio A (2007) MAD contortions: conformational dimerization boosts spindle checkpoint signaling. *Curr Opin Struct Biol* **17:** 716-725

Maresca TJ, Salmon ED (2010) Welcome to a new kind of tension: translating kinetochore mechanics into a wait-anaphase signal. *J Cell Sci* **123:** 825-835

Marshall OJ, Chueh AC, Wong LH, Choo KH (2008) Neocentromeres: new insights into centromere structure, disease development, and karyotype evolution. *Am J Hum Genet* **82:** 261-282

Martin-Lluesma S, Stucke VM, Nigg EA (2002) Role of Hec1 in spindle checkpoint signaling and kinetochore recruitment of Mad1/Mad2. *Science* **297:** 2267-2270

Masumoto H, Masukata H, Muro Y, Nozaki N, Okazaki T (1989) A human centromere antigen (CENP-B) interacts with a short specific sequence in alphoid DNA, a human centromeric satellite. *The Journal of cell biology* **109:** 1963-1973

Mayer TU, Kapoor TM, Haggarty SJ, King RW, Schreiber SL, Mitchison TJ (1999) Small molecule inhibitor of mitotic spindle bipolarity identified in a phenotype-based screen. *Science* **286:** 971-974

McCleland ML, Gardner RD, Kallio MJ, Daum JR, Gorbsky GJ, Burke DJ, Stukenberg PT (2003) The highly conserved Ndc80 complex is required for kinetochore assembly, chromosome congression, and spindle checkpoint activity. *Genes & development* **17:** 101-114

Meraldi P, Draviam VM, Sorger PK (2004) Timing and checkpoints in the regulation of mitotic progression. *Dev Cell* **7:** 45-60

Murray AW, Kirschner MW (1989) Dominoes and clocks: the union of two views of the cell cycle. *Science* **246:** 614-621

Musacchio A, Hardwick KG (2002) The spindle checkpoint: structural insights into dynamic signalling. *Nature reviews Molecular cell biology* **3:** 731-741

Musacchio A, Salmon ED (2007) The spindle-assembly checkpoint in space and time. *Nat Rev Mol Cell Biol* **8:** 379-393

Nasmyth K (2005) How do so few control so many? *Cell* **120:** 739-746

Neef R, Preisinger C, Sutcliffe J, Kopajtich R, Nigg EA, Mayer TU, Barr FA (2003) Phosphorylation of mitotic kinesin-like protein 2 by polo-like kinase 1 is required for cytokinesis. *The Journal of cell biology* **162:** 863-875

Neumann B, Walter T, Heriche JK, Bulkescher J, Erfle H, Conrad C, Rogers P, Poser I, Held M, Liebel U, Cetin C, Sieckmann F, Pau G, Kabbe R, Wunsche A, Satagopam V, Schmitz MH, Chapuis C, Gerlich DW, Schneider R, Eils R, Huber W, Peters JM, Hyman AA, Durbin R, Pepperkok R, Ellenberg J (2010) Phenotypic profiling of the human genome by time-lapse microscopy reveals cell division genes. *Nature* **464:** 721-727

Nilsson J, Yekezare M, Minshull J, Pines J. (2008) The APC/C maintains the spindle assembly checkpoint by targeting Cdc20 for destruction. *Nat Cell Biol*, Vol. 10, pp. 1411-1420.

Okada T, Ohzeki J, Nakano M, Yoda K, Brinkley WR, Larionov V, Masumoto H (2007) CENP-B controls centromere formation depending on the chromatin context. *Cell* **131:** 1287-1300

Pan J, Chen RH (2004) Spindle checkpoint regulates Cdc20p stability in Saccharomyces cerevisiae. *Genes & development* **18:** 1439-1451

Paweletz N (2001) Walther Flemming: pioneer of mitosis research. *Nature reviews Molecular cell biology* **2:** 72-75

Perpelescu M, Fukagawa T (2011) The ABCs of CENPs. *Chromosoma* **120:** 425-446

Peter M, Heitlinger E, Haner M, Aebi U, Nigg EA (1991) Disassembly of in vitro formed lamin head-to-tail polymers by CDC2 kinase. *The EMBO journal* **10:** 1535-1544

Peters JM (2006) The anaphase promoting complex/cyclosome: a machine designed to destroy. *Nat Rev Mol Cell Biol* **7:** 644-656

Pines J (2011) Cubism and the cell cycle: the many faces of the APC/C. *Nature reviews Molecular cell biology* **12:** 427-438

Portier N, Audhya A, Maddox PS, Green RA, Dammermann A, Desai A, Oegema K (2007) A microtubule-independent role for centrosomes and aurora a in nuclear envelope breakdown. *Developmental cell* **12:** 515-529

Poser I, Sarov M, Hutchins JR, Heriche JK, Toyoda Y, Pozniakovsky A, Weigl D, Nitzsche A, Hegemann B, Bird AW, Pelletier L, Kittler R, Hua S, Naumann R, Augsburg M, Sykora MM, Hofemeister H, Zhang Y, Nasmyth K, White KP, Dietzel S, Mechtler K, Durbin R, Stewart AF, Peters JM, Buchholz F, Hyman AA (2008) BAC TransgeneOmics: a high-throughput method for exploration of protein function in mammals. *Nat Methods* **5:** 409-415

Potapova TA, Daum JR, Pittman BD, Hudson JR, Jones TN, Satinover DL, Stukenberg PT, Gorbsky GJ (2006) The reversibility of mitotic exit in vertebrate cells. *Nature* **440:** 954-958

Rahmani Z, Gagou ME, Lefebvre C, Emre D, Karess RE (2009) Separating the spindle, checkpoint, and timer functions of BubR1. *J Cell Biol* **187:** 597-605

Reddy SK, Rape M, Margansky WA, Kirschner MW (2007) Ubiquitination by the anaphase-promoting complex drives spindle checkpoint inactivation. *Nature* **446:** 921-925

Rudner AD, Murray AW (2000) Phosphorylation by Cdc28 activates the Cdc20-dependent activity of the anaphase-promoting complex. *The Journal of cell biology* **149:** 1377-1390

Santaguida S, Musacchio A (2009) The life and miracles of kinetochores. *EMBO J* **28:** 2511-2531

Santaguida S, Tighe A, D'Alise AM, Taylor SS, Musacchio A (2010) Dissecting the role of MPS1 in chromosome biorientation and the spindle checkpoint through the small molecule inhibitor reversine. *J Cell Biol* **190:** 73-87

Santamaria A, Neef R, Eberspacher U, Eis K, Husemann M, Mumberg D, Prechtl S, Schulze V, Siemeister G, Wortmann L, Barr FA, Nigg EA (2007) Use of the novel Plk1 inhibitor ZK-thiazolidinone to elucidate functions of Plk1 in early and late stages of mitosis. *Mol Biol Cell* **18:** 4024-4036

Santamaria A, Wang B, Elowe S, Malik R, Zhang F, Bauer M, Schmidt A, Sillje HH, Koerner R, Nigg EA (2010) The Plk1-dependent phosphoproteome of the early mitotic spindle. *Mol Cell Proteomics*

Schulze WX, Mann M (2004) A novel proteomic screen for peptide-protein interactions. *The Journal of biological chemistry* **279:** 10756-10764

Scott RJ, Lusk CP, Dilworth DJ, Aitchison JD, Wozniak RW (2005) Interactions between Mad1p and the nuclear transport machinery in the yeast Saccharomyces cerevisiae. *Molecular biology of the cell* **16:** 4362-4374

Screpanti E, De Antoni A, Alushin GM, Petrovic A, Melis T, Nogales E, Musacchio A (2011) Direct binding of Cenp-C to the Mis12 complex joins the inner and outer kinetochore. *Current biology : CB* **21:** 391-398

Shah JV, Botvinick E, Bonday Z, Furnari F, Berns M, Cleveland DW (2004) Dynamics of centromere and kinetochore proteins; implications for checkpoint signaling and silencing. *Curr Biol* **14:** 942-952

Shannon KB, Canman JC, Salmon ED (2002) Mad2 and BubR1 function in a single checkpoint pathway that responds to a loss of tension. *Mol Biol Cell* **13:** 3706-3719

Shevchenko A, Wilm M, Vorm O, Mann M (1996) Mass spectrometric sequencing of proteins silver-stained polyacrylamide gels. *Anal Chem* **68:** 850-858

Sillje HH, Nagel S, Korner R, Nigg EA (2006) HURP is a Ran-importin beta-regulated protein that stabilizes kinetochore microtubules in the vicinity of chromosomes. *Curr Biol* **16:** 731-742

Simonetta M, Manzoni R, Mosca R, Mapelli M, Massimiliano L, Vink M, Novak B, Musacchio A, Ciliberto A (2009) The influence of catalysis on mad2 activation dynamics. *PLoS Biol* **7:** e10

Sironi L, Mapelli M, Knapp S, De Antoni A, Jeang KT, Musacchio A (2002) Crystal structure of the tetrameric Mad1-Mad2 core complex: implications of a 'safety belt' binding mechanism for the spindle checkpoint. *EMBO J* **21:** 2496-2506

Sironi L, Melixetian M, Faretta M, Prosperini E, Helin K, Musacchio A (2001) Mad2 binding to Mad1 and Cdc20, rather than oligomerization, is required for the spindle checkpoint. *EMBO J* **20:** 6371-6382

Skinner JJ, Wood S, Shorter J, Englander SW, Black BE (2008) The Mad2 partial unfolding model: regulating mitosis through Mad2 conformational switching. *J Cell Biol* **183:** 761-768

Sliedrecht T, Zhang C, Shokat KM, Kops GJ (2010) Chemical genetic inhibition of Mps1 in stable human cell lines reveals novel aspects of Mps1 function in mitosis. *PLoS One* **5:** e10251

Stegmeier F, Rape M, Draviam VM, Nalepa G, Sowa ME, Ang XL, McDonald ER, 3rd, Li MZ, Hannon GJ, Sorger PK, Kirschner MW, Harper JW, Elledge SJ (2007) Anaphase initiation is regulated by antagonistic ubiquitination and deubiquitination activities. *Nature* **446:** 876-881

Sudakin V, Chan GK, Yen TJ (2001) Checkpoint inhibition of the APC/C in HeLa cells is mediated by a complex of BUBR1, BUB3, CDC20, and MAD2. *J Cell Biol* **154:** 925-936

Tang Z, Bharadwaj R, Li B, Yu H (2001) Mad2-Independent inhibition of APCCdc20 by the mitotic checkpoint protein BubR1. *Dev Cell* **1:** 227-237

Tighe A, Staples O, Taylor S (2008) Mps1 kinase activity restrains anaphase during an unperturbed mitosis and targets Mad2 to kinetochores. *J Cell Biol* **181:** 893-901

Vassilev LT, Tovar C, Chen S, Knezevic D, Zhao X, Sun H, Heimbrook DC, Chen L (2006) Selective small-molecule inhibitor reveals critical mitotic functions of human CDK1. *Proc Natl Acad Sci U S A* **103:** 10660-10665

Vink M, Simonetta M, Transidico P, Ferrari K, Mapelli M, De Antoni A, Massimiliano L, Ciliberto A, Faretta M, Salmon ED, Musacchio A (2006) In vitro FRAP identifies the minimal requirements for Mad2 kinetochore dynamics. *Curr Biol* **16:** 755-766

Wan X, O'Quinn RP, Pierce HL, Joglekar AP, Gall WE, DeLuca JG, Carroll CW, Liu ST, Yen TJ, McEwen BF, Stukenberg PT, Desai A, Salmon ED (2009) Protein architecture of the human kinetochore microtubule attachment site. *Cell* **137:** 672-684

Wang Q, Liu T, Fang Y, Xie S, Huang X, Mahmood R, Ramaswamy G, Sakamoto KM, Darzynkiewicz Z, Xu M, Dai W (2004) BUBR1 deficiency results in abnormal megakaryopoiesis. *Blood* **103:** 1278-1285

Wassmann K, Liberal V, Benezra R (2003) Mad2 phosphorylation regulates its association with Mad1 and the APC/C. *EMBO J* **22:** 797-806

Westhorpe FG, Diez MA, Gurden MD, Tighe A, Taylor SS (2010) Re-evaluating the role of Tao1 in the spindle checkpoint. *Chromosoma*

Wolf F, Wandke C, Isenberg N, Geley S (2006) Dose-dependent effects of stable cyclin B1 on progression through mitosis in human cells. *The EMBO journal* **25:** 2802-2813

Xia G, Luo X, Habu T, Rizo J, Matsumoto T, Yu H (2004) Conformation-specific binding of p31(comet) antagonizes the function of Mad2 in the spindle checkpoint. *EMBO J* **23:** 3133-3143

Yang M, Li B, Liu CJ, Tomchick DR, Machius M, Rizo J, Yu H, Luo X (2008) Insights into mad2 regulation in the spindle checkpoint revealed by the crystal structure of the symmetric mad2 dimer. *PLoS Biol* **6:** e50

Yang M, Li B, Tomchick DR, Machius M, Rizo J, Yu H, Luo X (2007) p31comet blocks Mad2 activation through structural mimicry. *Cell* **131:** 744-755

Acknowledgements

I would like to thank Prof. Erich Nigg for providing me with the invaluable opportunity of being a member of his lab. I also thank him for the scientific and intellectual freedom he gave me, always accompanied by his expert guidance. I feel that it has been an exceptional experience, leading an enormous scientific and personal growth.

I am grateful to Dr. Anna Santamaria, who supervised this work. I could count on Anna´s continuous support, during both successful and difficult times. I am grateful for comments and corrections on this manuscript. Furthermore, I am also glad cause thanks to our parallel growth I became aware of the challenges of my future career.

I would like to thank Prof. Elmar Schiebel, who has been my first mentor. He introduced me to science as an investigator and continued providing me with his important input. Furthermore, I thank him for reviewing this manuscript and for his participation to my Ph.D. exam as co-referee.

Special thanks go to Dr. Zuzana Storchova, who joined my Thesis Advisory Committee meetings, providing a precious source of constructive criticism.

I would like to express my gratitude to Dr. Andrea Musacchio, not only for the numerous reagents that he shared with us and that have made this work possible, but also for his intellectual contribution. The work on Mad2 by his laboratory originally raised my interest on this field and it has been therefore a special honor to receive his suggestions.

I would like to thank Elena Nigg, Anja Wehner and Dr. Fabien Cubizolles for expert lab help. Furthermore I am grateful to Dr. Andreas Uldschmidt for precious reagents and to Drs. Kalyan Dulla and Roman Körner for their support in mass spectrometry experiments.

I am grateful to the present and past members of the Nigg lab, for generating a stimulating and joyful environment. Among them, I would like to thank the persons with whom I shared my time outside of the lab, making the Ph.D. an experience at 360°: Manuel Kaulich, Gernot Guderian, Gary Chan, Ina Mayer, Tom Gaitanos, Christian Arquint and Nadja Hübner. I also thank Anna Baron for joining the Mad1 project and Conrad von Schubert for bringing new curiosity in the lab.

Lastly, I would like to thank the IMPRS-LS coordinators in Martinsried and especially Dr. Hans-Jörg Schäffer, for providing great help beyond his duties in many situations and our secretaries Alison Dalfovo and Nadine Iberl for administrative support.

Curriculum Vitae

Name: Luca
Surname: Fava
Place of birth: Bolzano, Italy
Date of birth: 10th of August, 1983
Nationality: Italian

Education

Sep. 2009 – present
PhD studies, continuation: University of Basel, Switzerland (while maintaining the affiliation with IMPRS-LS, see below). Expected date of graduation: October 21st, 2011

Aug. 2007 – Aug. 2009
PhD studies: International Max Planck Research School for Molecular and Cellular Life Sciences (IMPRS-LS), Martinsried, Germany

Sep. 2005 – Jul. 2007
Master in Molecular Biology: (Laurea Magistrale) completed with First Class Honours (score of 110/110, with distinction), University of Padua, Italy

Sep. 2002 – Jul. 2005
Bachelor in Molecular Biology: (Laurea Triennale) completed with First Class Honours (score of 110/110, with distinction), University of Padua, Italy

Research experience

Sep. 2009 – present
Characterization of mitotic checkpoint complexes, continuation of the PhD Thesis. Work carried out in Prof. Erich Nigg's laboratory under the supervision of Dr. Anna Santamaria, Growth & Development, Biozentrum, University of Basel, 4056 Basel, Switzerland

Aug. 2007 – Aug. 2009
Characterization of mitotic checkpoint complexes, PhD Thesis. Work carried out in Prof. Erich Nigg's laboratory under the supervision of Dr. Anna Santamaria, Department of Cell Biology, Max Planck Institute of Biochemistry, 82152 Martinsried, Germany

Sep. 2006 – Jul. 2007
Functional and structural characterization of the γ-Tubulin complex in *S. cerevisiae*, Master Thesis. Work carried out in Prof. Elmar Schiebel's laboratory, Center for Molecular Biology of the University of Heidelberg (ZMBH), 69120 Heidelberg, Germany

May 2005 – Jul. 2005
Characterization of chimeric lentiviral vectors based on the Human Immunodeficiency Virus type 1 (HIV-1) and the Semliki Forest Virus (SFV), Bachelor Thesis. Work carried out in Prof. Cristina Parolin's laboratory under the supervision of Dr. Claudia Del Vecchio, Department of Histology, Microbiology and Medical Biotechnology, University of Padua, Italy

Publications

Fava LL, Kaulich M, Nigg EA, Santamaria A (2011) Probing the in vivo function of Mad1:C-Mad2 in the spindle assembly checkpoint. *The EMBO journal* **30:** 3322-3336

Chan YW, Fava LL, Uldschmid A, Schmitz MH, Gerlich DW, Nigg EA, Santamaria A (2009) Mitotic control of kinetochore-associated dynein and spindle orientation by human Spindly. *J Cell Biol* **185:** 859-874

Presentations at international meetings

Jun. 2010, EMBO Workshop: Chromosome Segregation and Aneuploidy, Edinburgh, United Kingdom. "A Closed-Mad2 monoclonal antibody highlights the Mad1:C-Mad2 template action *in vivo*". Poster

Aug. 2009, FEBS/EACR Advanced Lecture Course in Molecular Mechanisms in Signal Transduction and Cancer, Spetses, Greece. "Towards the *in vivo* visualization of Mad2 conformers". Poster and selected talk

Awards and Scholarships

Aug. 07-present	IMPRS-LS (Max Planck Institute of Biochemistry) student membership, providing support in terms of travel grants, access to scientific and soft skill workshops and salary (partly)
Aug. 2009	Prize for the best selected talk at FEBS/EACR Advanced Lecture Course in Molecular Mechanisms in Signal Transduction and Cancer, Spetses, Greece
Academic Year 2006-2007	ZMBH fellowships for the Master work at the University of Heidelberg

Academic Year 2006-2007 Socrates/Erasmus fellowships for the Master work at the University of Heidelberg

Academic Year 2006-2007 Academic Merit Award of the Province of Bolzano, assigned to the best 80 university students resident in Alto Adige according to score of the final exam (110/110, with distinction)

Academic Year 2005-2006 Academic Merit Award of the Province of Bolzano, assigned to the best 180 university students resident in Alto Adige according to the average score of the university exams (29.1/30)